

dti

A NATIONAL MEASUREMENT
GOOD PRACTICE GUIDE

No. 98

Elastic Modulus
Measurement



The DTI drives our ambition of 'prosperity for all' by working to create the best environment for business success in the UK. We help people and companies become more productive by promoting enterprise, innovation and creativity.

We champion UK business at home and abroad. We invest heavily in world-class science and technology. We protect the rights of working people and consumers. And we stand up for fair and open markets in the UK, Europe and the world.

This Guide was developed by the National Physical Laboratory on behalf of the NMS.

Measurement Good Practice Guide No. 98

Elastic Modulus Measurement

J D Lord and R Morrell

Abstract:

Elastic modulus is an intrinsic material property and a key parameter in engineering design and materials development. A wide range of test methods is available for measuring modulus, but there is currently some uncertainty within parts of the user community about the reliability of modulus data, to the extent that many use standard handbook values in their calculations and designs. This is not recommended and can be addressed through good experimental practice and careful measurement.

Both static and dynamic modulus methods are covered in this Guide, presented in separate sections with details on the different test methods and on practical issues affecting the quality and accuracy of the measurement. The Good Practice Guide draws together some of the background to the techniques, discusses the current standards, and highlights a number of key factors crucial to obtaining good quality measurement. Examples are given where appropriate to highlight aspects of the test methodology, based both on measurements made at NPL and from a number of intercomparison exercises.

Practical issues relevant to the current test methods are discussed, including test-piece preparation, alignment, strain measurement, data analysis methods, uncertainty budgets and the use of reference materials, together with a range of examples, and recommendations for obtaining good quality modulus data.

Results presented show that it is possible to obtain good modulus data from the tensile test, but this generally requires a separate and dedicated test set-up using high quality averaging strain measurement and data analysis procedures, focusing only on the early part of the stress-strain curve. Dynamic methods are generally more versatile, and can be more readily applied to high temperature measurement and to brittle materials with good accuracy.

In both cases, following the procedures recommended, accurate values of modulus can be realised, with typical uncertainties in the measured values as low as 1-2%.

© Crown copyright 2006
Reproduced with the permission of the Controller of HMSO
and Queen's Printer for Scotland

ISSN 1744-3911

National Physical Laboratory
Hampton Road, Teddington, Middlesex, TW11 0LW

For further information on *Materials Measurement* contact Jerry Lord or the Materials Enquiry Point at the National Physical Laboratory:

Jerry Lord
Tel: 020 8943 6340
Fax: 020 8943 2989
E-mail: jerry.lord@npl.co.uk

Materials Enquiry Point
Tel: 020 8943 6701
Fax: 020 8943 7160
E-mail: materials@npl.co.uk

Elastic Modulus Measurement

CONTENTS

1	Scope	1
2	Terms and Definitions	2
3	Introduction	3
4	Static Methods	6
4.1	Overview of existing tensile testing standards	6
4.2	Example modulus data from intercomparison exercises	8
4.3	Practical issues	12
4.3.1	Strain measurement	12
4.3.2	Misalignment and bending	14
4.3.3	Data analysis techniques	17
4.3.4	Development of the NPL web-based modulus analysis software	19
4.3.5	Strain range issues	24
4.3.6	Use of reference materials	25
4.3.7	High temperature measurements	26
4.4	Software validation using ASCII datafiles	27
4.5	Uncertainty budgets	31
4.6	Summary and recommendations on tensile testing	33
4.7	Flexural modulus testing	34
4.7.1	Introduction	34
4.7.2	Machine displacement method	35
4.7.3	Linear displacement transducer methods	38
4.7.4	Strain gauge method	39
4.7.5	Tests at elevated temperature	40
5	Resonance and Impact Excitation Methods	41
5.1	Principle	41
5.1.1	Vibration modes of beams	41
5.1.2	Vibration modes of discs	44
5.2	Calculations	44
5.2.1	Standards	44
5.2.2	Beam flexure	45
5.2.3	Beam torsion	46
5.2.4	Beam longitudinal mode	46
5.2.5	Discs	46
5.2.6	Other shapes	47
5.3	Practical issues	48
5.3.1	Test-piece dimensions and surface finish	48
5.3.2	Suspension and support methods	48
5.3.3	Resonance excitation	50
5.3.4	Impact excitation	50
5.3.5	Vibration detection	51

5.3.6	Measurement to high temperatures	51
5.3.7	Damping	52
5.3.8	Example data	52
5.3.9	Method accuracy and uncertainty	59
5.4	Differences between dynamic and static moduli	62
5.4.1	Theory	62
5.4.2	Validation	62
5.5	Summary and recommendations on dynamic testing	65
6	Acknowledgements	66
7	References	66
	Annex 1: Equations for resonance or natural frequency methods	69
	Annex 2: Selection of prismatic bar test-piece dimensions for resonance or impact excitation	78
	Annex 3: Impact excitation method applied to disc test-pieces	83
	Annex 4: Resonance and impact excitation methods applied to single crystals	89

1 Scope

The aim of this Good Practice Guide (GPG) is to provide an overview of some of the issues associated with making accurate elastic modulus measurements from static and dynamic tests. It is not possible to cover all methods in detail, so the focus is primarily on measurements from the tensile test, and on dynamic methods based on the impact excitation technique. The static and dynamic methods are covered in two separate sections.

The test methods described in the document are not material specific and the general procedures and approach can be applied to a range of materials, but the tensile test method described is probably more suitable for metallic materials and some composites, and the dynamic methods for both metals and ceramics. This Good Practice Guide mainly deals with room temperature tests although some comment and advice on high temperature measurement is included where appropriate.

In both cases, consideration is given to some of the practical factors that affect the quality and accuracy of the measurements – such as specimen preparation, dimensional accuracy, strain measurement techniques, aspects of the test set-up, uncertainty calculations and data analysis methods, illustrated with examples wherever possible. Key issues are highlighted in bold throughout the text and summarised at the end of each section.

Many of the experimental data presented in this GPG have been generated through research programmes at NPL, although some of the data relevant to measuring modulus from a tensile test was produced as part of a recent EU project, *TENSTAND*, in which various aspects of the tensile test procedure relevant to computer controlled testing were investigated.

2 Terms and Definitions

Symbol or Term	Definition	Units
E	Young's modulus	GPa
σ	Stress	MPa
ε	Strain	%
$Rp_{0.2}$	0.2% proof stress	MPa
Rm	Tensile strength	MPa
ν	Poisson's ratio	-
G	Shear modulus	GPa
Ea	Adiabatic modulus	GPa
Ei	Isothermal modulus	GPa
f	Fundamental frequency (subscripts f,t refer to flexure and torsion)	Hz
F	Load	N
L	Test-piece length	m
b	Test-piece width	m
t	Test-piece thickness	m

The list is not exhaustive, and other dimensional, mass and density parameters are defined in the appropriate places throughout the document.

3 Introduction

Although elastic modulus is an intrinsic material property and a key parameter in engineering design and materials development, the current test methods for measuring it are not well established. An accurate knowledge of the engineering value of elastic modulus is vital for design, for finite element and modelling calculations, and for giving reliable fits to the constitutive equations for the stress-strain curve. From the tensile test, accurate values of modulus are also necessary for obtaining reliable values for proof stress, because inaccuracies in the slope or modulus fit can give significant errors in proof stress, particularly if the material has a high work hardening rate in the early stages of yield.

The existing tensile standards EN 10002-1 [1] and ASTM E8 [2] focus predominantly on measuring the full stress-strain curve, of which the elastic part is often only a small proportion. ASTM E111 [3] is the only standard currently addressing some of the issues relevant to making accurate modulus measurements from a tensile test, although a number of in-house proprietary procedures exist. Results from the detailed test programme carried out within the recently completed EU TENSTAND project confirm that there are still major difficulties with obtaining reliable modulus measurements from the tensile test, and contrary to expectations, the majority of partners revealed that they normally measured modulus by alternative techniques. Of those who used the tensile test, the modulus measurements were usually made using a different set up and test conditions than would be used for measuring the full stress-strain curve according to EN 10002-1. From the analysis of the datafiles generated as part of the TENSTAND project, the uncertainty in modulus was the highest of all the parameters examined. This further illustrates the difficulty of obtaining good quality data, but perhaps such large uncertainty should not be unexpected as the tests were carried out according to the current procedures in EN 10002-1, which does not specifically cover the measurement or calculation of Young's modulus. More specific guidance on the determination of the slope of the curve in the elastic range is given in Section A.4.9 in Annex A in the latest draft of EN 10002-1, but this is still inadequate.

It is possible to obtain good quality modulus data from the tensile test, but this generally requires a separate and dedicated test set-up using high quality averaging strain measurement focusing only on the early part of the stress-strain curve. These are specialised tests, and it might be neither feasible nor realistic to carry them out in a cost effective way on a high throughput computer controlled test machine.

Generally the main driver for measuring modulus is for product and material specification, modelling data or customer request. In some cases the need is material specific, for example much of the modulus measurement work at NPL has arisen because of the work on metal matrix composites (MMCs). To realise the potential of these materials for higher strength and stiffness compared with conventional unreinforced alloys, accurate methods for measuring the properties are required. In some cases the identification of the linear part to the curve was difficult, due to presence of high tensile residual stresses that developed in the matrix material during processing and heat treatment, leading to very low proportional limits and a short elastic portion of the curve. In other situations the need for accurate measurement is driven by legislation.

Within the tensile test itself, there are many practical difficulties associated with achieving a straight portion at the beginning of the stress-strain curve, and the modulus of some materials is notoriously difficult to measure. However, an accurate value is important for design purposes and for subsequent calculation of proof stress values and non-proportional elongation values in the full tensile test. The stress-strain curve in Figure 1 [4] shows the effect that different values for the modulus can have on these parameters.

In Figure 1, two lines for the slope or modulus are shown, with values of 205 GPa and 199 GPa, and it can be seen that the variation in modulus has an impact on the calculated values for R_p and A . Although, in this case, the difference in proof stress values is small ($\sim 0.5\%$) they might be expected to be greater for materials with significant work hardening since small variations in the modulus may result in large differences in the values of R_p .

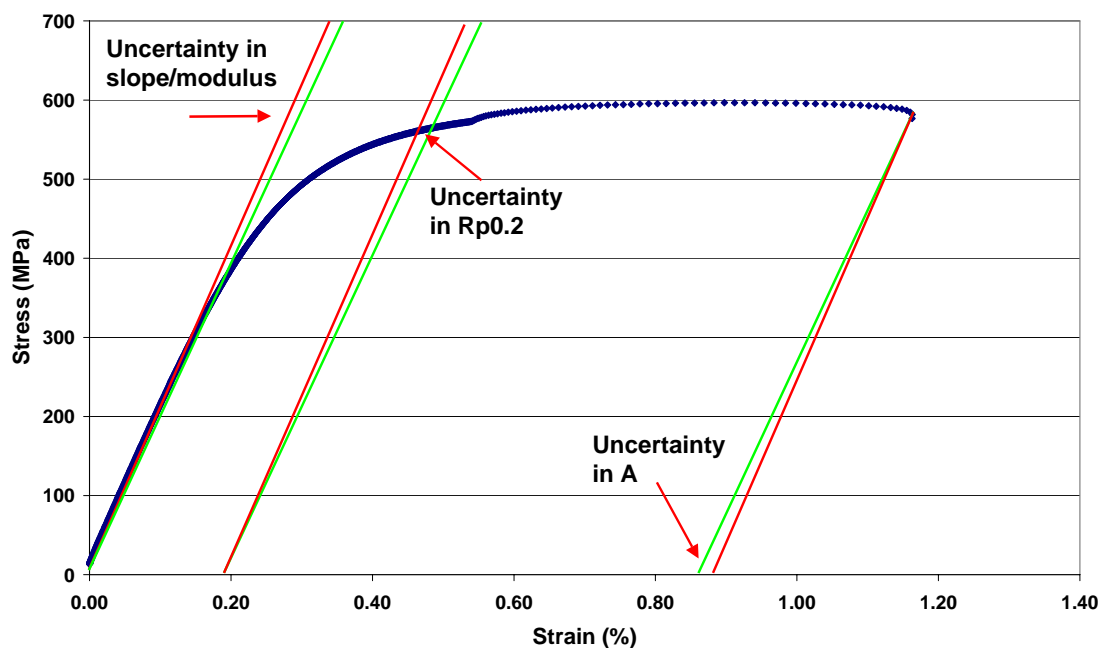


Figure 1: The influence of the variation in modulus on other parameters [4]

As mentioned above, because of the practical difficulties of obtaining reliable modulus values from the tensile test some organisations abandon the calculation of modulus altogether and use pre-determined or handbook values for the initial slope and modulus values, which they then use to calculate the proof stress; others turn to dynamic techniques. A large variety of dynamic modulus methods is available including flexural resonance methods, the impact excitation technique (IET), and various ultrasonic, resonance or acoustic wave propagation methods [5-8]. The most commonly used dynamic methods for metals are probably the resonance techniques, and Table 1 summarises the relative merits of the tensile and dynamic modulus approaches.

The tensile test realises an engineering value of modulus, through the representation of the linear part of the stress-strain curve, and many engineers are more comfortable dealing with this as it is a parameter that they can relate directly to their design requirements. Generally however modulus measurements from the tensile test show larger variation and scatter compared with dynamic measurements, and issues such as alignment, strain measurement and

data analysis are important factors. The measurement of modulus at high temperatures is not trivial from the tensile test.

Dynamic methods generally have the advantage that they are relatively quick and simple and involve small elastic strains and high strain rates. Some can be readily modified to enable high temperature measurements, and it is also possible to obtain Young's modulus, shear modulus and Poisson's ratio from a single test if an appropriate test-piece geometry and set-up is used. Dynamic methods are used routinely for measurements on ceramics, where it is very difficult to obtain good experimental modulus data from static mechanical test methods, particularly tensile tests, because of the brittle nature of the material, gripping and alignment issues. Dynamic methods typically use a small and simple specimen geometry, which might be beneficial if only small amounts of material are available, but the methods can be sensitive to machining damage, surface finish and poor dimensional tolerances, all of which affect the accuracy of the result. A variety of commercial equipment is available and the theoretical errors in measurement of modulus by dynamic methods are small, typically of the order of $\pm 1\%$.

Table 1: Summary of relative merits of the dynamic and tensile approaches for measuring modulus

Tensile Test	Dynamic Methods
<p>Advantages:</p> <ul style="list-style-type: none"> ▪ “Engineering value” for modulus ▪ Generation of stress-strain curve ▪ Widely available test equipment 	<p>Advantages:</p> <ul style="list-style-type: none"> ▪ Quick, simple, non destructive ▪ Good inherent accuracy ▪ Uses small specimens ▪ High temperature measurement ▪ Can readily measure shear modulus and Poisson's ratio
<p>Disadvantages:</p> <ul style="list-style-type: none"> ▪ High accuracy strain measurement required ▪ Need averaging extensometry ▪ Specialised test ▪ Larger specimens required ▪ Large interlaboratory scatter ▪ Accurate high temperature measurements are difficult 	<p>Disadvantages:</p> <ul style="list-style-type: none"> ▪ Relevance of dynamic modulus to engineering applications & design? ▪ Sensitive to dimensional tolerances ▪ Methods do not always work well for some materials and composites ▪ Calculations require some knowledge of other material parameters ▪ Equipment not widely available

4 Static Methods

Static methods for measuring modulus include tensile tests and flexure tests. Depending on the application, material availability and data requirement users may consider using either approach, and both give a value for the modulus of the material. Most of the detail in the following section refers specifically to the measurements made during a tensile test, the flexure test is only covered briefly in the current version of the GPG, but many of the issues relative to strain measurement, alignment, specimen preparation and data analysis are common to both.

4.1 Overview of existing tensile testing standards

Young's modulus can be defined as the ratio of stress to strain during elastic loading. Traditionally, modulus has been determined 'by eye' from a straight line drawn on the linear part of the stress-strain curve, but more recently automatic testing machines using computer control and data acquisition use some form of curve fitting to get a best fit to the data. With the general tensile testing standards at present, there is little guidance on how modulus should be measured, and aspects of strain measurement are covered only briefly. Both EN 10002-1 [1] and ASTM E8 [2] give no formal definition for modulus, and yet accurate measurement of the slope of the stress-strain or load-displacement curve is necessary for calculating reliable proof stress data. ASTM E111 [3] covers the measurement of Young's modulus, tangent modulus and chord modulus in more detail, the latter two being recommended for non-linear materials. Table 2 [9] overleaf shows a comparison of the scope and test conditions of the current tensile testing standards and their relevance to modulus measurement.

The main differences between ASTM E111, EN 10002-1 and ASTM E8 are the scope of testing and the level of detail relevant to testing at low strain values. ASTM E111 covers the measurement of modulus in both tension and compression testing and by the use of dead weight loading; EN 10002-1 and ASTM E8 cover ramped load tensile testing only. In all three standards averaging extensometry is recommended, but only ASTM E111 gives specific guidelines for the uniformity of strain measurements over the range of the test, stating that the strain increments on opposite sides of the test-piece must not differ by more than 3%. ASTM E111 also notes that the specimen should be free from residual stress as this can affect the length of the linear portion of the curve, depending on whether compressive or tensile residual stresses are present. Although modulus is not generally affected by the heat treatment condition, it is not always possible to stress relieve or carry out annealing to remove residual stresses, because the user will want to measure the properties in the heat treatment state most relevant to the application. ASTM E111 also advocates the use of a higher resolution extensometer compared with the conventional tensile test methods, and also gives detailed advice on data analysis.

To some extent the difficulties in measuring the slope at the beginning of the stress-strain curve are recognised in Section 13.1 of EN 10002-1, and the use of hysteresis loops and preloading is recommended. Further advice is also given in the Annex (Section A.4.9) of the latest draft of EN 10002-1, but more explicit details and recommendations are still required.

ASTM E111 notes that the uncertainties in the measurement should be reported, but offers no advice on how this should be calculated; EN 10002-1 does give some background on uncertainty but does not cover modulus specifically.

Table 2: Comparison of EN 10002-1, ASTM E8 and ASTM E111 [9]

	EN 10002-1	ASTM E8	ASTM E111
Scope	Tensile testing of metals at ambient temperatures Modulus is not explicitly defined in either standard		Young's modulus, Tangent modulus and Chord modulus.
Test conditions	Uniaxial tensile testing Elevated temperature testing in EN 10002- 5	Tensile testing of metallic materials Room Temperature (RT) only	Tension or compression RT, elevated temp (below creep), sub zero
	Continuous loading		Continuous or incremental loading (via dead weights). Measurements during the loading or unloading cycle
	Hysteresis tests can be used to measure modulus/slope Preloads permitted but the value must be noted		Preload is recommended; Specimen should be free of residual stress. Tests should be carried out below elastic limit, and below 0.25% strain
Speed of testing	Recommendations given for various materials and conditions		Not specified
Extensometry	Class 1 for R_p Class 2 elsewhere	Class B-2 for R_{eL} , R_{eH} and A_t Averaging extensometry recommended for R_{eL} , R_{eH}	Class B-1 Averaging extensometry recommended
Strain uniformity and alignment	No recommendations, other than general guidelines to reduce misalignment and bending		As ASTM E8, E9 Recommend that strain increments on opposite sides should differ by less than 3%
Repeat measurements	Not applicable		Minimum of three runs recommended, but single test is permissible
Uncertainty	Example calculations given for a number of parameters (not Modulus) in Annex A of prEN 10002-1.	Some advice regarding precision statistics, but no uncertainty calculations	Should be included with the report. No examples or guidelines.
Data fitting	No recommendations – some guidelines on data sampling and measuring the slope included in Annex A of prEN 10002-1.	Only basic advise on data analysis.	Linear elastic: Least squares fit and/or strain deviation Non-linear elastic materials: Polynomial approximation and chord modulus

4.2 Example modulus data from intercomparison exercises

A number of examples are given to illustrate the typical variation in modulus obtained from tensile test intercomparison exercises. Of course the list is by no means exhaustive, and different groups around the world have carried out a large number of similar measurements, but the results do highlight some of the issues and difficulties associated with modulus measurement.

Figure 2 shows data from one of the earliest recorded intercomparison exercises on mild steel, organised by Unwin in 1895 [10]. Four different bars of material were examined by five different participants. The uncertainty in the measurements, expressed as ± 2 standard deviations is $\sim 2\%$, is quite remarkable, even today. It is possible that rounding and the limited resolution of the measurement equipment available at the time has affected the results.

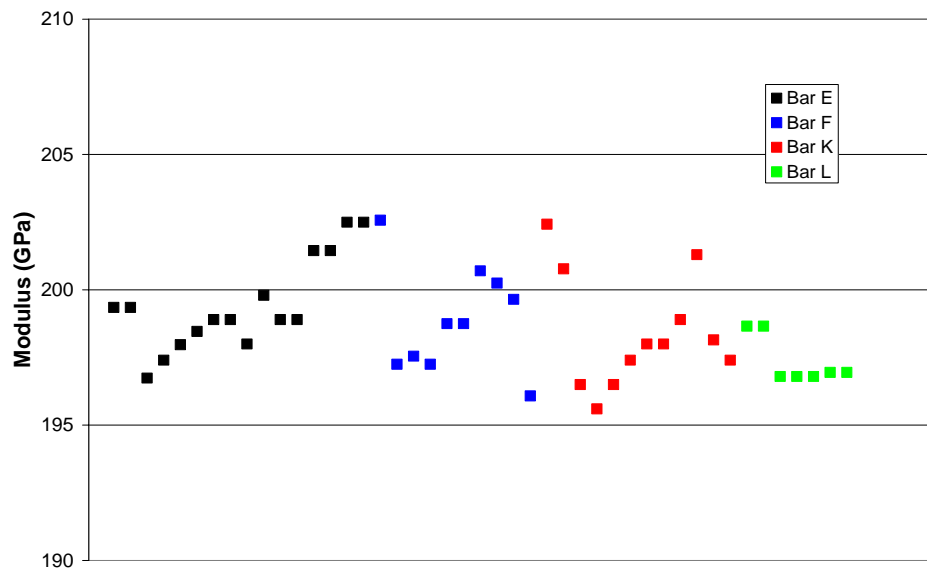


Figure 2: Data from the Unwin intercomparison exercise (1895) [10].

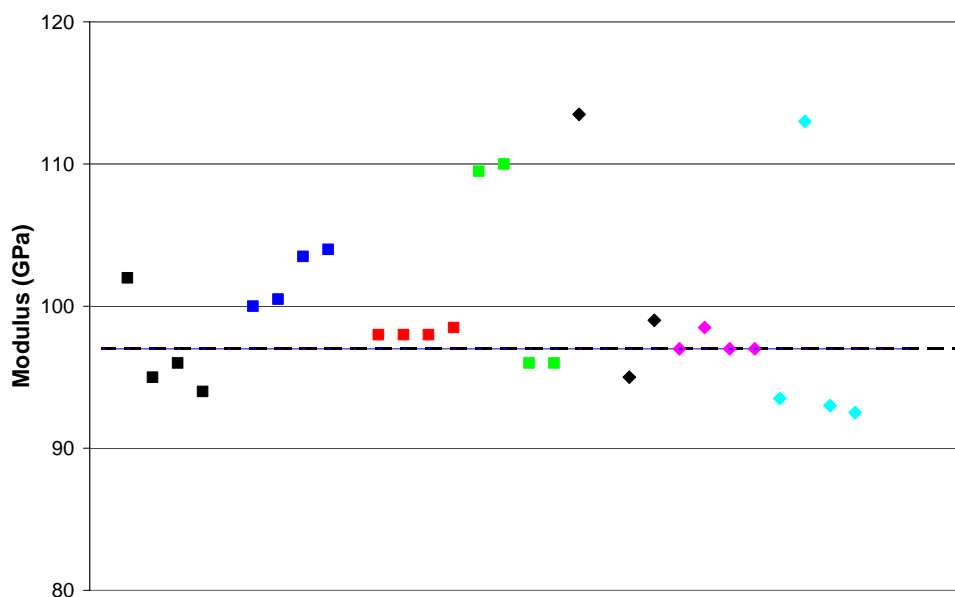


Figure 3: Data from the VAMAS intercomparison exercise on MMC [11].

Figure 3 shows similar data from a recent VAMAS international intercomparison exercise on a SiC reinforced Al MMC [11]. It is interesting to note that the results show higher levels of scatter and uncertainty than that measured by Unwin 100 years earlier, but clearly some laboratories are performing better than others.

Figure 4 shows the data generated on the BCR Nimonic 75 tensile reference material as part of the certification exercise on this material [12]. It should be noted that the material is not certified for modulus and the data plotted in Figure 4 was generated from tensile tests to failure. There is quite a large variation in the measured values, and clear differences between individual bars and organisations. Lab E was the only participant that used a special high resolution averaging extensometer and the reduced scatter and repeatability of the measurement (the uncertainty was $\pm 2\%$ compared to $\pm 12\%$ for all tests) illustrates the importance of the test set-up and strain measurement in particular. This will be addressed in more detail in the following sections.

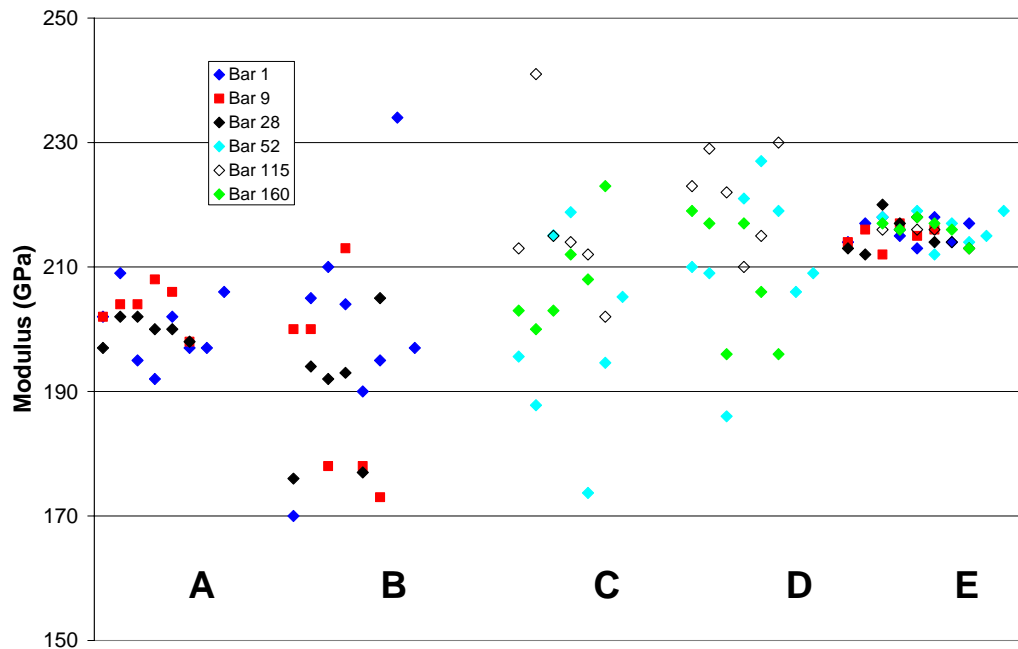


Figure 4: Data from the certification exercise on the BCR tensile reference material [12].

Figures 5 and 6 show data from the recently completed TENSTAND project [4, 13]. Figure 5 details the modulus values measured from an intercomparison exercise on 6 different materials (some in different forms), with 8 participants and 3 different sets of test conditions. Tensile tests were carried out to failure on a wide variety of test machines and test conditions. Some laboratories performed well, but generally there was large uncertainty in the measurements.

The uncertainties in the measured modulus values from this exercise were alarmingly large, but the mean modulus values for a particular material batch were generally very good, and in agreement with what might be expected for the particular material. The lowest uncertainties were obtained with the aluminium specimens, and some of the highest from tests on stainless steel. There does not appear to be a trend in the uncertainty values consistent with the test

conditions. In the data presented above, the only comparison of the flat and round test-piece geometry can be made with the S355 results. For the same conditions, tests on the round specimens showed less scatter and variability, and lower uncertainties, probably as a result of better alignment of the test-pieces with the threaded ends.

Figure 6 shows a summary of the data from a further exercise examining the software methods and algorithms used to calculate modulus. In this case a series of identical data files were distributed to the participants for analysis, the results are on the same set of data and any differences and uncertainty is a factor only of the data analysis. Even so the uncertainties, excluding outliers, are in the range 1-6%.

Table 3 shows a summary of the uncertainties from the exercises described above.

Table 3: Summary of data from intercomparison exercises

Reference	Year	Material	Uncertainty (± 2SD) %
Unwin [10]	1895	Mild steel	2
VAMAS [11]	1997	SiC/Al MMC	6
BCR Report [12]	2000	Nimonic 75	12
TENSTAND WP4 [13]	2005	Various	5-25
TENSTAND WP2 [4]	2005	Various - ASCII datafiles	1-6

Clearly there are still issues with obtaining reliable modulus data from the tensile test and, as will be highlighted later, there is a real need for a separate dedicated tensile modulus test, carried out over a limited strain range, using high-resolution strain measurement.

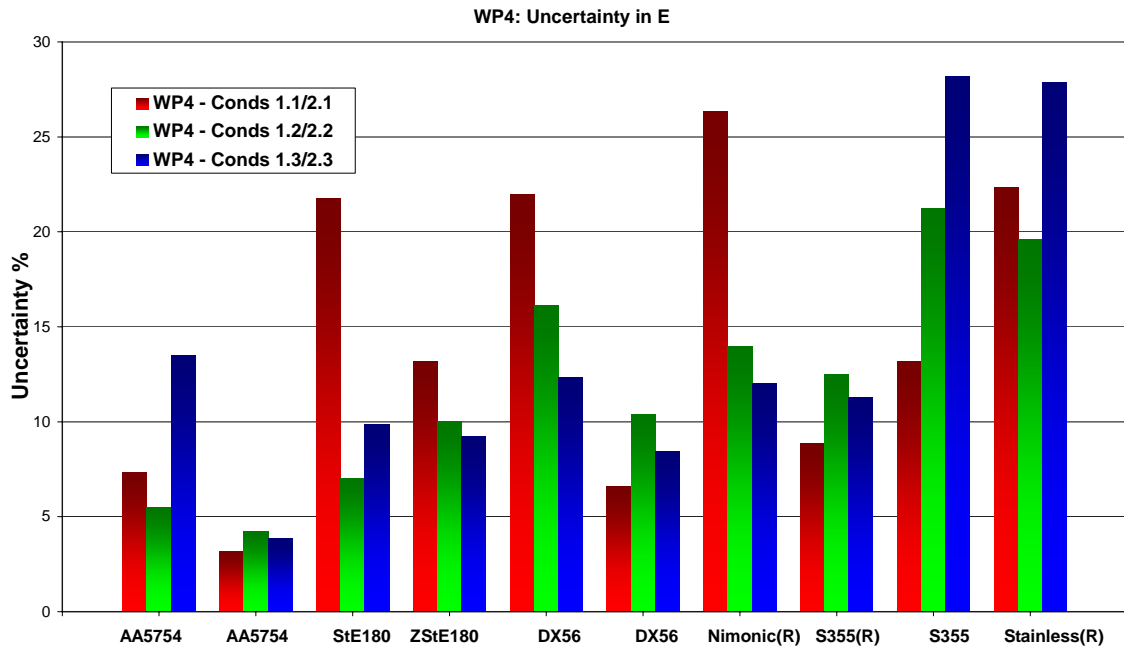


Figure 5: Data from the TENSTAND intercomparison exercise [13].

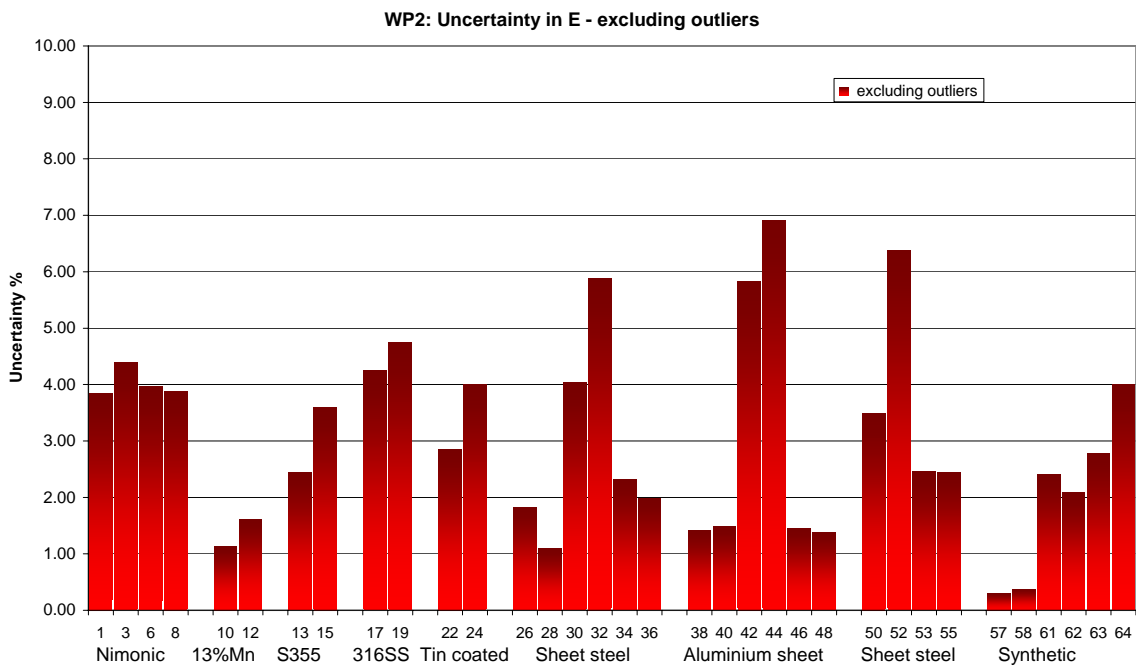


Figure 6: Data from the TENSTAND data analysis intercomparison exercise [4].

4.3 Practical issues

Some of the practical issues to consider when carrying out a tensile modulus test are described in the following sections including specific advice on strain measurement, misalignment and bending, data analysis techniques, and the use of reference materials.

4.3.1 Strain measurement

A wide variety of strain measurement methods exist, but most of the standards only discuss the use of extensometers. Strain gauges should not be ignored and in many respects offer a better solution than extensometers in the dedicated modulus test, as will be discussed later.

Extensometers come in a range of designs, gauge lengths, travels and may be single-sided or averaging (double-sided) models. For the highest possible accuracy, a Class 0.2 averaging high-resolution extensometer, calibrated according to EN ISO 9513 [14] **over the restricted strain range appropriate to the test**, is recommended for modulus measurement. An example of such a design is shown in Figure 7. Unfortunately Class 0.2 and 0.5 extensometers are not widely available, nor do many users have the appropriate equipment to calibrate these devices over the low strain range encountered in modulus testing, so in many cases Class 1 extensometers are used. For such devices the total bias error is $\pm 1\%$ or $3\ \mu\text{m}$, whichever is the greater, and this can lead to significant errors at low strains. The bias error associated with the various class of extensometer, according to EN ISO 9513, is summarised in Table 4.

Table 4: Bias error associated with various class of extensometer [14]

Class of Extensometer	Bias Error	
	Relative, %	Absolute, μm
0.2	± 0.2	± 0.6
0.5	± 0.5	± 1.5
1	± 1.0	± 3.0
2	± 2.0	± 6.0

Consideration of Figure 8 [15] illustrates the problem. Because of the $\pm 1\%$ or $3\ \mu\text{m}$ lower limit, the absolute error in strain measurement increases as the strains become smaller. For a 25 mm gauge length and 0.1% strain, the error in modulus can be as high as $\pm 12\%$, and these are the typical uncertainties that can be attributed to the measurement of strain for a Class 1 extensometer.

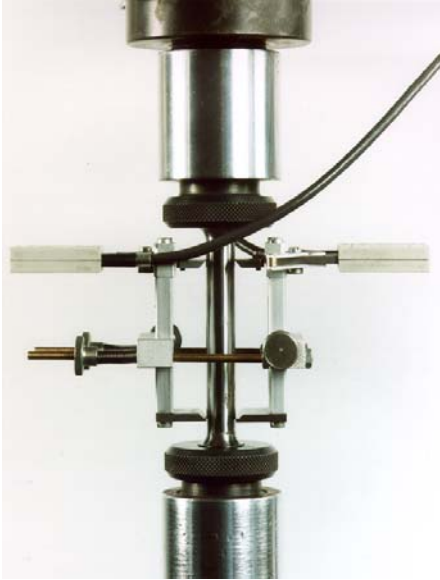


Figure 7: Typical high resolution averaging extensometer (courtesy of BAM).

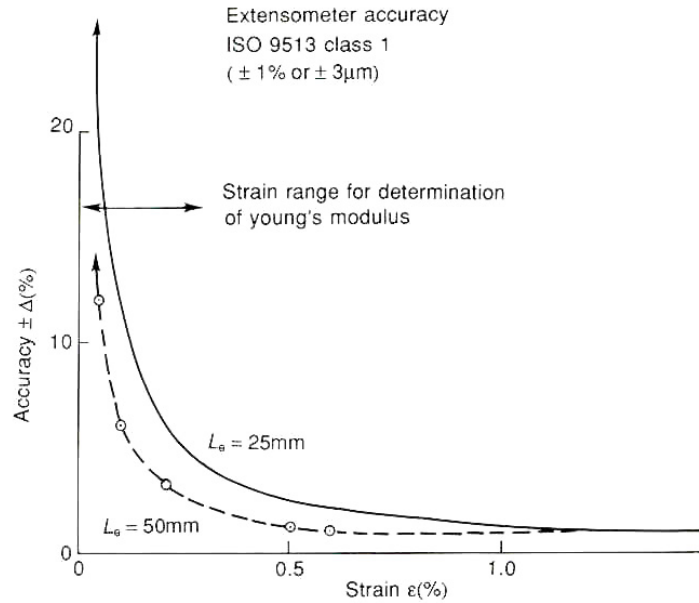


Figure 8: Typical errors likely in determining Young's modulus with a Class 1 extensometer [15].

Due to the difficulties associated with calibrating and setting up a high precision averaging extensometer, consideration should be given to using strain gauges bonded to each side of the test-piece to measure the strain during the test. At present none of the tensile testing standards directly advocate or support the use of strain gauges, but they are an attractive and cost effective alternative to the high-resolution extensometer. A number of practical issues must be considered however to ensure accurate and reliable results:

- **The strain gauge is a precision instrument and installation should only be carried out by suitably qualified staff.**
- **A high instrument gain should be chosen to give the greatest strain resolution and full-scale output over the limited strain range during the modulus test.**
- **An accurate gauge factor must be used.**
- **Calibration of the strain gauge instrumentation should be carried out over a similar strain range to that used in the test.**

Strain gauges are only suitable for measuring the full tensile properties if the failure strains are less than about 3%, and the resolution of the strain gauge reading depends on the gauge factor and instrumentation gain. Modern strain gauge instrumentation typically has a resolution of $\pm 1\mu\epsilon$, (although higher resolution instrumentation is available) but for these settings the maximum strain that can be measured may be limited to only 0.5% (5000 $\mu\epsilon$). If gauges are used to measure the stress-strain curve at higher strain values, then a compromise must be reached between the maximum strain that can be measured and the measurement resolution required, and **they should not be used for machine control.**

Strain gauge installations may also be susceptible to other uncertainties that are difficult to quantify. The instrumentation itself can be calibrated by using a shunt resistor, but the

individual gauge installation on the test-piece itself cannot be calibrated easily. Errors can arise due to misalignment of the gauge, poor gauge installation and bonding, temperature effects, Wheatstone bridge non-linearities and transverse sensitivity. All are important factors but are difficult to quantify. However, for modulus measurements at low strain levels, uncertainties in the strain readings of better than $\sim \pm 1\%$ should be readily achievable. As with extensometry, it is vital that the gauges should be applied to both sides of the test-piece and averaged to take account of out-of-plane bending.

4.3.2 Misalignment and bending

Misalignment and bending of the test-piece in the test machine is a major contributor to uncertainty and scatter in the modulus measurement, and all efforts should be taken to minimise its effect by ensuring that the test machine, load train and fixtures are well aligned. General guidelines are given in EN 10002-1 and ASTM E8, and EN10002-2 [16] for test machine alignment, with more specific advice in ASTM E111 that strain increments on opposite sides of the test-piece should not differ by more than 3%. This is quite challenging.

Misalignment and bending can be manifest as a non-linear part of the stress-strain curve, to which it is both impossible and meaningless to fit a straight line to represent the modulus of the material. It can be identified by employing strain measurement on opposite sides of the test-piece, such as a double-sided extensometer, or multiple strain gauges applied to different parts of the gauge length, although a double-sided averaging extensometer that gives only a single mean value will not be able to identify whether bending is present.

Bending can be reduced through the use of special alignment fixtures, test-piece location jigs and accurately machined specimens, but it is very difficult to eliminate completely. With some set-ups a universal joint in the load train is beneficial and offers a degree of self-alignment. The test machine set-up can be verified and classified using an instrumented “reference” specimen, following procedures similar to those adopted in other areas of mechanical testing, such as strain controlled low cycle fatigue testing [17]. This should be repeated if there are changes to the system configuration, grips or test-piece design.

At the very least, it is recommended that individual strain channel readings be examined for signs of non-linearity and bending. Preliminary checks can be made by carrying out a loading cycle below that set in the actual test itself, to examine the extensometer or strain readings, and test-piece alignment, which can then be adjusted if necessary.

Figure 9 shows data from a dedicated modulus tensile test carried out on a rectangular section test-piece with strain gauges bonded to opposite faces. The individual outputs from the two strain channels are shown, together with the mean value. Clearly there is some misalignment and bending in this case. The data are shown plotted on scales of 0.1% and 200 MPa, which are below the proportional limit for this material. This was a full tensile test and the difference between the two strain channels at 0.1% strain was $\sim 15\%$.

Analysis of the respective single strain channels gave “modulus” values of 193.5 GPa and 220.0 GPa; the mean of the strain readings gave a linear portion to the curve and a more realistic modulus value of 208.4 GPa.

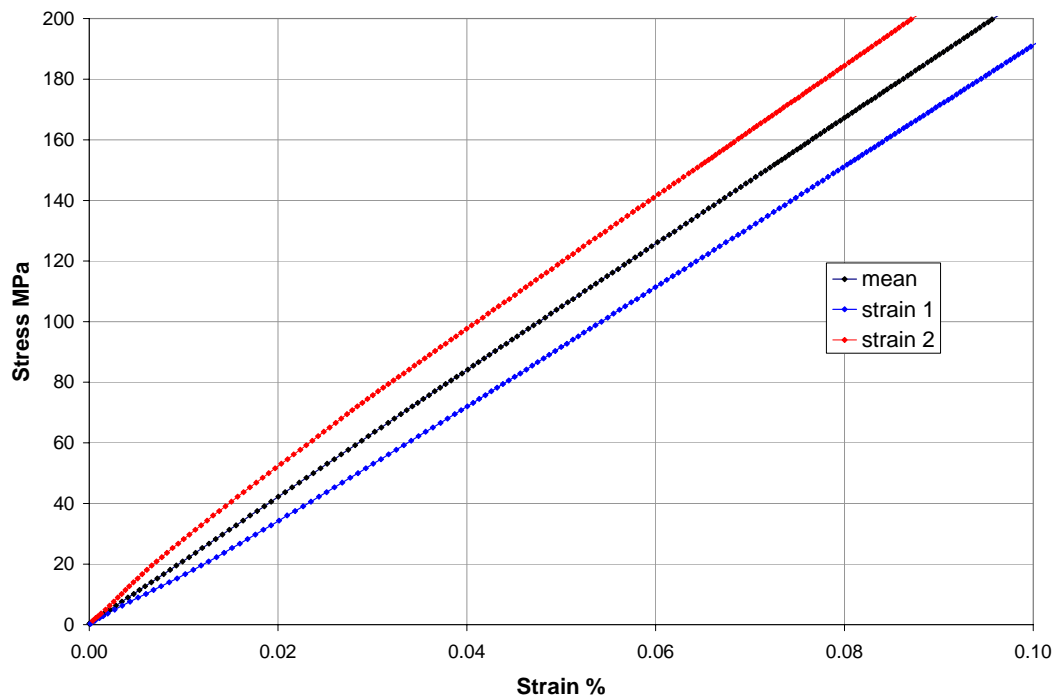


Figure 9: Comparison of individual strain readings from a tensile test.

Figure 10 shows corresponding strain data from a dedicated modulus tensile test on the NPL “modulus reference specimen”, carried out using strain gauges and high instrument gain, over a limited strain range. In this case the strain readings are in much closer agreement; the individual gauges give modulus values of 203.6 GPa and 196.1 GPa compared to the mean of 199.7 GPa, and the difference between the two strain channels at 0.1% strain was ~ 3%.

Figure 11 shows results from a series of measurements on the NPL “modulus reference specimen”, which is used to check the test system, set-up and data analysis procedures. The specimen is a unidirectional SiC fibre reinforced Ti composite, which has been loaded over 80 times in a 10-year period, with tests being carried out below the proportional limit to ensure that behaviour remains elastic. The mean modulus value for all tests (excluding outliers – see below) is 200.3 GPa with a standard deviation of ± 1.2 GPa.

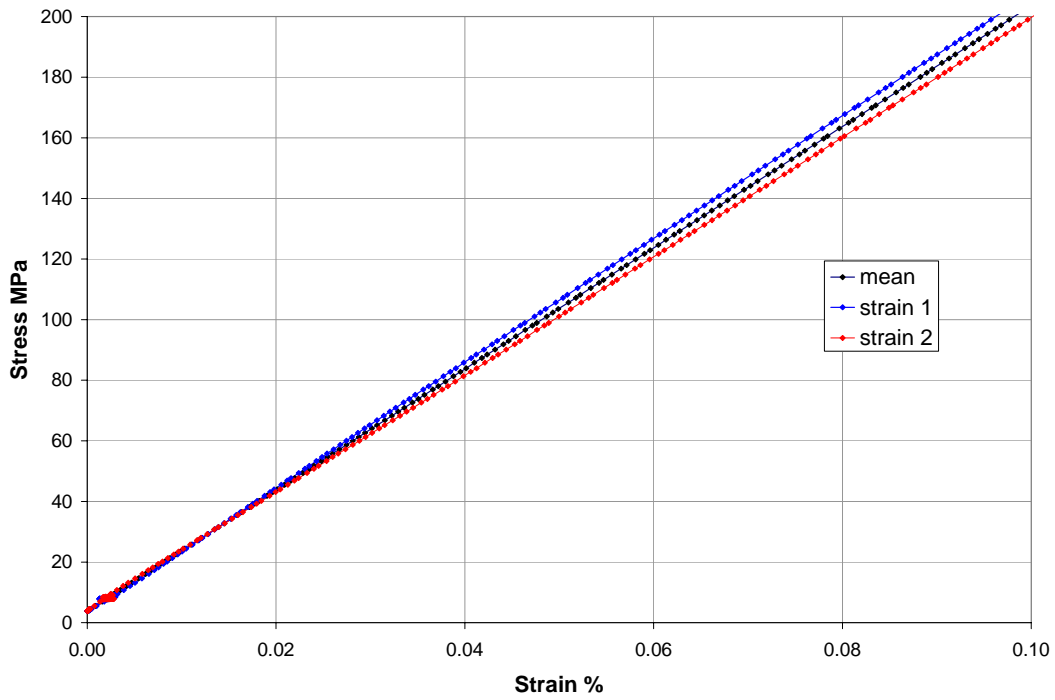


Figure 10: Comparison of individual strain readings from a dedicated modulus test.

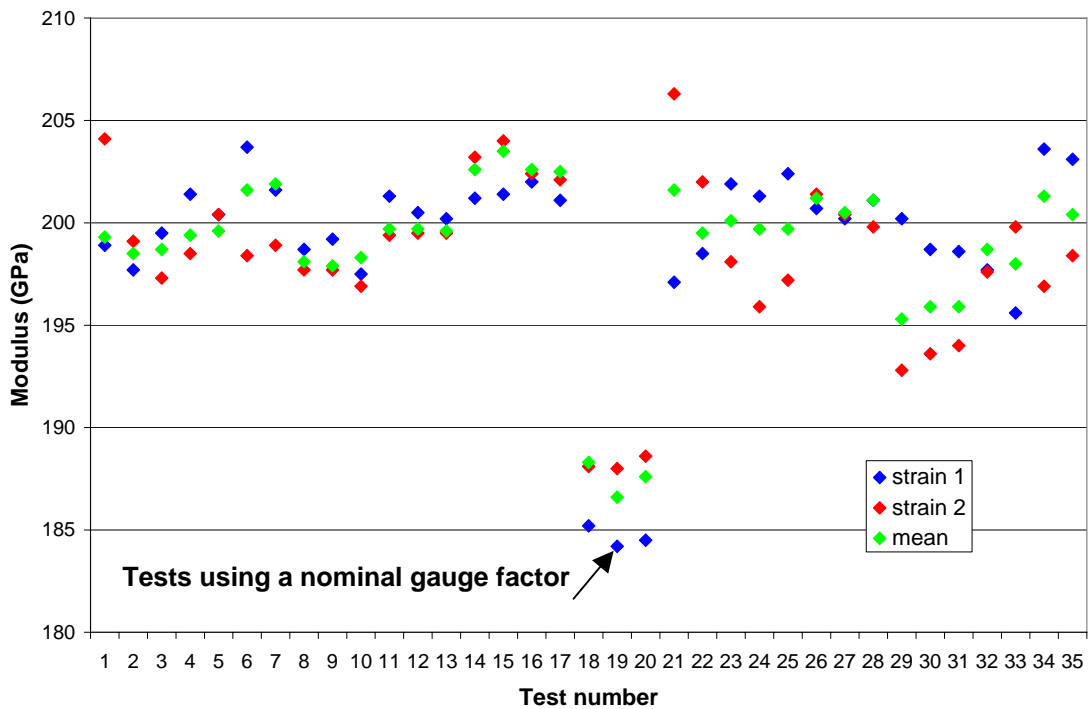


Figure 11: Data on the NPL “reference” modulus specimen.

Results show only a small variation in the mean value for modulus, but larger scatter in the values calculated from individual gauges. The mean value for each test is not simply the arithmetic average of the two modulus measurements, but is based on re-analysis of the stress/strain curve based on the average strain measurements. Tests were carried out using different types of strain gauges, and it is important to note that tests 18-20 used gauges supplied with a nominal gauge factor of 2.0. Inaccuracies in the gauge factor in this case has led to an offset and error in the true strain reading, with an associated error in modulus – and these were identified as outliers in the data set. As noted previously, accurate values for the gauge factor must be used, and it is also recommended that a reference specimen be used for regular checks and validation.

In some cases there may be nonlinearity in the early part of the stress-strain curve caused by “bedding in” of the test-piece into the grips. To avoid this a small pre-load may be applied to the specimen prior to testing, or the problem might be resolved by carrying out a series of repeat loading-unloading tests, both of which are allowed in the current standards.

4.3.3 Data analysis techniques

Although the concept of fitting a straight line to the linear part of the stress-strain curve is simple, in reality a number of factors affect the modulus value calculated including the noise and variability in the quality of the data, the linearity of the stress-strain curve itself, and the choice of procedures for carrying out the data fitting. A major concern exists with the large variety of algorithms available to the user because, without specific guidance or consideration, the algorithms can give very different values for modulus.

In some cases graphical techniques are still used but most systems today use computer-based analyses. Commercial test machine software such as *Zwick testXpert* and *Instron Merlin* offer a wide range of analysis options relating to the calculation of the slope or modulus, some of which are illustrated schematically in Figure 12 [15] and listed below:

- Maximum slope
- Tangent modulus
- Chordal modulus
- Secant modulus
- Segment modulus
- Initial tangent modulus
- Hysteresis loop measurements
- Combined tangent/secant
- Combinations and variations of the above

It is not the intention of this GPG to discuss in detail the aspects of all the individual options, but to highlight some of the issues that the user should consider in their choice of test method and analysis procedures.

The preferred procedure is to examine the early part of the stress-strain curve (below the elastic limit) and automatically optimise the fit of the modulus line to the data by consideration of least squares regression analyses or other statistical fitting techniques, **with little or no operator intervention**. Many of the data analysis procedures are carried out between discrete data points, and others use some sort of fitting or interpolation between automatically or user selected limits, either as a simple straight line or by use of least squares

regression. Some algorithms only consider part of the curve, while some split the curve into a fixed number of discrete regions (which may or may not overlap) and then calculate values of the slopes according to particular criteria, such as the region with maximum slope. Others are designed to take account of anomalies at the start of the test such as non-linearity associated with bedding in, specimen straightening and initial slackness in the load train etc.

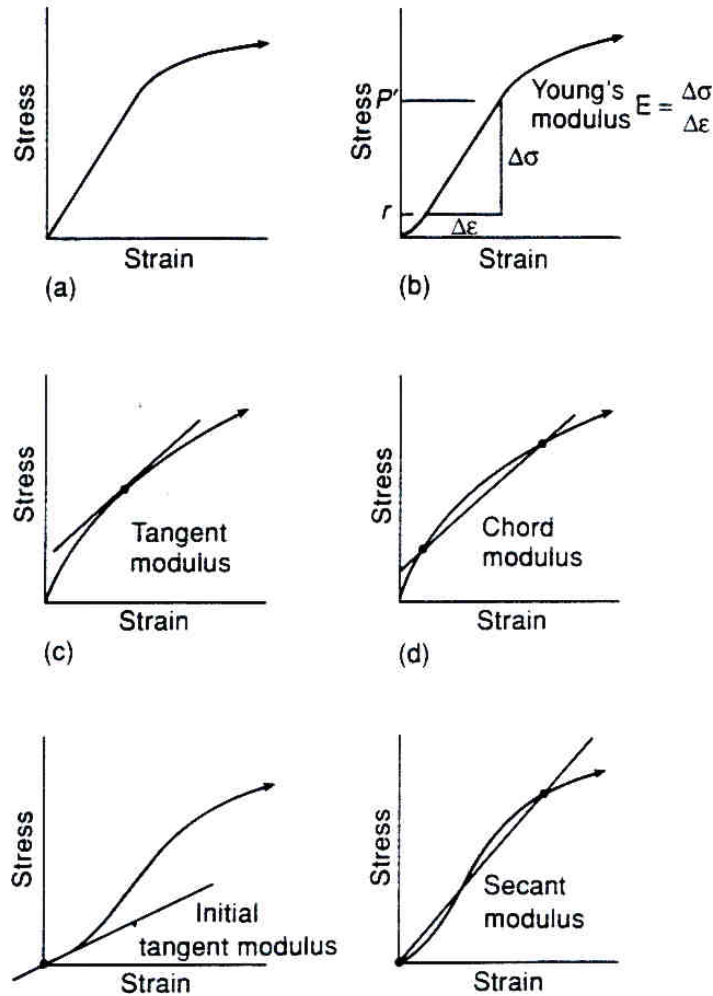


Figure 12: Schematic of modulus definitions and calculations [15].

The accuracy in modulus calculation is also affected by the quality of the data and test set-up. Ideally the data should be free from excessive noise and contain sufficient data points in the elastic range for detailed analysis. The number of data points is an important issue because, if the tensile test was designed to measure the whole of the stress-strain curve, there may be insufficient data points in the early part for accurate calculation of modulus. From analysis of the ASCII datasets developed in the TENSTAND project [13], the typical number of datapoints varied between 150-500 using a high sampling rate (50Hz) and a strain range of 0.2%. The high sampling rates recommended for the full tensile test are required to capture the pertinent features in the stress-strain curve, such as the upper or lower yield points. Data acquired at significantly lower sampling rates can lead to problems due to the limited number of datapoints in the elastic part of the curve, but this is not really an issue for the dedicated tensile modulus test.

For the dedicated modulus test it is recommended that:

- The stress-strain data is captured using a computer based acquisition system, with at least 100 data points sampled for each strain increment of 0.1%;
- Some knowledge of the function of the particular algorithm used to calculate the modulus from the stress-strain data is desirable (and should be recorded in the test report);
- The software should be able to analyse the data automatically with minimal operator intervention.

4.3.4 Development of the NPL web-based modulus analysis software

NPL has developed software for analysing stress-strain data [18], whereby the tangent and secant moduli are calculated at each data point, and used to define the straight line fit to the early part of the stress-strain curve (see schematic in Figure 13).

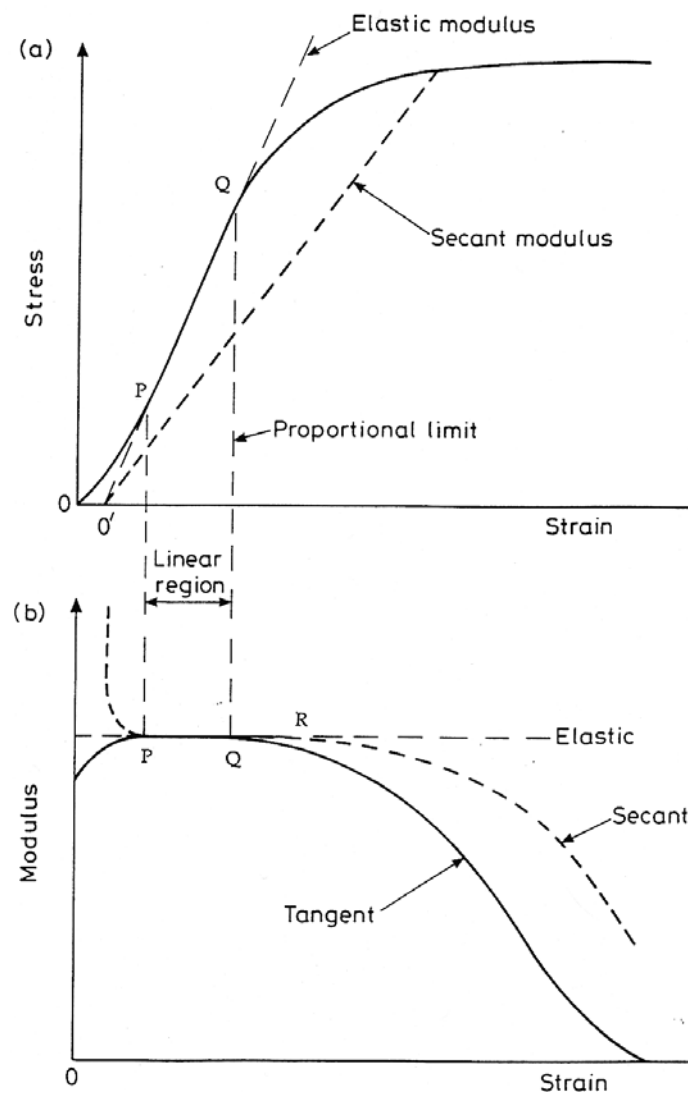


Figure 13: Schematic of NPL modulus software and analysis procedure [18].

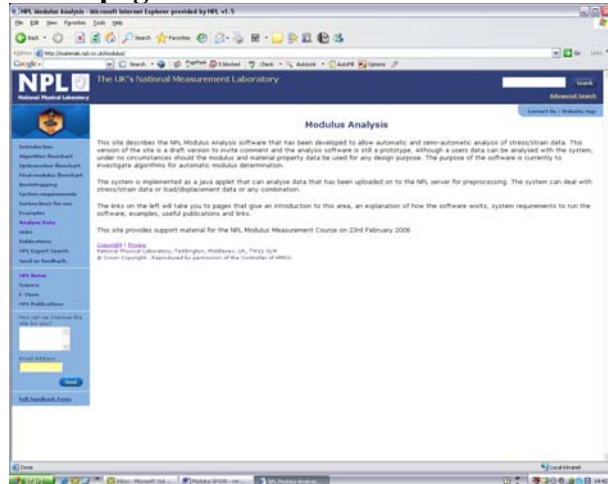
The analysis works by sequentially fitting a quadratic polynomial to the stress-strain data, point by point along the curve, by a least squares regression analysis. The fitted polynomial is then differentiated at each point to obtain a value for the tangent modulus, which is then plotted against strain. The best fit to the tangent modulus-strain curve is then obtained and this modulus value is used to define a new origin for the stress-strain data. The data are then replotted with a new origin, and the secant modulus-strain curve is calculated. For a good fit to the linear part of the curve, the tangent and secant moduli should coincide and this is taken to represent the true value of Young's modulus from the test. The analysis of the secant and tangent moduli data is a very sensitive method for checking whether the value selected is a good fit to the stress-strain curve. It has been used to analyse data in various intercomparison studies and been adopted by a number of users and commercial software packages [19-22].

A web-based version of the modulus analysis software has recently been implemented, which is currently available to access at <http://materials.npl.co.uk/modulus>. Users can import their own stress-strain data in the form of ASCII or Excel datafiles, and analyse the data to calculate modulus. Example screenshots are given in Figure 14.

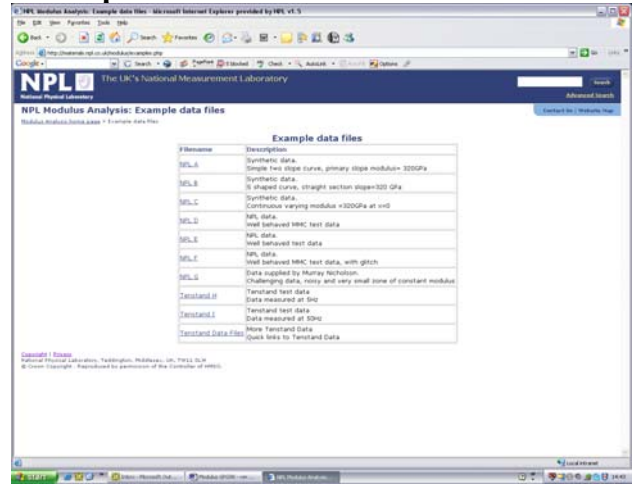
Figure 15 shows a stress-strain curve from the TENSTAND ASCII dataset [4] that has been analysed using three different algorithms to show the sensitivity of the tangent-secant moduli approach. In each case the plot of the tangent and secant moduli vs. strain are shown on the left hand side, and the corresponding stress-strain curve, with the modulus fit overlaid on the curve on the right. The value selected for the best fit (top figure) gave a modulus of 192.0 GPa, with 194.4 GPa and 190.2 GPa for the middle and bottom cases respectively. Although the fit to the stress strain curve looks reasonable in all cases, there is a clear difference in the tangent/secant moduli curves. Only in the top figure do the tangent and secant coincide, and the value from this analysis has been chosen as the “correct” modulus for the test. The differences between the values calculated from the other analyses are only 2.4 GPa and 1.8 GPa respectively, but do not give as good a fit to the data and are in error by about 1%.

Figure 16 shows typical stress-strain data obtained from modulus tests at NPL, and analysed using the web-based software. The data have been generated from dedicated tensile modulus tests on flat rectangular specimens, using strain gauges bonded to both sides of the specimen. The tests were carried out to failure, but a high data-sampling rate was used to ensure sufficient datapoints were captured in the early part of the curve. Three different materials are shown and in all cases there is excellent agreement between the tangent and secant modulus values in the early part of the curve, and excellent modulus fits.

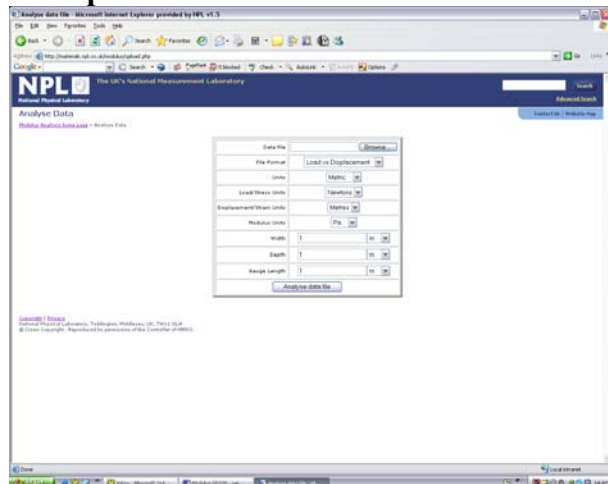
Home page



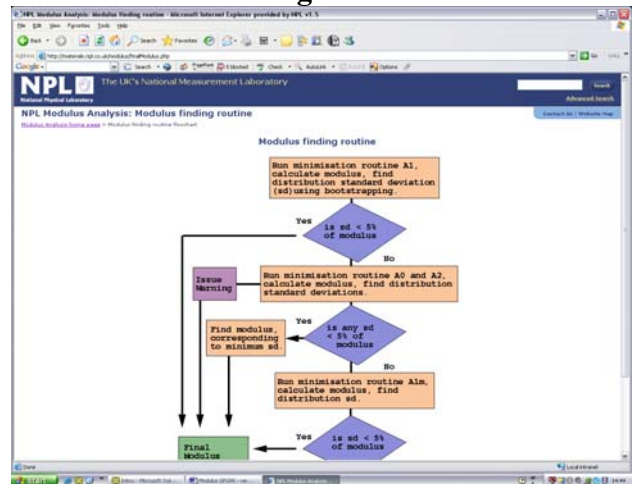
Example Files



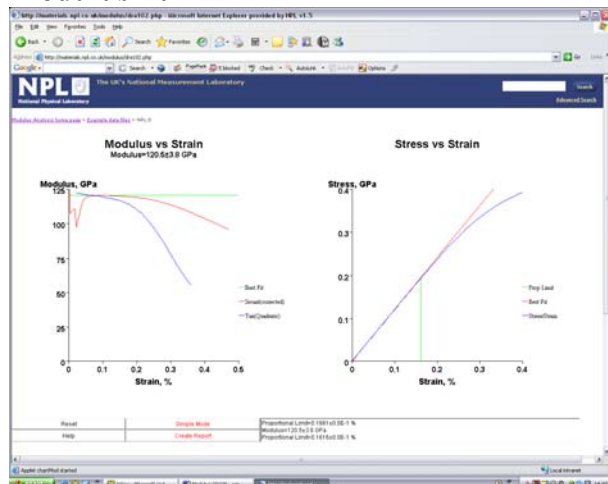
File upload



Details of Modulus algorithm



Modulus fit



“Bootstrapping” page

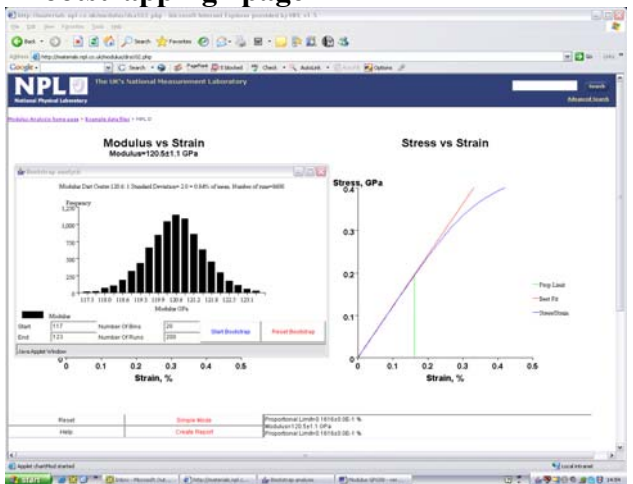


Figure 14: Example screenshots of the NPL web-based modulus analysis software.

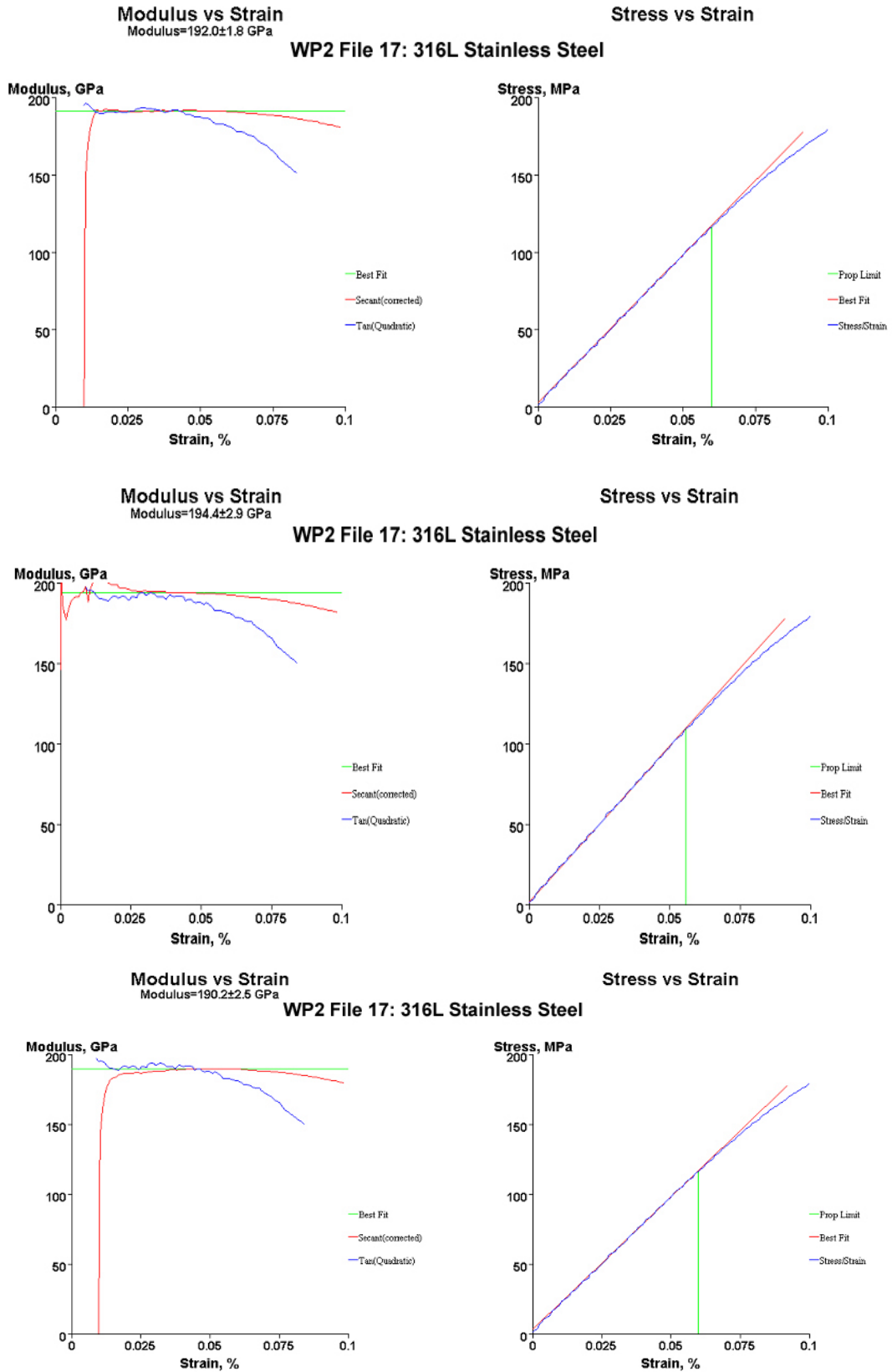


Figure 15: Examples showing the sensitivity of the tangent/secant approach.

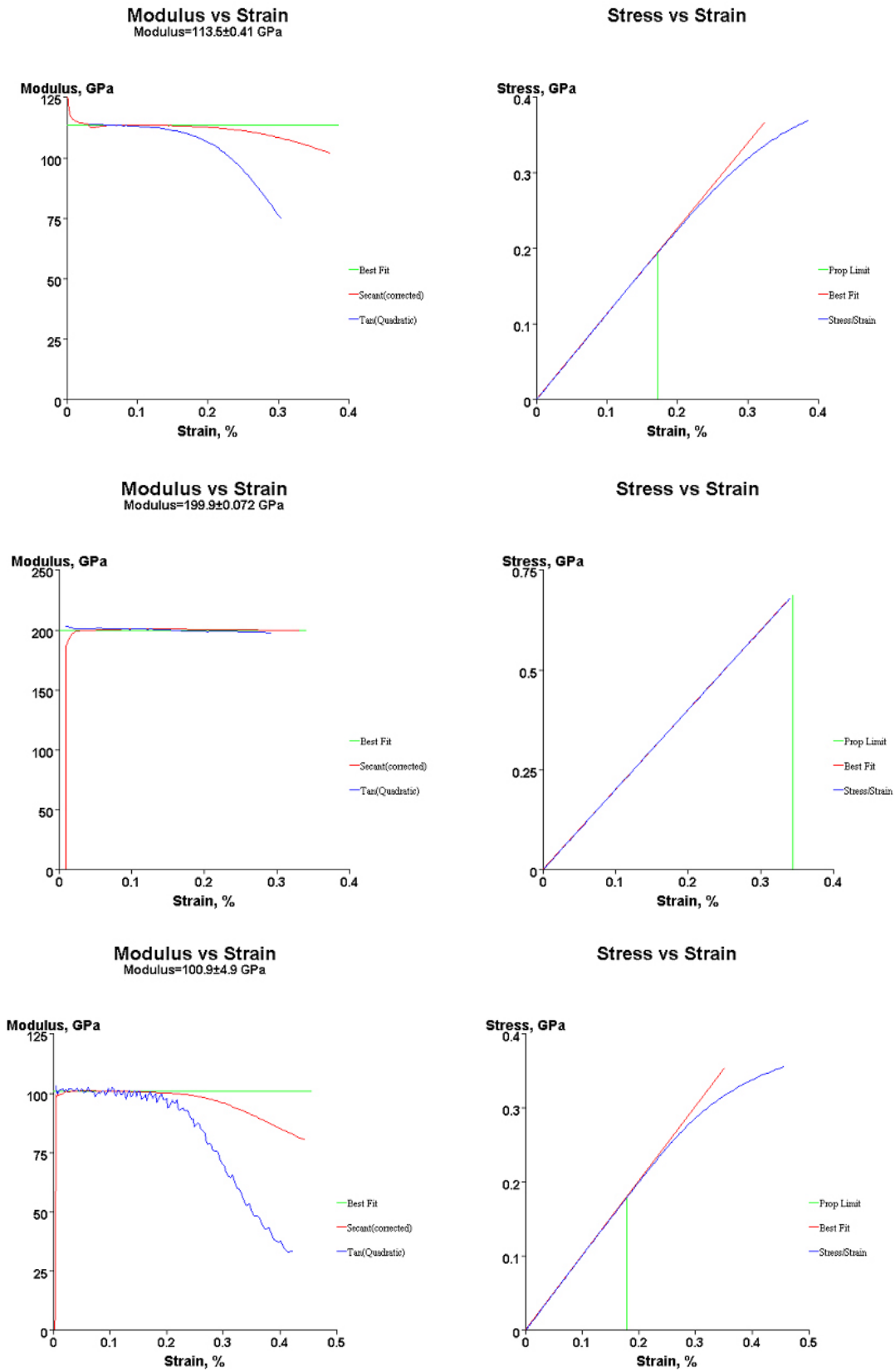


Figure 16: Typical stress-strain data obtained from a dedicated modulus tests at NPL.

4.3.5 Strain range issues

The strain range over which both the modulus test is carried out and the modulus fit to the stress-strain curve is made have an important influence on the quality of the measurement and the modulus value calculated. Some of the results presented previously in Section 4.3.2 and the stress-strain data in 4.3.4 illustrate this point, and the recommendation of this GPG is that a dedicated tensile modulus test be carried out over a restricted strain range.

For many materials the elastic part of the stress-strain curve corresponding to the Young's modulus may extend only to 0.1-0.2% strain. In a dedicated modulus tensile test, it makes little sense therefore to carry out measurements beyond this value. **Indeed there are significant advantages to remaining below the proportional limit because the test can then be repeated if necessary with no change in properties.**

Some users advocate the use of hysteresis testing and measurements of the modulus on the unloading part of the stress-strain curve, but this should not be necessary if the test is set up correctly. For some materials such as fibre-reinforced composites, hysteresis testing must be carried out carefully as damage to the brittle fibre reinforcement will result in a reduction of the load carrying capacity and hence to the modulus values measured. This can be identified by a reduction in modulus with loading to higher plastic strains.

The range over which the modulus is fitted can also have an impact on the calculated value. Generally, modulus values tend to fall with increasing strain range, particularly if analysis methods based on fitting a straight line between discrete points on the curve are used, as one of these might occur in a region beyond the proportional limit, where the material has started to yield. An advantage of the NPL-type approach that calculates the moduli at each individual data point is that the proportional limit can be more readily identified, and the tangent and secant values are seen to fall beyond this point (see Figure 16).

Table 5 shows results of detailed analysis of some of the datafiles generated in the TENSTAND project [4]. Each individual datafile was analysed using the NPL software over the range 0-0.1%, 0-0.15% and 0-0.2% strain to determine whether the range selected had an influence on the modulus calculation. In total over 150 analyses were carried out. Five different analysis approaches were used with the NPL software: **Method A** minimises the difference between the secant modulus and the calculated value for Young's modulus; **Method B** minimises the difference between the tangent and secant moduli; **Method C** minimises the difference between the tangent modulus and the calculated value for Young's modulus and **Method D** selects the value obtained from A, B or C based on the minimum standard deviation. Values were also calculated using simple linear regression.

The uncertainties from the exercise based on the range of analysis methods and strain range covered were very low, typically below 0.5%, and illustrate the quality of modulus data that can be obtained from a dedicated tensile modulus test.

Generally the values for modulus calculated using simple linear regression were in good agreement with those using other algorithms (and this probably reflects the fact that the dedicated modulus test has resulted in good quality data), but in some cases (*e.g.* Files 2, 9, 10) the value of modulus calculated using simple linear regression varied considerably depending on the strain range over which it was calculated, even though there was no evidence of yielding and deviation from the elastic behaviour.

Table 5: Modulus analysis tests carried out on a variety of materials at NPL, analysed using different algorithms with the NPL modulus software.

File No.	Material	Strain range	A	B	C	D	Mean	SDev	U%	LinReg	From mean
1	F15	0.10%	113.5	113.5	113.5	113.5	113.5	0.0	0.0	113.6	0.1
		0.15%	113.7	113.7	113.7	113.7	113.7	0.0	0.0	113.4	-0.3
		0.20%	113.6	113.6	113.1	113.6	113.5	0.3	0.4	113.6	0.1
2	F44	0.10%	142.9	143.1	143.3	143.1	143.1	0.2	0.2	142.1	-1.0
		0.15%	142.9	142.7	142.7	142.7	142.8	0.1	0.1	140.9	-1.8
		0.20%	142.9	142.7	142.5	142.7	142.7	0.2	0.2	139.9	-2.8
3	R1	0.10%	100.4	100.4	100.2	100.4	100.4	0.1	0.2	100.0	-0.3
		0.15%	99.9	100.4	99.6	100.0	100.0	0.3	0.7	99.6	-0.4
		0.20%	99.9	99.7	99.3	99.7	99.7	0.3	0.5	99.2	-0.5
4	R6	0.10%	101.5	101.4	101.4	101.4	101.4	0.0	0.1	101.1	-0.3
		0.15%	101.5	101.5	101.1	101.1	101.3	0.2	0.5	100.9	-0.4
		0.20%	101.0	101.5	101.1	101.1	101.2	0.2	0.4	100.5	-0.7
5	T1	0.10%	173.1	173.1	172.6	173.1	173.0	0.3	0.3	173.6	0.6
		0.15%	174.1	173.8	173.3	174.1	173.8	0.4	0.4	173.9	0.1
		0.20%	174.1	173.8	173.3	174.1	173.8	0.4	0.4	173.6	-0.2
6	T5	0.10%	172.8	172.8	172.8	172.8	172.8	0.0	0.0	173.3	0.5
		0.15%	173.2	173.2	173.7	173.2	173.3	0.2	0.3	173.8	0.5
		0.20%	173.2	173.2	173.7	173.2	173.3	0.2	0.3	173.8	0.5
7	N43	0.10%	201.1	201.7	201.8	201.7	201.6	0.3	0.3	201.4	-0.2
		0.15%	201.5	201.6	201.6	201.6	201.6	0.0	0.0	201.3	-0.3
		0.20%	201.2	201.2	201.2	201.2	201.2	0.0	0.0	201.0	-0.2
8	NPL D	0.10%	121.4	121.4	121.4	122.2	121.6	0.4	0.7	121.6	0.0
		0.15%	121.6	121.6	121.6	121.6	121.6	0.0	0.0	120.8	-0.8
		0.20%	121.0	121.0	120.3	121.0	120.8	0.3	0.6	119.7	-1.1
9	NPL E	0.10%	105.0	105.0	105.1	105.1	105.1	0.1	0.1	104.9	-0.2
		0.15%	105.0	105.1	104.8	104.9	105.0	0.1	0.2	103.8	-1.1
		0.20%	104.9	105.0	104.9	104.9	104.9	0.0	0.1	102.2	-2.7
10	NPL F	0.10%	114.6	114.6	114.6	114.6	114.6	0.0	0.0	115.3	0.7
		0.15%	115.8	115.8	115.8	115.8	115.8	0.0	0.0	112.6	-3.2
		0.20%	114.5	114.5	114.5	114.5	114.5	0.0	0.0	106.1	-8.4

4.3.6 Use of reference materials

The use of reference materials as a quality check is recommended, but there is a problem because no recognised material is yet generally available for the validation of modulus test set-ups. In Section 4.2 data was presented from the certification exercise on the BCR Nimonic 75 tensile reference material [12], and this is currently the only certified tensile reference material available. But it is not certified as a modulus reference material because the tests carried out were full tensile tests to failure and the modulus results returned from these showed considerable scatter. On further inspection the batch of material appeared to have a bi-modal modulus distribution, with modulus values depending on the location from which the test-pieces were taken.

Another approach is to use a stable, well-defined material as an in-house quality check, and this is the approach taken at NPL, using a unidirectional SiC fibre reinforced Ti composite test-piece, which has been loaded over 80 times in a 10-year period. Some of the early results

were presented in Section 4.3.2, but Figure 17 shows the full set. The data includes results from measurements using gauges from 4 different suppliers. The results show excellent repeatability with a mean value from the 80 tests of 200.3 GPa (excluding the sg3 data as mentioned previously), and permit a check that the test set-up and data analysis procedures are functioning correctly.

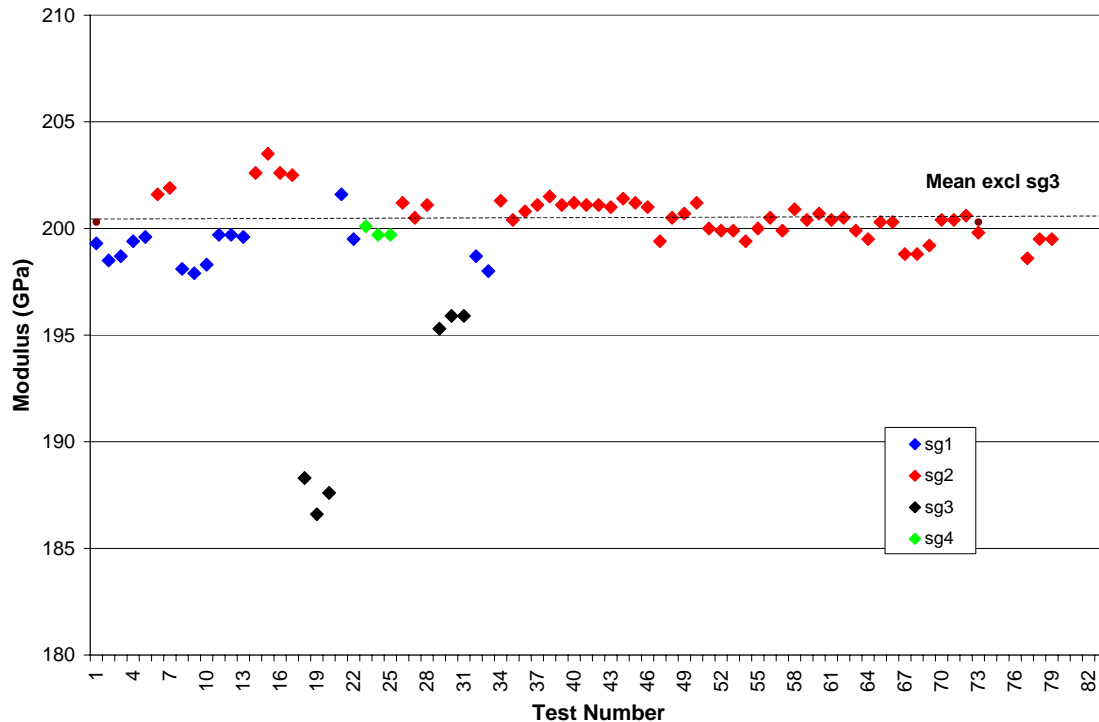


Figure 17: Modulus data from NPL “reference modulus specimen”.

It is recommended that a check be made:

- Before a series or batch of tests, or
- Whenever the test machine configuration (grips, load cell, alignment fixture etc) is changed, or
- If a different batch of strain gauges are used, or
- At regular periods, in line with the customer’s quality procedures

4.3.7 High temperature measurements

The procedures for obtaining high temperature modulus measurements from the tensile test are not covered in this edition of the GPG. A similar set of requirements as those for the dedicated room temperature modulus test is necessary, with the added complication of high quality strain measurement at temperature. In the author’s opinion it is probably more practical and cost effective at this stage to use the dynamic techniques described in Section 5.

4.4 Software validation using ASCII datafiles

Physical reference materials can be used to check and validate the whole test set-up, including the software algorithms or procedures used to calculate modulus from the stress-strain curve, but this approach will always include some uncertainty due to the practical aspects of doing the test. The software can be validated independently by analysing datafiles with known properties, which can be generated either from the tensile test data itself, or synthetically using computer models.

A set of datafiles for validating tensile testing software and data analysis routines was developed as part of the TENSTAND project [4] and was used for an intercomparison exercise – the exercise included detailed analysis of real physical data, and synthetic data generated by NPL. All the tensile testing was carried out according to EN10002-1, as the exercise was designed to examine the ability of the software to analyse the whole stress-strain curve and to calculate a range of tensile parameters.

The files covered a range of different materials and stress-strain behaviour, and included the Nimonic 75 BCR reference material, aluminium alloys, structural steels, stainless steels, tin coated packaging steels and a series of synthetic data files with different levels of noise. The files are presented in a single agreed ASCII format.

Analysis of the modulus data returned from the exercise showed larger variations than expected, especially considering that all the participants were analysing the same data and the scatter was due to the software and analysis alone. The data have been shown previously in Figure 6, with ten datasets showing uncertainties in modulus in excess of 10%. Closer examination of the stress-strain curves indicated that although few test showed significant non-linearity, the quality of the data itself (noise, number of datapoints, offsets) was probably the likely cause of the large scatter, and this was probably a consequence of the test method and type and of the class of extensometry used to generate the stress-strain curve. In many cases long travel extensometers were used and these remained on the specimen up to the point of failure. **It is unrealistic for such devices to be suitable for measuring modulus in the first 0.2% of the stress-strain curve, when they are designed for elongations of 40% or more.**

The identification of the agreed values for the ASCII dataset was a long and difficult process. For each datafile agreed values and outliers were chosen by careful examination of the data and inspection of the individual stress-strain curves. For some parameters - such as the maximum force and tensile strength - an absolute value (in most cases) could be agreed, but for others such as the modulus a range of values were agreed. These modulus values were selected by analyzing each curve using the NPL modulus software and selecting a range of representative values that gave a reasonable visual fit to the early part of the curve. Typically the variation in modulus expressed by the range is 4-5%, and based on these modulus values, a corresponding range of values for $R_{p0.1}$ and $R_{p0.2}$ was calculated. A summary of the agreed values is given in Table 6.

Table 6: Agreed values for the TENSTAND ASCII Reference datafiles [4]

No.	Material	$R_{p0.2}$ (MPa)	R_m (MPa)	F_m (N)	A (%)	E (GPa)
1	Nimonic 75, CRM 661	309.6 - 310.1	764.4	59973	41.2	200.8 - 216.5
6	Nimonic 75, CRM 661	308.0 - 308.6	761.1	59780	41.4	182.7 - 195.8
10	13%Mn Steel	337.1 - 337.2	937.0	72667	51.4	180.6 - 184.0
13	S355 Structural Steel		567.2	44503	29.4	228.8 - 221.0
17	316L Stainless Steel	261.0 - 261.2	575.7	45278	51.1	189.8 - 202.3
22	Tin Coated Steel	562.5 - 564.6	596.7	2369	0.9	198.7 - 207.3
30	Sheet steel - DX56	162.7 - 162.9	301.5	4272	39.9 - 40.1	195.0 - 207.4
38	Al AA5182 Sheet	396.4 - 397.1	434.3	2007	4.7	68.1 - 69.3
42	Al AA1050 Sheet	30.01 - 30.05	83.6	1210	44.5	68.7 - 72.0
46	Al AA5182 Sheet	134.5 - 134.8	284.6	8420	22.6 - 22.7	68.7 - 70.0
50	Sheet steel - DX56	163.9 - 164.0	303.9	2665	43.4 - 43.9	162.2 - 165.3
53	Sheet steel - ZStE		318.9	3782	40.3 - 40.8	198.7 - 208.9
57	Synthetic data - zero noise	434.3	738.5	58000	50.0	207.5 - 208.0
61	Synthetic data - 0.5% noise	438.1 - 441.6	748.1	58754	50.0	201.6 - 211.5
63	Synthetic data - 1% noise	446.5 - 448.2	759.3	59632	50.0	203.0 - 211.6

The uncertainty in modulus was the highest of all the calculated parameters in the exercise, and the mean value for the uncertainty of all the modulus values before and after the outliers were removed were respectively 8.2% and 3.1%.

Figure 18 shows representative stress-strain curves for selected datafiles. Clearly the quality of the data varies considerably. Some of the stress-strain curves (such as File 22, 30, 42 and 63) show some of the problems encountered. Files 22 and 63 are somewhat noisy and this is reflected in the tangent/secant plots, and participants probably had difficulty in identifying the best fit to the data in such cases. Files 30 and 42 caused difficulties because the stress-strain curves do not appear to have significant linear sections over which the modulus could be calculated. Many of the curves were generated with offsets and preloading. In itself this should not be detrimental to the quality of the data, but files with this behaviour did tend to have problems and increased scatter in the calculated modulus values.

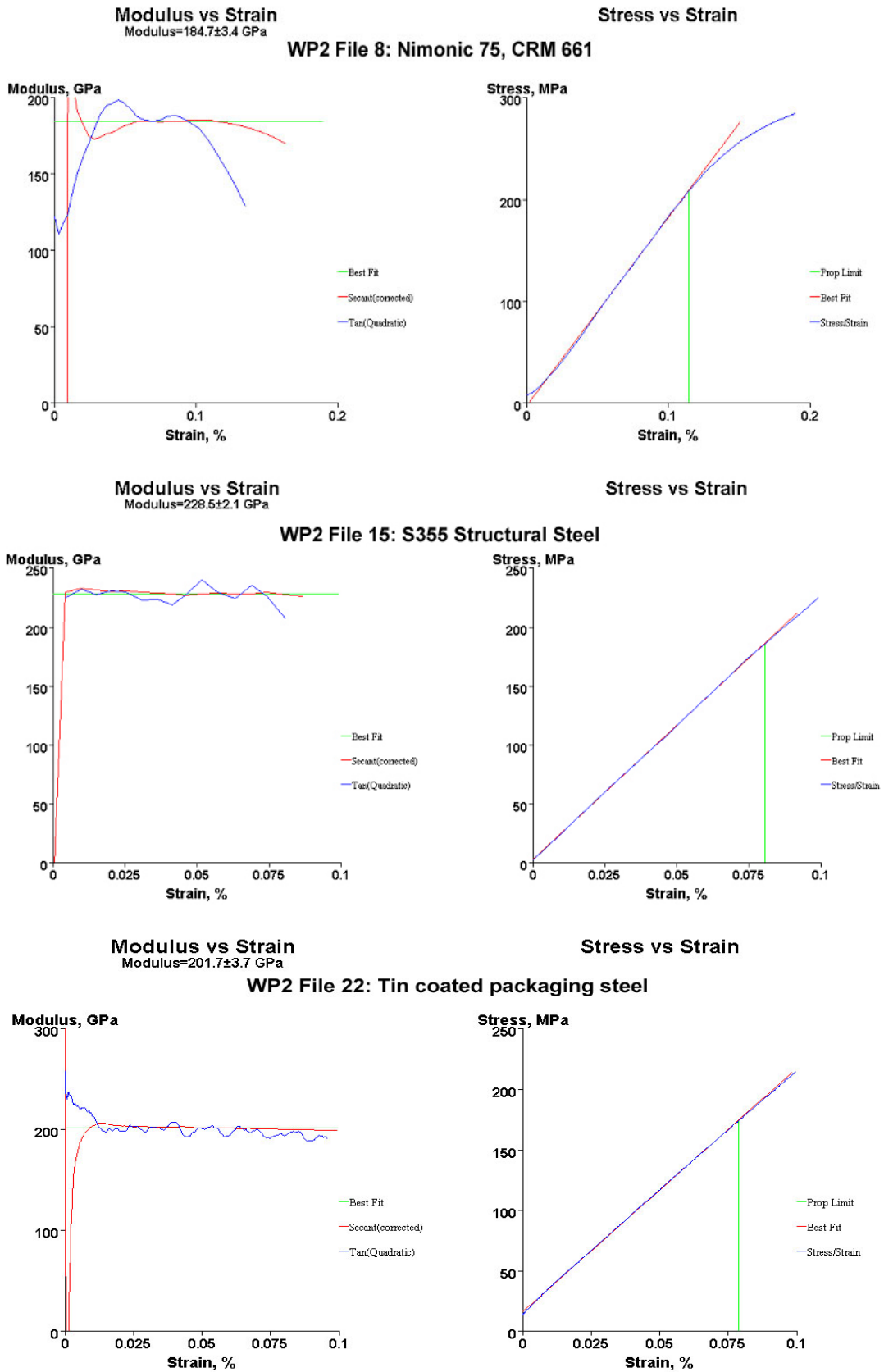


Figure 18: Representative WP2 ASCII datafiles.

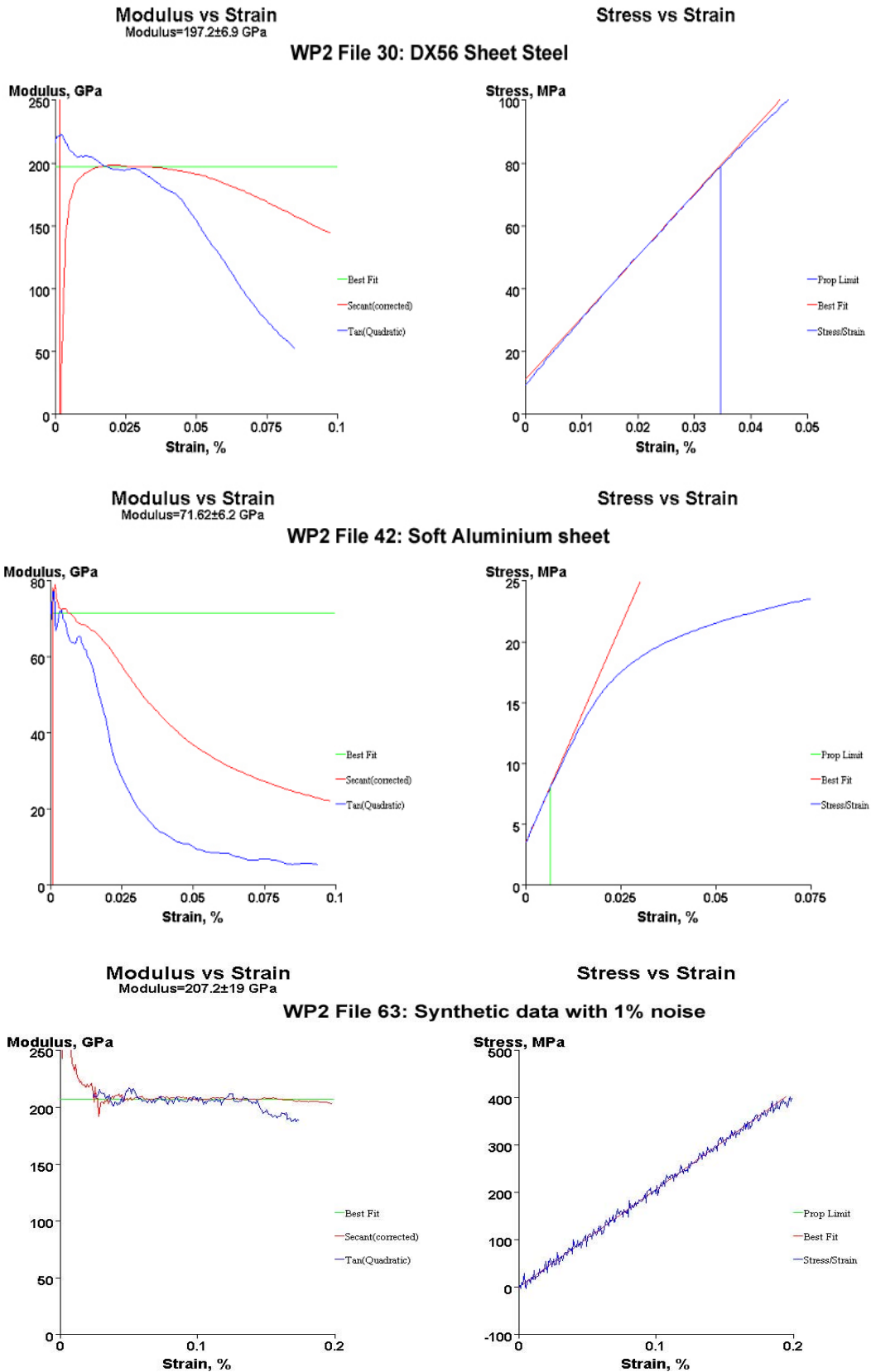


Figure 18 (cont.): Representative WP2 ASCII datafiles.

It is important to stress that the NPL algorithms are not the only approach for calculating modulus. The major test machine manufacturers such as Instron and Zwick offer comprehensive analysis software that offer a wide range of options, and many organisations have developed their own analysis procedures. Results from the study do show that the modulus value measured depends on a number of factors including aspects of the test set-up, the accuracy of strain measurement, the strain range examined, the number of datapoints and method of evaluation. Care and consideration should be made by the test machine operator to ensure the best quality data is achieved.

It is recommended that users validate their own software on a routine basis by carrying out analyses of the TENSTAND ASCII datafiles, which are available from NPL. If possible several files should be examined. If the values calculated differ significantly from the agreed values, the use of the particular software package or algorithm should be stopped until the discrepancies can be resolved. Some variation in the calculated values for modulus is to be expected, and should be included as a factor in the uncertainty budget developed for the modulus test, and quoted with the value for modulus. Further details, together with an example uncertainty budget for a tensile modulus test are given in the following section.

4.5 Uncertainty budgets

It is good practice in any measurement to quote the uncertainties associated with the measurement itself, but this is not always carried out and rarely reported. For the tensile modulus test it is reasonably straightforward to make some estimate of the uncertainties associated with the test method, and this is a valuable approach which should be encouraged as it can help to identify which experimental parameters or aspects of the test are likely to give rise to the greatest uncertainty. If used properly it can help to refine the experimental set up by identifying which aspects of the test are contributing most to the uncertainty in the measurement.

A number of documents are available to help develop an understanding of uncertainty, providing guidance and advice. Some guidelines are included as an annex in the proposed revision to EN10002-1, but more general advice on uncertainty calculations can be found in Refs 23-26. The key document is the ISO TAG4 guide [23], but this can be a little over-complicated, so the reader is recommended to look at some of the other publications [24-26]. A Code of Practice (CoP) for determining the uncertainties associated with the tensile testing technique was produced as part of a recent EU UNCERT project [26]. In this project a series of documents were produced, in a common format, for determining the uncertainties in a variety of mechanical tests on metallic materials. CoP 7, which deals with the tensile testing technique, was one of 17 produced by the UNCERT consortium. The document contains a standard procedure for estimating uncertainties, together with some background to the technique and worked examples.

In all the documents, the basic procedure for estimating uncertainty is the same, and can be broken down into the following steps:

- 1: Identifying the parameters for which the uncertainty is to be estimated
- 2: Identifying all sources of uncertainty in the test
- 3: Classifying the type of uncertainties

- 4: Estimating the sensitivity coefficient and standard uncertainty for each major source
- 5: Computing the combined uncertainty
- 6: Computing the expanded uncertainty
- 7: Reporting of results

The key issue is to identify which are the major contributing factors, and estimate their uncertainties. In the tensile test a number of factors can contribute to the uncertainty in the quoted modulus value, including the class of extensometer or strain gauge resolution, uncertainty in the dimensional measurements, the classification and resolution of the load cell, misalignment of the specimen or strain measurement device, temperature effects, operator dependent factors, data fitting routines and analysis methods etc. All can have an impact on the overall uncertainty in the modulus measurement.

These individual uncertainties are usually summed using the root mean square method, and then multiplied by a coverage factor to give an expanded uncertainty for the measurement to a known confidence level (typically $\pm 95\%$ or 2 standard deviations).

Table 7 shows an example uncertainty budget calculation for the measurement of modulus from a dedicated tensile modulus test.

Table 7: Example uncertainty budget for the tensile modulus test

Source of Uncertainty	Uncertainty	Measured Value	Uncertainty u (%)	Probability distribution	Divisor	u (E_{spec}) (%)
Force, F	From load cell calibration certificate		0.22	Normal	1	0.22
Area, A	0.02 mm ²	9 mm ²	0.22	Rectangular	$\sqrt{3}$	0.13
Accuracy of strain measurement, ϵ	10 $\mu\epsilon$	1000 $\mu\epsilon$	1.00	Rectangular	$\sqrt{3}$	0.58
Modulus analysis method	0.25 GPa	210.0 GPa	0.12	Rectangular	$\sqrt{3}$	0.07
Repeatability of E measurement	0.6 GPa	210.0 GPa	0.29	Normal	1	0.29
Combined Standard Uncertainty						0.70
Expanded Uncertainty ($k = 2.00, 95\%$)						1.40

In the above example, the uncertainty in the force is a function of the load cell accuracy and classification and can usually be taken from the calibration certificate for the test machine. There will be a contribution associated with measuring the test-piece dimensions, and this might be affected by both the resolution and accuracy of the micrometer used for the measurements, and the variation of dimensions of the test-piece itself. The accuracy and resolution of the strain measurement system is also important. The data in the Table above is based on the typical uncertainty in the strain gauge readings at 0.1% strain, from the NPL dedicated modulus test set-up; the figure has been derived from consideration of the accuracy and resolution of the gauge readings and from experimental data and, according to this calculation, is the largest contributing factor to the uncertainty in the measurement. A factor

has been included to cover the uncertainty associated with the software algorithms and the uncertainty in the ability to fit a line to the linear part of the stress-strain curve, together with variability associated with repeat tests – and this might be either on the same sample or on different samples from a batch of material, or both. The list of factors contributing to the overall uncertainty is not exhaustive and other parameters could be included. The reader is encouraged to examine their own test set-up and practice and develop their own uncertainty budget, based on the example above and the guidelines given in the various documents.

Finally, based on the results from the test and the uncertainty budget, the modulus should be reported as:

$$E = 210.0 \pm 2.9 \text{ GPa} \quad \text{.. to a confidence level of 95\%}.$$

With the caveat that ... **the reported expanded uncertainty is based on a standard uncertainty multiplied by a coverage factor, which provides a level of confidence of approximately 95%.**

A similar uncertainty budget for the dynamic modulus measurement is presented in Section 5.3.9.

4.6 Summary and recommendations on tensile testing

From consideration of the modulus data results presented in this GPG and other studies, it is clear that the current tensile test procedure outlined in EN10002-1 is generally unsuitable for obtaining accurate and reliable modulus data.

Results have shown that it is possible to obtain good quality modulus data from the tensile test, but this generally requires a separate and dedicated test set-up using high quality averaging strain measurement, focusing only on the early part of the stress-strain curve. It is important to recognise that these are specialised tests, and it might be neither feasible nor realistic to carry them out in a cost effective way in a high throughput computer controlled test machine.

The accuracy in modulus determination is strongly affected by the quality of the data and test set-up. Ideally the data should be free from excessive noise and contain sufficient data points in the elastic range for detailed analysis. This is an important point, because if a test was designed to measure the whole of the stress-strain curve, there may be insufficient datapoints in the early part for accurate calculation of modulus. To obtain better quality measurements from the tensile test, there are a number of practical issues and specific recommendations for the user to consider, including....

- The use of a dedicated tensile modulus test, with a more closely defined test definition and scope, particularly relating to the strain range examined, test speed, alignment, data analysis procedures and test conditions.
- The mandatory use of averaging strain measurement methods, with extensometry (Class 0.5 or better) or strain gauges calibrated specifically over the limited strain range relevant to the modulus measurement

- Appropriate choice of test conditions and sampling rates to give sufficient data points for analysis. It is recommended that the stress-strain data is captured using a computer based acquisition system, and that at least 100 data points are sampled for each strain increment of 0.1%.
- The use of specimen geometries with longer gauge lengths and improved alignment, to reduce bending.
- Careful consideration of the data analysis techniques used. Some knowledge of the function of the particular algorithm used to calculate the modulus from the stress-strain data is desirable, and should be recorded in the test report. Ideally the software should be able to analyse the data automatically with minimal operator intervention.
- Calibration and validation of software algorithms using the TENSTAND ASCII datafiles.
- The use of reference specimens, either the BCR Nimonic 75 tensile reference material (CRM661) or an in-house reference test-piece.
- Development of uncertainty budgets for the modulus measurement, which will help to identify particular areas of the test set-up that contribute most to the scatter and variability.

Although the preference is to measure modulus from the stress-strain curve, the use of dynamic techniques should be considered if sensible values of modulus cannot be measured because of plastic deformation of the material or problems with the practical set up, or to validate and support the use of using handbook values. It is recommended that wherever possible measurements be made rather than relying on default handbook values because these might not be available for the specific material grade being tested. If realistic values of modulus cannot be achieved through the tensile tests it is an indication that the test set-up is inappropriate. In such cases, users are encouraged to examine aspects of the tests such as machine and test-piece alignment, gripping, strain measurement and the use of different test conditions and data analysis procedures that might help them achieve better quality results.

4.7 Flexural modulus testing

4.7.1 Introduction

As an alternative to tensile testing, flexural testing in three or four-point bending is possible. In this case, much smaller forces are applied, and larger displacements are achieved, but care has to be taken concerning a number of factors in order to obtain consistent and correct results. Calculations are usually based on thin-beam flexure equations, such as those developed by Timoshenko [27]. There are basically three methods that can be applied (described in standard EN 843-2 [28] for advanced technical ceramics), depending on the available facilities:

- Measuring the displacement of the testing machine crosshead;
- Measuring the net out-of-plane displacement between two well-defined points on the surface of the test-piece;
- Applying strain gauges to both faces of the test-piece at the span centre (four-point bend only).

The key points to note when using one or other of these methods are:

- When using mechanical measurement, test-pieces should be thin and parallel-faced (if flat) or of small consistent diameter (if rods);
- The test jig and fixtures should have freely rolling rollers with some capability for minimisation of test-piece twist, and some capability of self-aligning and equal distribution of the force between the two loading rollers in four-point bending;
- If using the machine displacement method, it should be noted that machine movement is not necessarily reproducible, and techniques have to be adopted to ensure that consistent behaviour is obtained, and that any region of initial load take-up is avoided. This is dealt with in more detail below.

The method is ideal for brittle materials, which are difficult to subject to significant tensile stress, but there is a risk of permanent deformation in materials which show plasticity or yield resulting from an inappropriate stress distribution in the test-piece or indentation by loading rollers.

4.7.2 Machine displacement method

4.7.2.1 System design

In this method, the machine displacement is imposed on the loading roller(s) relative to the support rollers, causing the test-piece to bend (Figure 19, top left). The calibrated displacement as a function of time at a given displacement rate of the cross-head or ram in a conventional universal mechanical testing machine is used as the measure of deflection.

The deflection of the test-piece is actually equal to the machine displacement less the deflection of the machine itself. This latter deflection can be a combination of compliant elements in the load train, the load cell, flattening of loading rollers or their indentation into the test-piece, or the mechanics of the machine itself. ‘Bedding-in’ usually occurs at low applied force levels as contacts are pushed together, so the force/displacement traces are often somewhat non-linear, and may not be repeatable. It is therefore advantageous to make the test span as long as possible and the test-piece as thin as possible, subject to there being representative microstructure through the thickness. However, it should be noted that making the test-piece too thin results in non-linear behaviour if the deflection exceeds about half the thickness of the test-piece, owing to the introduction of contact point tangency errors (see NPL Good Practice Guide No. 7 [29]), and also increases the effects of surface non-planarity and of the error in measurement of test-piece thickness. The thickness should ideally be at

least 1 mm. The test-piece width should be no more than 10 mm to minimise the effects of anticlastic curvature (*i.e.* curvature developed from Poisson effects in the transverse plane).

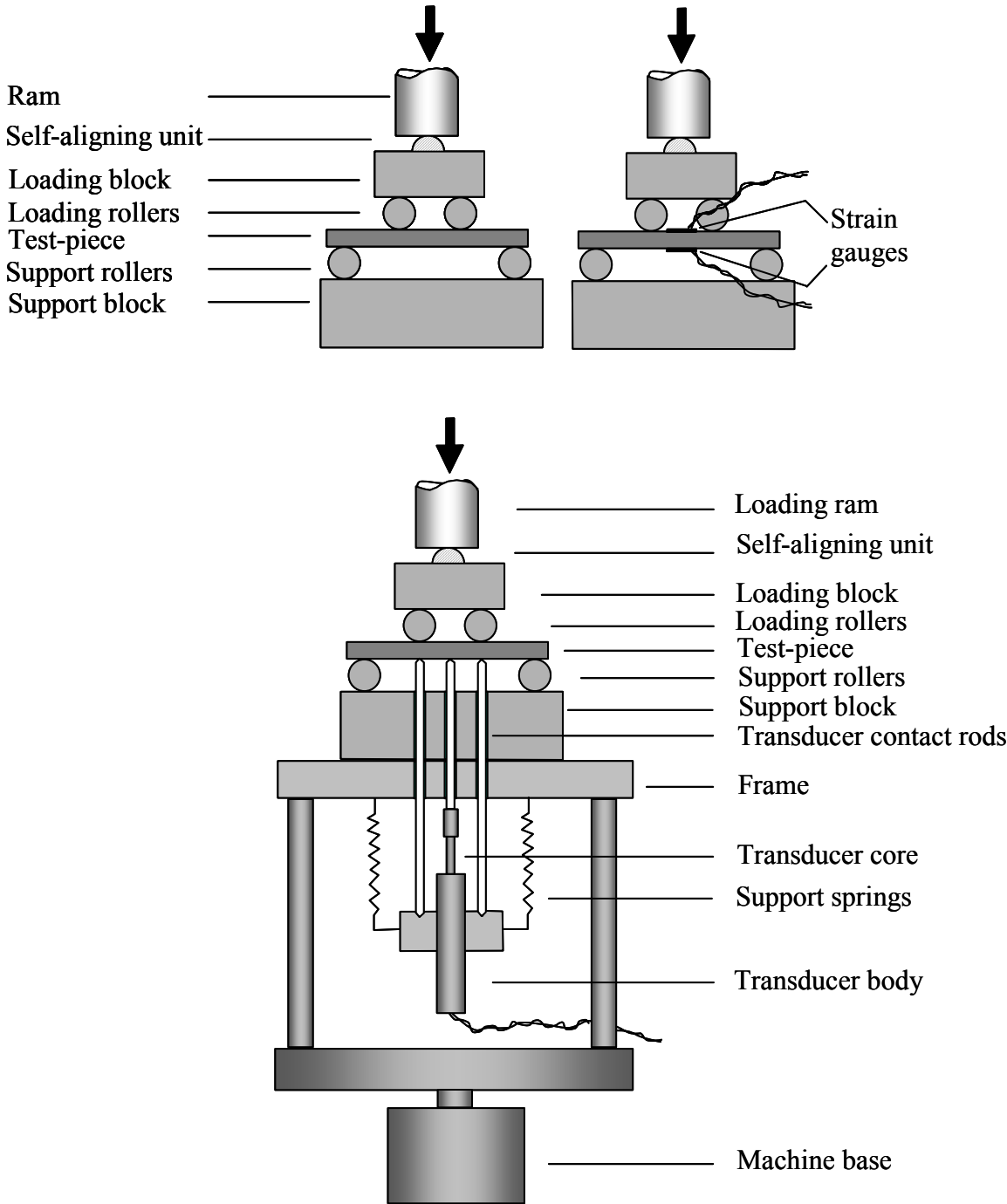


Figure 19: Schematic diagrams of (top left) four-point flexure using machine displacement measurement, (top right) strain gauges applied to both sides of the test-piece, and (lower) direct measurement of deflection between fixed points on the test-piece surface using a single linear displacement transducer.

The flexure facility should comprise a pair of smooth, hard support rollers that rest with their axes parallel, a defined distance apart on a flat surface. The roller diameter is typically 3 - 5 mm and made of hardened steel or hardmetal to minimise the risk of damage or deformation. The single (for three-point bending) or pair (for four-point bending) of loading rollers are similarly located symmetrically and should be free to rotate and articulate to allow a degree of self-alignment on the test-piece. The use of carefully machined test-pieces minimises the requirements for full articulation of all rollers, but there still needs to be some articulation of the loading unit to take up out-of-alignment in the machine itself.

4.7.2.2 Procedure

Before commencing a test it is helpful to minimise the risks of fracturing or permanently bending the test-piece. If the flexural strength or yield stress is known, the well-known flexural stress equations can be used to compute a safe maximum force that can be applied to the test-piece that will avoid problems. Typically the maximum stress applied should be about half of the mean strength or yield stress.

Having centralised a test-piece within the test facility, it is then advisable to apply several loading and unloading cycles, recording the force and apparent machine displacement. The first cycle can generally be ignored to avoid the 'bedding-in' effects.

In order to determine the machine displacement over the same loading cycle, the simplest method is to replace the thin test-piece with a thick steel bar and to repeat the load cycling. In doing it this way, account is taken of loading roller flattening and all other contributions to load train compliance.

The analysis of the results is then straightforward. Selecting force levels of about 10% and 90% of the maximum applied (thus avoiding the initial transient and any effects due to machine reversal) the apparent test-piece deflection is determined for each loading and unloading after the first. The same procedure is used for the thick steel bar results. Young's modulus E can then be calculated as follows:

For the displacement of loading points in three-point bending:

$$E = \frac{(F_2 - F_1)l^3}{4bh^3(\delta_c - \delta_s)} \quad (1)$$

For the displacement of loading points in four-point bending:

$$E = \frac{2(F_1 - F_2)d_1^2(d_1 + 3d_2)}{bh^3(\delta_c - \delta_s)} \quad (2)$$

where:

- E = Young's modulus in N m^{-2} or Pa;
- F_1 = Lower load level selected from recordings in N;
- F_2 = Upper load level selected from recordings in N;
- l = Test jig outer span in three-point or four-point bending in m;
- d_1 = Test jig inner roller to outer roller spacing in four-point bending in m;

- d_2 = One half of the test jig inner span in four-point bending in m;
 b = Test-piece width in m;
 h = Test-piece thickness in m;
 δ_c, δ_s = Displacement recorded for the test-piece and the steel bar respectively in the jig over load interval F_1 to F_2 , in m;

For the case of quarter-point bending, $d_1 = d_2$, and Equation 2 reduces to:

$$E = \frac{(F_2 - F_1)l^3}{8bh^3(\delta_c - \delta_s)} \quad (3)$$

The average Young's modulus figures can then be calculated for the loading and unloading curves. If these values differ by more than 2 %, the tests should be repeated. If they differ by less than 2 %, the overall average can then be determined.

4.7.2.3 Accuracy

The accuracy of this method depends primarily on the fixtures employed and the dimensions of the test-piece. For a long thin test-piece an accuracy of $\pm 2\%$ is typically achievable, but this becomes worse for smaller displacements. Ideally, the displacements recorded using the steel bar should be small compared with those of the test-piece so the corrections are small.

4.7.3 Linear displacement transducer methods

4.7.3.1 System design

For this method a special facility has to be constructed which is capable of supporting the displacement transducers in the correct position beneath the test-piece in order that the locations of the contacts for the sensing probes are maintained, and that the force applied by these probes is small compared with the forces being applied to the test-piece by the test machine. A typical construction is shown in Figure 19 (lower). The transducer is suspended on springs within a cage below the flexural loading jig such that it can record the displacement, say, of the centre of the test-piece relative to the loading roller positions, i.e. in the region of a test-piece in four-point bending which is subject to pure bending, and thus has uniform curvature, making computation easier.

The critical element of this method is the transducer sensitivity and repeatability, and the ability to adjust its location appropriately. The transducer should be of a high-specification, capable of detecting displacements of less than 1 μm with good linearity and the minimum of friction. The core should be of the guided type to ensure repeatable location. A calibrator is also required.

Test-pieces can be thicker and spans can be smaller than in the case of the machine deflection method, but thicker test-pieces deflect less and thus the fractional errors increase. This type of method has been found to work adequately for high-stiffness materials (engineering ceramics) tested over a 40 mm span at a thickness of 3 mm, producing Young's modulus values to within 5% of the values from other methods.

4.7.3.2 Procedure

Load cycling is used as for the machine displacement method, and the Young's modulus is computed as follows:

For three-point bending using defined points at the span centre and under one or both support rollers:

$$E = \frac{(F_2 - F_1)l^3}{4bh^3\delta_t} \quad (4)$$

where:

δ_t = transducer displacement recorded between the test piece centre and the inner loading point in four-point bending over the selected load range, expressed in metres (m).

For four-point bending using defined points at the span centre and under one or both loading rollers, calculate Young's modulus from the equation:

$$E = \frac{3(F_2 - F_1)d_1d_2^2}{bh^3\delta_t} \quad (5)$$

For the case of quarter-point bending, $d_1 = d_2$, and Equation 5 reduces to:

$$E = \frac{3(F_1 - F_2)l^3}{64bh^3\delta_t} \quad (6)$$

4.7.3.3 Accuracy

The accuracy with which the modulus can be determined using this method depends crucially on the quality of the transducer and the engineering of the unit, which guides and locates the deflection probes. The repeatability of the transducer output with defined displacements should be targetted as being within 1% of the displacement measured. In addition, it can be seen from equation (5), for example, that the accurate determination of the sensing positions, using for example a travelling microscope, is essential, as well as accurate measurement of the thickness of the test-piece.

4.7.4 Strain gauge method

4.7.4.1 System design

This method uses a conventional flexural jig for four-point bending and a test-piece of any 'thin-beam' thickness, taking the same precautions as for the displacement method in terms of jig design. The essential difference is that strain gauges are bonded to opposing faces of the

test-piece near the centre between the loading rollers so that axial strain can be determined during loading and unloading.

4.7.4.2 Procedure

Strain gauge selection and their attachment to the test-piece are critical steps that require some skill, and users should refer to section 4.3.1 for advice on their application. For flexural testing the gauges should be small and not interfere with the deflection of the test-piece. They should have an accurate gauge factor, and be attached to appropriate instrumentation with a driving bridge circuit, which has good linear response. Gauges can be applied to one side or both sides of the test-piece, the latter arrangement being preferable particularly if the material behaviour is suspected to be non-linear, or different in tension and compression, as may arise in some composite materials, or materials which develop microstructural damage during loading.

The procedure for measurement is essentially the same as for the previous methods. Several load cycles are made, and the strain determined is correlated with the force applied according to:

$$E = \frac{3(F_2 - F_1)d_1}{bh^2\varepsilon} \quad (7)$$

where ε is the strain determined.

4.7.4.3 Accuracy

Unlike the mechanical methods, the strain gauge method has potential for being more accurate, and better at following non-linearities. The overall accuracy is dominated by the quality of the gauge and the accuracy of the gauge factor, as well as the skill in their application to the test-piece. In principle, results to better than $\pm 2\%$ can be achieved without any special requirements on the geometry of the test-pieces as long as the thin beam condition is maintained.

4.7.5 Tests at elevated temperature

The mechanical methods described above can also be used to elevated temperature by designing the loading systems, jigs and fixtures from appropriate refractory materials. Examples of facilities and high temperature set-ups are shown in the standard EN821-2 [28] for advanced technical ceramics. The key issues with elevated temperature measurements are to ensure that in the machine displacement method the load train remains elastic and has no viscoelastic elements, while in the transducer method temperature stability needs to be achieved to minimise thermal expansion effects which can interfere with differential measurement.

5 Resonance and Impact Excitation Methods

These methods are essentially equivalent. Using usually a beam test-piece with uniform cross-section (round, square or rectangular), the characteristic vibration frequencies are determined either by continuously driving the vibration and sweeping the frequency to detect resonances, or by striking it, allowing it to ‘ring’, and then deconvoluting the recorded sound spectrum. The latter method is often termed the ‘natural frequency’ method. The same set of equations is employed for both methods in order to relate frequency to elastic modulus.

The methods and key issues are described in the following sections, with more detailed information relevant to particular set-ups or measurements – such as more detailed background on the equations and geometric correction factors, advice on selection of bar dimensions appropriate for different test modes, disc specimens and single crystal materials - given in the annexes.

5.1 Principle

5.1.1 Vibration modes of beams

5.1.1.1 Modes

The first step in understanding these methods is to appreciate the modes of vibration of the test-piece. These will depend to some extent on how and where the beam is supported, and the location at which the vibration is driven or excited by striking. For a prismatic beam, there are basically four vibration modes of interest:

- Out-of-plane flexural
- In-plane flexural
- Torsional
- Longitudinal

The *flexural vibration frequencies* are controlled primarily by the Young’s modulus (E) of the test-piece *in the longitudinal direction*, essentially independently of any material anisotropy.

The *torsional mode vibrations* for an *isotropic material*, are controlled primarily by the shear modulus (G) of the test-piece. If the material is anisotropic, things become more complicated, and it is best if the principal axes of the test-piece are parallel to the axes of anisotropy. The vibrations are controlled by a mix of shear stiffness in the principal planes of the test-piece containing the longitudinal direction.

The *longitudinal mode vibrations* are controlled primarily by the Young’s modulus (E) of the test-piece and the Poisson’s ratio *in the longitudinal direction*.

5.1.1.2 Out-of plane flexure

There is a series of nodes (minimum vibration) and antinodes (maximum vibration) along the length of the freely supported beam (a ‘free-free’ beam in mathematical terminology). At the lowest resonant or natural frequency (the fundamental mode), the nodes are 0.223 of the length of the beam from each end, with antinodes at each end and in the centre. For overtones or harmonics, there are more closely spaced nodes and antinodes, and these are shown schematically in Figure 20.

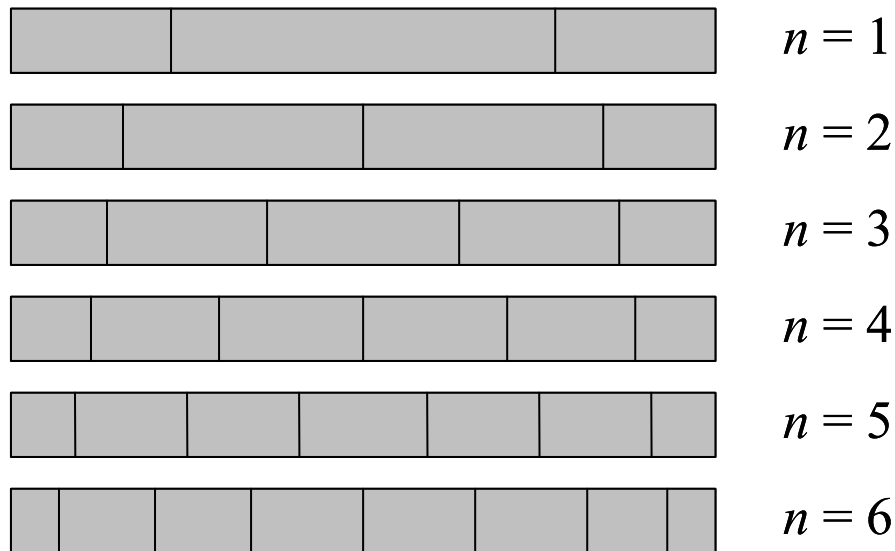


Figure 20: Out-of-plane vibration modes of a ‘free-free’ beam with the nodal lines indicated

From Figure 20 it can be seen that the fundamental mode can be driven or arise during impact if the beam is supported at the nodes so as not to damp out the vibration, and excited elsewhere, especially midway between nodes or at either end. It can also be deduced that driving or striking it in the beam centre will not result in harmonics $n = 2, 4, 6$, etc., because these also have a node in the centre, so only alternating modes will be detected. All modes can be excited if the beam is driven or impacted near the end.

Since in most cases the interest is in identifying the fundamental ($n = 1$) mode, it is general practice to support the test-piece at or close to the fundamental flexural node positions and to drive or impact the test-piece in the centre. If a suspension method (e.g. a loop of thread or wire) is used both to support and to drive the test-piece in resonance, then the usual practice is for the loops to be positioned just outside the nodal positions.

However, it is also of interest, but sometimes a necessity, to be able to identify the series of frequencies to ensure that the fundamental has been detected and correctly identified. This often arises with long thin test-pieces where higher modes are more easily excited than the fundamental. For flexure, these higher mode frequencies are not in a convenient simple relationship to the fundamental mode as a result of beam end inertia effects, and for a long thin beam the series is in the ratio (see Annex 2):

1 : 2.757 : 5.404 : 8.933 : 13.344 : 18.638 :

The ratios become a little smaller as the length to thickness ratio of the beam is reduced. By comparing the measured ratios with these predicted values, a clear identification of the series

can be made and, importantly, the flexural modes can be distinguished from other modes that may be excited.

5.1.1.3 In-plane flexure

Turning the test-piece by 90° about an axis parallel to its length produces another fundamental and series of harmonics that relate to the geometry of the test-piece. The pattern will be the same as in Figure 20.

5.1.1.4 Torsion

Unlike the flexural modes, torsional vibration modes for a long thin isotropic ‘free-free’ beam are in a convenient ratio sequence of:

1 : 2 : 3 : 4 : 5 : 6 : as shown in Figure 21.

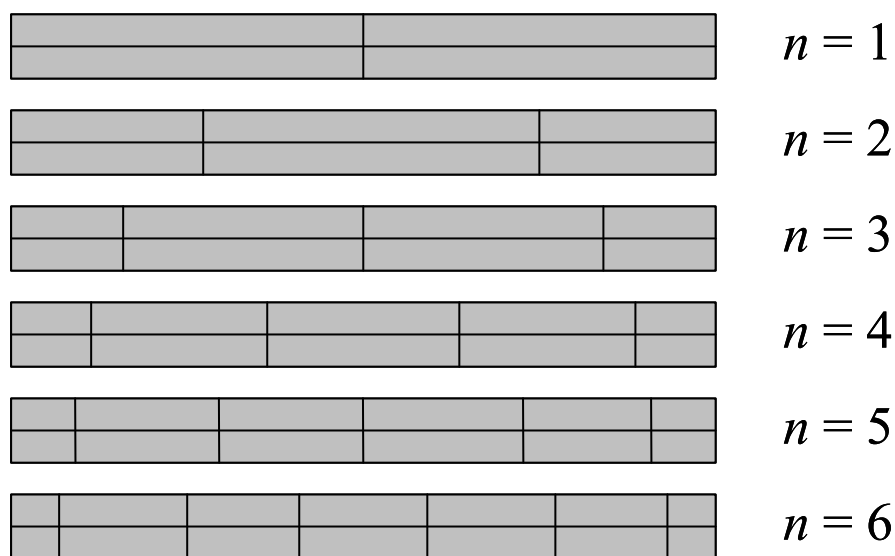


Figure 21: Torsional vibration modes of a ‘free-free’ beam with the nodal lines indicated.

In order to obtain the fundamental mode, the beam therefore has to be supported at its centre, and vibrated at or near its ends by driving or impacting at a location off the centre line, so that most of the energy goes towards twisting the test-piece rather than flexing it. This is more difficult to achieve than the simple support or suspension that can be used for the flexural mode. This aspect will be dealt with later. An alternative approach that has been tried at NPL is to target the $n = 2$ mode. By comparing Figures 20 and 21 it can be seen that the nodal positions for fundamental flexure and second mode torsion have similar geometries. With these support positions, if a vibration driver or a strike is applied near the beam centre, but to one side of the centre line, both $n = 1$ flexure and $n = 2$ torsion will be preferentially excited. If the system employed can detect both modes simultaneously, a second geometry set-up is not needed to obtain the two key parameters of Young’s modulus and shear modulus.

In order to identify whether a torsional mode interferes with a flexural mode excited at the same time, the information given in Annex 2 can be used. The dimensions of the test-piece, typically the width to thickness ratio, can be selected to ensure separation of flexural and torsional frequencies to make identification clear.

To calculate Poisson's ratio (ν) for an isotropic material, both Young's modulus (E) and shear modulus (G) need to be determined. Then the following formula can be used:

$$\nu = \frac{E}{2G} - 1 \quad (8)$$

Accurate values of both E and G are needed for an accurate value of Poisson's ratio. A 1% error in either E or G results in typically a 4% error in ν when $\nu \approx 0.33$!

5.1.1.5 Longitudinal

Exciting longitudinal mode vibrations is commonly undertaken, but care has to be taken to ensure that rather lower frequencies due to simultaneous flexure or torsion are not also identified as the fundamental longitudinal mode. **Typically, the fundamental longitudinal mode frequency is five to ten times greater than that of the fundamental flexural mode, and so should be easy to identify.** Higher longitudinal harmonics are seldom encountered, but for a long thin test-piece they can be assumed to be an integral multiplier of the fundamental mode. This assumption becomes invalid when the ratio of the cross-sectional dimension to wavelength exceeds about 0.2.

5.1.2 Vibration modes of discs

An alternative approach that has been found to work well for isotropic materials is to use disc-shaped test-pieces and to excite the out-of-plane vibration. There are two series of vibration modes, one of which is symmetrical about the disc axis with concentric ring nodes (termed 'flexural' or 'diaphragm mode' here), and the other has a series of radial nodes and antinodes (termed 'torsional', or 'saddle' mode). Figure 22 shows the lowest order modes of each type.

The ratio of the frequencies of the two lowest modes gives Poisson's ratio through a look-up table. Either of the two frequencies with Poisson's ratio gives Young's modulus. Shear modulus can then be computed from Young's modulus and Poisson's ratio. See Annex 3 for further details.

5.2 Calculations

5.2.1 Standards

There are a number of standards which specify the formulae to be used for calculating elastic moduli. The formulae generally have a long and well-developed pedigree, and generally have their simplest form for long thin beams. With shorter aspect ratios there are usually correction functions with increasing complexity. Within the accuracy of determining the dimensions or density of the test-piece, these more complex forms can generally be avoided or truncated without significant error provided that the beam test-pieces are 'thin', i.e. length to thickness ratio typically > 20 . In the following sections, the simpler forms of these equations are given, and the fundamental mode frequency is assumed in all cases. Further details of their validity are given in Annex 1.

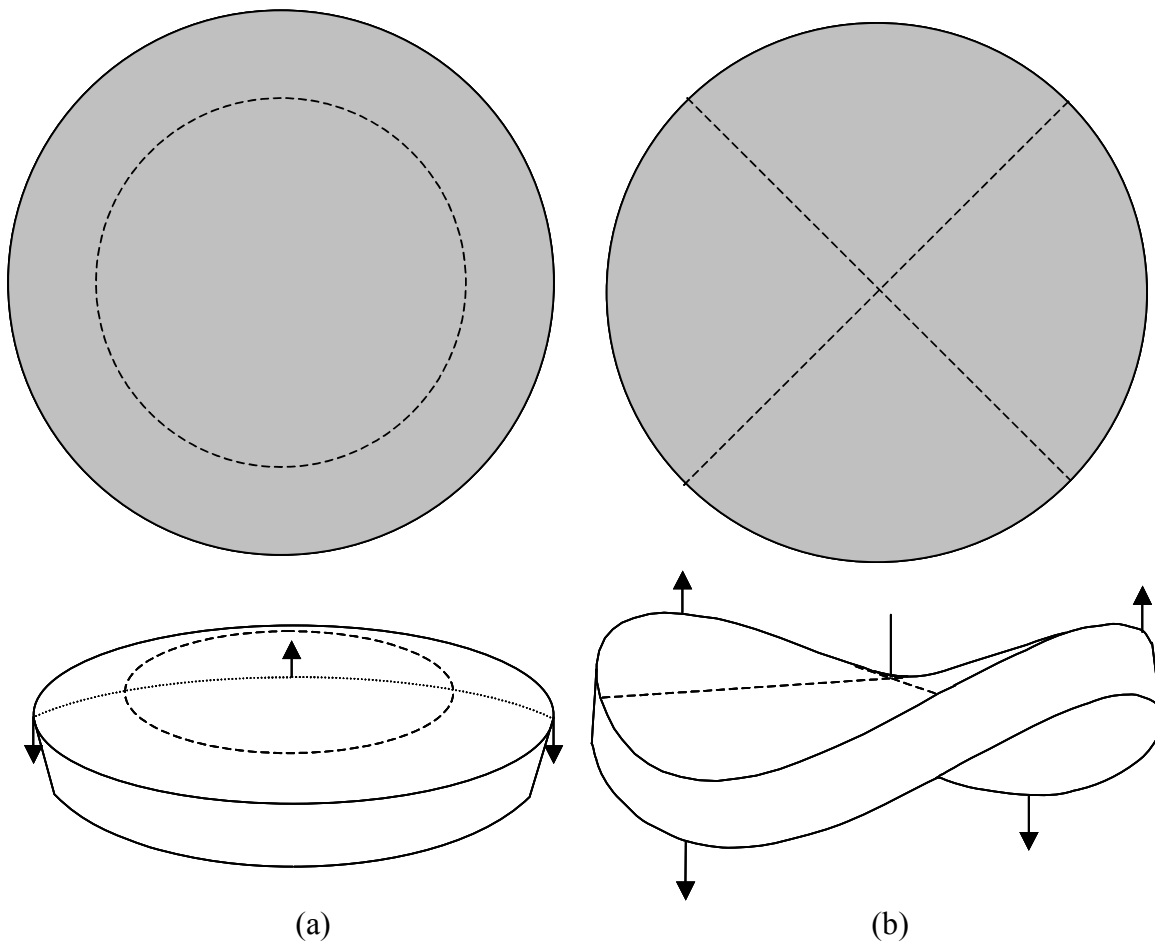


Figure 22: The first two modes of vibration of a disc, (a) flexural or ‘diaphragm’ mode, (b) torsional or ‘saddle’ mode. The dashed lines indicate the nodal lines and the arrows the direction of motion.

5.2.2 Beam flexure

For rectangular section beams (e.g. ISO 17561, CEN EN 843-2, ASTM C623, C848, C1198, C1259):

$$E = 0.9465 \left(\frac{mf_f^2}{b} \right) \left(\frac{L^3}{t^3} \right) T \quad \text{where } T = 1 + 6.858(t/L)^2 \quad (9)$$

For round section beam/rod:

$$E = 1.6067 \left(\frac{L^3}{d^4} \right) mf_f^2 T' \quad \text{where } T' = 1 + 4.939(d/L)^2 \quad (10)$$

5.2.3 Beam torsion

For a rectangular section beam with $b > t$ (e.g. ISO 17561, CEN EN 843-2, ASTM C623, C848, C1198, C1259):

$$G = \frac{4Lmf_t^2}{bt} \left[\frac{B}{1+A} \right] \text{ where } B = \left[\frac{b/t + t/b}{4(t/b) - 2.52(t/b)^2 + 0.21(t/b)^6} \right] \quad (11)$$

The term A can be ignored if the ratio $1 < b/t < 2$ (see Annex).

For a round section beam/rod:

$$G = 16 \left(\frac{L}{\pi d^2} \right) mf_t^2 \quad (12)$$

5.2.4 Beam longitudinal mode

For a rectangular section beam:

$$E = 4L\rho f_l^2 K \quad (13)$$

where $\rho = m/Lbt$ and $1/K \approx 1 - \frac{\pi^2 v^2 (b^2 + t^2)}{12L^2}$

Note that this is outside the scope of ASTM standards, and is not accurate unless $b \sim t$ (see Annex 1). It is usually recommended to use the flexural mode as it is more accurate.

For a round section beam/rod (e.g. ISO 17561, CEN EN 843-2, ASTM C623, C848, C1198, C1259):

$$E = \frac{4Lmf_l^2 K}{\pi r^2} \quad (14)$$

where $1/K = 1 - \frac{\pi^2 v^2 r^2}{2L^2} \approx 1$ for long thin rods.

5.2.5 Discs

This method is included in EN 843-2 Annex and ASTM C1259 Annex. The first step is to determine Poisson's ratio, ν from the ratio of first two frequencies (flexural, $n = 2$; torsional, $n = 1$) via a look-up table. The next step is to use the following equation for both of the frequencies

$$E = \frac{37.6991md^2(1-\nu^2)f_n^2}{K_n^2 t^3} \quad (15)$$

where K_n is determined from separate look-up tables for $n = 1$ and $n = 2$. Details are given in Annex 3.

5.2.6 Other shapes

5.2.6.1 Grinding wheels

Vibration modes for discs with small central holes undergoing out-of-plane vibration have been analysed with particular application to grinding wheels and the use of the impact excitation method to provide quality assurance of the integrity of the wheel material. The behaviour is similar to that of discs without holes.

For the *out-of-plane mode*, Rammersdorfer and Hastik [30] have provided the relationship:

$$E = \frac{48\pi^2 f^2 r_o^4 (1 - \nu^2) \rho}{\lambda^4 t^2} \quad (16)$$

where λ^2 is a function of the radius ratio r_i/r_o , f is the fundamental vibration frequency, ν is Poisson's ratio, and ρ is the density. The value for the parameter λ^2 of 5.2 is conventionally used, and is suitable for small holes only of diameter up to about 0.2 of the disc diameter.

5.2.6.2 Thin rings

Vibration modes of thin rings with vibration in-plane (Prescott [31]) and out-of-plane (Raju [32], Rammerstorfer and Hastik [30]) have been studied and relationships to Young's modulus are available.

For the *in-plane mode*, the relevant equation for a 'thin' ring is given as [31]:

$$E = \frac{\rho r^4 \cdot 4\pi^2 f^2 t (r_o - r_i)}{I} \cdot \frac{(n^2 + 1)}{n^2 (n^2 - 1)^2} \quad (17)$$

where $n = 2, 3, 4, \text{etc.}$, is the vibration mode, and I is the cross-sectional moment of inertia, taken as $t(r_o - r_i)^3/12$. It is unclear how 'thin' a ring should be for this equation to be valid, but the validity is most likely to be best for the lowest vibration mode.

For the *out-of-plane mode*, an extrapolation of the grinding wheel case has to be used. Based on the analysis of Raju a more appropriate value of λ^2 can be computed (see Annex 1) and used in Equation (16):

$$\lambda^2 = 5.908 - 3.4r_i / r_o \quad (18)$$

which appears to be valid at least over the range $0.4 < r_i/r_o < 0.8$.

5.3 Practical issues

5.3.1 Test-piece dimensions and surface finish

It is clearly best if the test-pieces are specially prepared for this measurement, and have dimensions and dimensional tolerances that are appropriate. In particular, there are three main issues to consider:

1. To ensure that the frequencies at which the test-pieces vibrate in the anticipated modes are within the capability of the measurement system. If appropriate, use an estimate of Young's modulus to calculate the frequency that is to be expected.
2. Test-piece dimensions should be scaled to ensure that the appropriate frequencies can be obtained, and are not confused by overlapping values for different modes.
3. The test-pieces should be prepared with accurate geometry and dimensions. The principal factor in flexural measurement is usually the thickness of the beam or disc, which enters into the equations as the third power. Ensure that the faces of the test-pieces are accurately parallel to better than 0.3% (*i.e.* parallelism better than 0.001 mm for a 3 mm thick test-piece). The test-piece ends, often ignored for other types of testing, also need to be square to the length and machined flat.

Test-pieces should also have a good surface finish. Thickness measurements are generally made on the raised parts of the surface, and not on the centre-line of the roughness. It can be imagined that the stiffness of the test-piece is determined by the thickness of the bulk material excluding the rough surface. Smooth, preferably lapped finishes are desirable, otherwise overestimation of the structural thickness of the test-piece will occur, leading to an underestimate of moduli.

5.3.2 Suspension and support methods

5.3.2.1 Main issues

Suspension/support methods for test-pieces depend on the arrangements made for excitation and detection. In some respects, there is no ideal solution. The key issue is to minimise the interaction between the test-piece and its environment, but at the same time keep it in position during the testing. This is particularly critical for high-temperature testing where readjustment of the position during the tests is usually not possible.

5.3.2.2 Room-temperature testing

For the **flexural resonance method**, there are several options:

- If the test-piece is to be driven in flexure by a mechanical vibrator, the test-piece can be suspended in loops of thread or fibre, using one loop to drive the vibration and the other to detect the vibration. These loops should contact the test-piece just outside the nodal positions in order to be capable of driving and detecting, and should have a minimum mass (Figure 23a)

- If the test-piece is to be driven electrostatically, it should be supported at its nodes (normally at the fundamental mode flexure nodes) using soft supports or taut strings, and can be lightly clamped at these positions. It is then driven centrally by an electrode placed beneath the test-piece. Note that the test-piece itself must be electrically earthed, or if an insulator, it must have a coating which can be earthed applied in the region opposite the driver electrode.

For the **torsional resonance method**, the best option is the suspension one. The method recommended in ASTM C1198 [35] is to use loops of thread or fibre near each end of the test-piece, but running from opposite corners (for a rectangular section bar, Figure 23b) or opposite sides of the diameter (for a round rod). This ensures that torsion is excited preferentially.

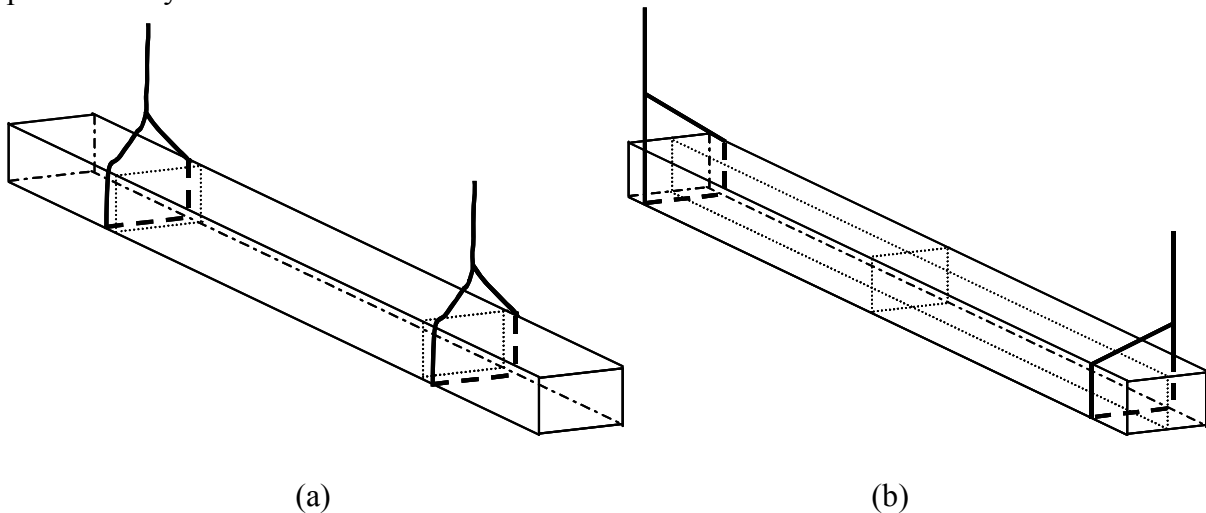


Figure 23: Suspension locations for the resonance method (a) flexural mode, with the suspension loops just outside the flexural nodal positions (dotted lines) and (b) torsional mode, with the suspension loops near opposite corners (torsional nodal lines dotted).

For the **longitudinal resonance method**, the test-piece can be rested on a compliant support such as cotton wool or ceramic fibre, such that the driver contacts one end and the detector contacts the other.

Similar issues exist for the **impact excitation method** but slightly different solutions can be adopted because of the reliance on transient impacts to ‘ring’ the sample, rather than continuously driving it in resonance. For the **flexural impact excitation method** simply resting the test-piece on cotton wool or ceramic fibre may be sufficient to allow support with minimum damping while the test-piece is struck. However, a better solution is to rest it on parallel taut nylon strings at the relevant nodal positions. The test-piece location can be made more stable by having taut strings over the top of the test-piece as well as underneath (Figure 24a).

For the **torsional impact excitation method**, similar methods to those for flexure may be used, but if strings are used, the support has to be predominantly at the test-piece centre. Support along the centre-line of the length of the test-piece is possible, i.e. along the nodal axis, but this can be difficult to arrange reliably. Reliance on centre support only means that the test-piece may not be well-balanced, but it has been found that supporting on a pair of strings about 5 mm to 10 mm apart enables sufficient balance provided that an acoustic method of detection is used. An alternative approach is to use the flexural nodal positions for

support, and to strike the second torsional mode which has nodes approximately in the same locations.

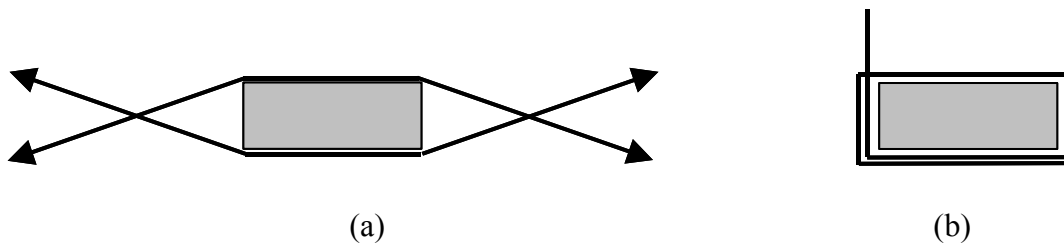


Figure 24: (a) Use of taut nylon strings to support and locate test-pieces at the appropriate nodal positions, and (b) wire suspension for use to high-temperatures with wire wrapped tightly around the specimen to prevent movement.

For **longitudinal impact excitation**, preventing the movement of the test-piece axially is difficult, (although the method shown in Figure 24a) is helpful.

5.3.2.3 High-temperature testing

Suspensions for high-temperature resonance use are more difficult to achieve, yet are more critical for preventing the test-piece from becoming dislodged during a prolonged thermal cycle. In the loop suspension method which can use cotton thread or nylon string at room temperature, carbon fibre or fine platinum wire have been suggested. Alternative fibres, such as ceramic fibre have been tried, but have limited success because of difficulties of tying off the loops because generally the fibre diameters are rather large, and the material is more brittle.

For impact excitation, less reliance is placed on the overall mass of the suspension, and it is possible to use platinum or nichrome wire loops. Silica fibre cord was used successfully by Sakata et al. [33] up to 900 °C. It has been found that test-piece location can be stabilised either by wrapping the wire tightly round the test-piece to restrict sliding (Figure 24b), or by using a metal wire version of Figure 24a in which the tension is provided by dead weights hanging over refractory bars.

5.3.3 Resonance excitation

The usual method with the resonance techniques is to employ a device which vibrates at a controllable level, and where the driving frequency can be swept over a wide range (typically 100 Hz to 200,000 Hz). A piezo-vibrator is ideal for this. Earlier references refer to a record stylus being used in reverse. A high-frequency loudspeaker is also possible, although the maximum frequency may be rather limited.

5.3.4 Impact excitation

The ideal impact is a single strike with a hard ball. The easiest method of doing this at room temperature is to glue a ball bearing or a ceramic grinding bead, typically 4-6 mm in diameter, onto the end of a plastic strip, such as a cable-tie. With a little practice, a single strike in a predetermined location becomes easy to do. For high temperature use, small balls can be dropped down a guide tube and allowed to bounce off the test-piece.

Automated impactors are also suitable, especially for high-temperature use. An electromagnetically driven pulser with a captive flier attached is typical. The flier strikes the

test-piece at the appropriate position and falls back into the pulser. It is probably true to say that more consistent and controllable impacts can be made using a pulser than can be achieved manually or by the ball-drop method.

5.3.5 Vibration detection

In resonance, the traditional method is to use a **record player pick-up**, but nowadays if this is not available a **sensitive piezosensor** is needed. A piezosensor can also be used for the impact excitation method. The tip of the sensor can be placed in direct contact with the test-piece, although this does risk affecting the dynamic mass of the test-piece. It is often better to lightly contact the test-piece close to, **but not at**, a node, using a thin extension probe to the sensor, so that there is minimum interference with the vibration developed.

If the surrounding environment is air or inert gas, a **microphone** can be used, but it is important to ensure that it is capable of detecting the ultrasonic frequencies that can be developed. It may be necessary to place it very close to the surface of the test-piece if the sound intensity is low.

A more sophisticated and expensive system which will work in vacuum and to high-temperatures is to use a **laser vibrometer**, which is aimed at the antinode position in the test-piece. The surface at or near free end of the test-piece is ideal, because there all frequencies will be detected.

5.3.6 Measurement to high temperatures

The dynamic methods lend themselves readily to use at elevated temperature provided that adequate support or suspension methods are used which are reliable to the highest temperature of interest. The key issue is to maintain the location of the test-piece such that it can continue to be vibrated or impacted at the appropriate positions (see 5.1.1).

The furnace system can be of any type appropriate to providing an environment in which the test-piece can be supported, vibrated and the vibration detected. There are two issues of importance:

- The test-piece temperature should be measured using a separate thermocouple to that used for furnace control, but its tip should not be in contact with the test-piece in case it damps the vibration. It is safest to ensure that it is in contact with the structure that supports the test-piece. Small temperature errors can usually be tolerated, since the temperature dependences of moduli are usually relatively low and monotonic.
- The test-piece will (generally) expand as the temperature is raised, and its density will fall. The 'true' elastic moduli are those which are based on true dimensions as a function of temperature, so if room-temperature dimensions have been used in the appropriate calculations, the nominal elastic moduli need to be corrected. Inspection of the equations shows that in all cases, the correction needs to be by a factor $1/(1+\alpha T)$ where α is the mean linear expansion coefficient and T is the temperature range over which the test-piece has been heated. This correction is typically of the order of 1-2% to 1000 °C. Some standards require that this correction is made, others do not. Whether this correction is made depends on how the data are to be used, so in any

event it should be made clear in the test report whether or not such a correction has or has not been made.

5.3.7 Damping

In addition to the identification of resonant frequencies, the dynamic methods can also be used to measure damping, or at least to undertake comparative measures of damping. To do this, the damping of vibration arising from the suspension system must be minimised, and this requires accurate positioning of the suspension or support system at the test-piece nodes. Damping has the effect of broadening the shape of the resonant peaks, and in most materials will usually increase markedly at temperatures at which the materials start to become plastic or where one or more of the phases begins to melt.

5.3.8 Example data

5.3.8.1 Nimonic 101

Figure 25 shows the series of frequency spectra obtained for a Nimonic 101 test-piece at room temperature using an IMCE RFDA system. The test-piece was 100 mm in length, 1.8 mm thick and 10 mm wide. Four different spectra are shown for different strike modes. The lowest spectrum is for the flexural mode. This shows the fundamental mode at 976 Hz, plus a series of harmonics. Because the test-piece was set up as described for mode $n = 1$ in Figure 23a, the second mode at 2698 Hz and the fourth mode at 7897 Hz almost do not appear because they are not strongly excited. The third mode, $n = 3$, appears at 5224 Hz, and the fifth mode, $n = 5$, appears at 12854 Hz. The peak at 10876 Hz is the second harmonic torsional mode. When set up in the torsional mode with central support (see Figure 23), it can be seen that the same flexural modes are produced, including stronger responses from the even-numbered modes. In addition, there are new peaks at 5407 Hz and 16455 Hz, which together with the 10876 Hz peak form the torsional series 1 : 2 : 3 : The closeness of the lowest torsional frequency to the third flexural mode 5224 Hz means that the two could easily be confused unless care is taken to identify their respective appearances when the test-piece is struck at relevant positions. When set up in the sideways flexural mode, peaks at 13537 Hz and 24707 Hz appear. These are not fundamental and second mode peaks respectively because the frequency ratio is less than 1. However, there is a moderate response at 5200 Hz, which gives a ratio of 2.6 with 13537 Hz, and is thus likely to be the fundamental mode. Finally, when set up for the longitudinal mode, only one strong peak appears, and this is the fundamental mode at 26208 Hz.

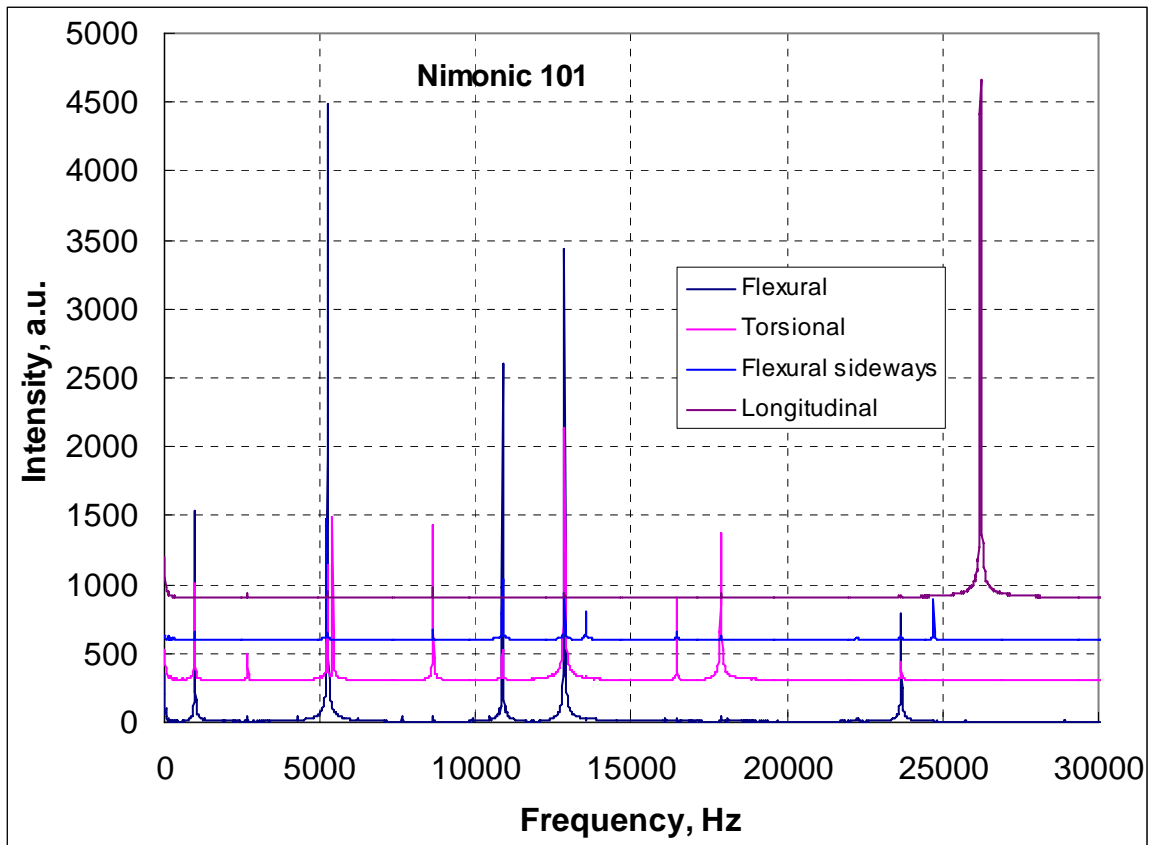


Figure 25: Frequency spectrum for Nimonic 101 tested in flexural, torsional, sideways flexural and longitudinal modes.

Using this process to identify the fundamental mode frequencies to use in the standard methods of computation of elastic moduli, the data in Table 8 can be produced. For the flexural and sideways flexural modes, a value of Poisson's ratio of 0.275 was initially assumed. Using the simultaneous detection of the flexural and torsional modes, the correct Poisson's ratio of 0.345 was computed. This was then used to re-compute the values for Young's modulus from the two flexural geometries and to calculate the longitudinal mode Young's modulus. There is good consistency between the different geometries and strike modes, and it can also be seen that for this particular material, for the test-piece geometry used, the outcomes are insensitive to the exact value of Poisson's ratio used in cases where it is not directly measured.

Table 8: Room-temperature analysis of Nimonic 101

Set-up mode	Assumed Poisson's ratio	Calculated Young's modulus, GPa	Calculated shear modulus, GPa	Calculated Poisson's ratio
Flexural	0.275	222.11	-	-
Flexural sideways	0.275	221.67	-	-
Torsional/flexural	-	223.71	83.18	0.345
Flexural	0.345	222.10	-	-
Flexural sideways	0.345	222.17	-	-
Longitudinal	0.345	222.60	-	-

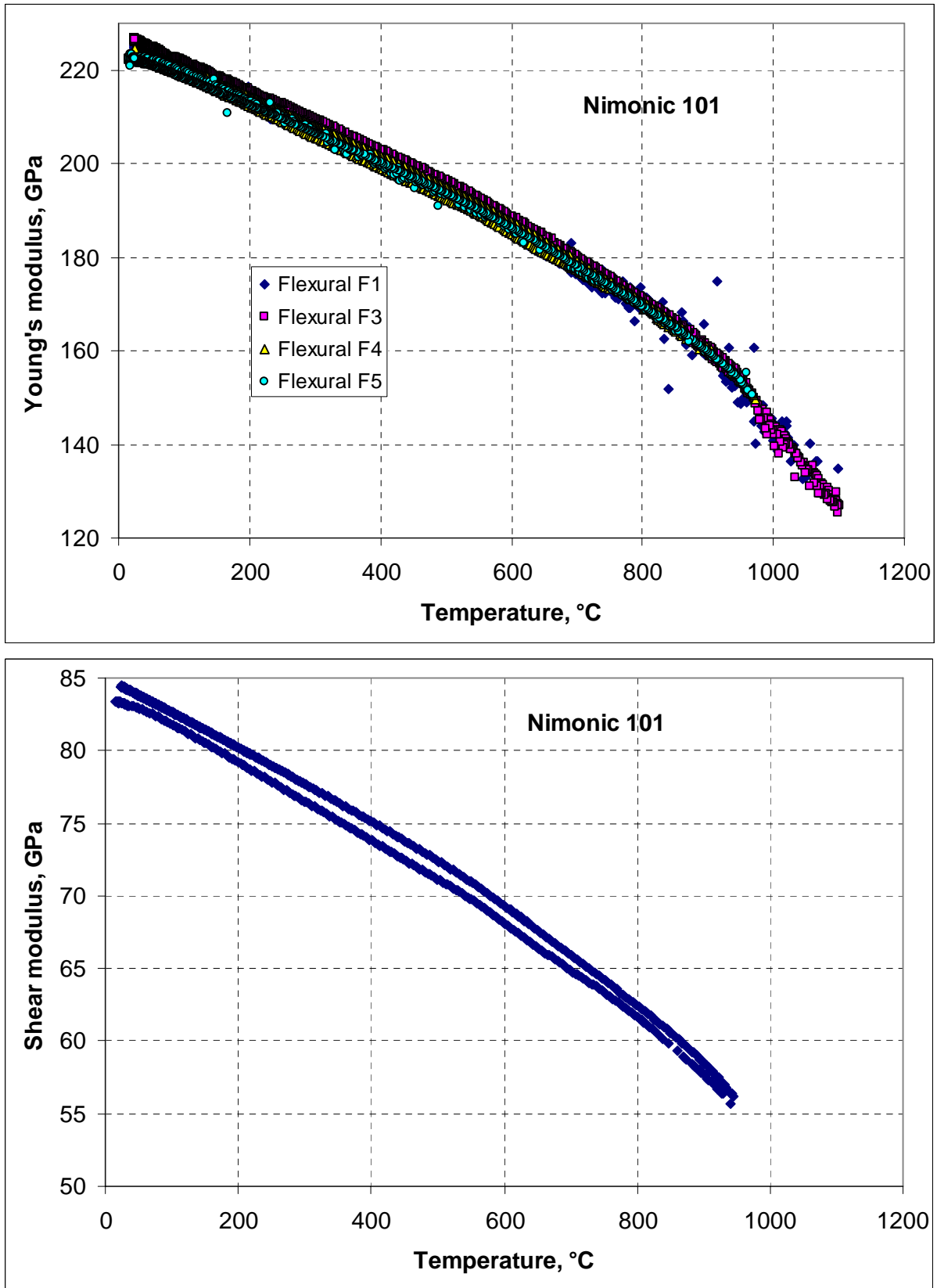


Figure 26: (top) Young's modulus of Nimonic 101 calculated from four flexural mode frequencies, and (bottom) shear modulus as a function of temperature calculated from the second torsional mode.

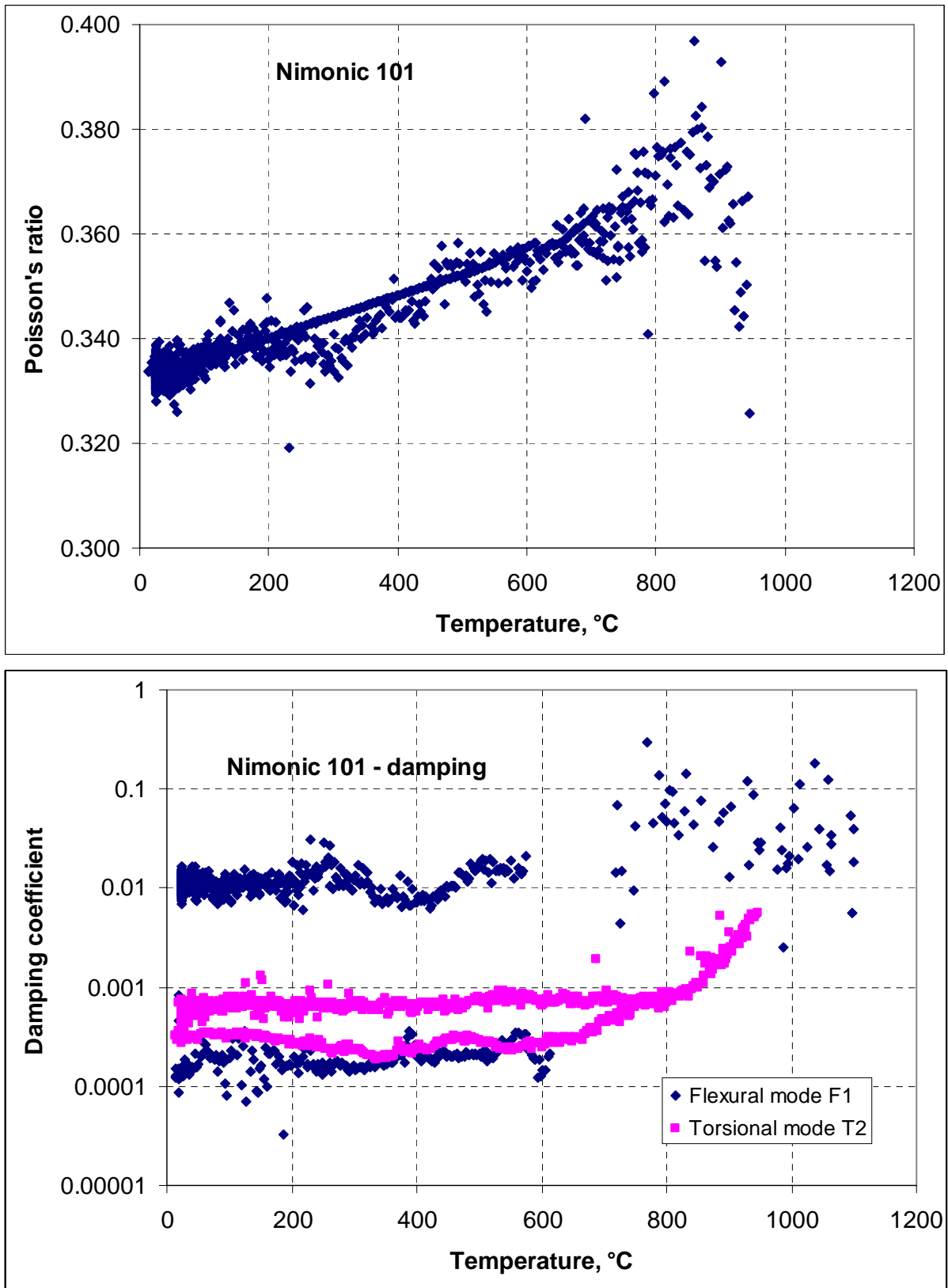


Figure 27: (top) Poisson's ratio of Nimonic 101 from the fundamental flexural mode Young's modulus and the second torsional mode shear modulus, and (bottom) damping coefficient for these two modes

The test-piece was then set up in NPL's high-temperature facility using nichrome wire suspension at the flexural nodal positions. The wire was wound tightly around the test-piece to lock it into position and prevent it slipping axially. The impactor was set up to strike the test-piece at the centre of its length, but offset to one side so that both flexural and torsional modes could be obtained. The test-piece was then heated in an argon atmosphere at 3 °C/minute to 1100 °C and cooled at the same rate, with impacts every minute. Figure 26 shows the results of the modulus calculations (uncorrected for thermal expansion). In the upper part of Figure 26a, four flexural modes have been used to demonstrate the equivalence of outcome, based on the determined room-temperature modal frequency ratio. It will be noted that the fundamental mode data are more scattered than the higher frequencies, and the third mode extends to higher temperatures than any of the others. Based on the third mode data, it can be seen that there is an inflection in the curve at about 950 °C, which is thought to be due to a phase change in the precipitate. In the lower part, Figure 26b, are the shear modulus data computed using the second torsional mode. The maximum temperature at which this mode was detected was about 950 °C. The small level of hysteresis between heating and cooling is possibly due to annealing of the test-piece during the test. Figure 27a shows Poisson's ratio computed from the data in Figure 26, and Figure 27b shows the damping coefficient for the fundamental flexural and second mode torsional vibrations indicating a marked increase in damping above about 850 °C.

5.3.8.2 High-alumina ceramic

In this example, a rectangular bar of alumina, 175 mm in length, x 12 mm wide x 4.2 mm thick, was set up and tested using a similar philosophy to that described for the Nimonic 101 test-piece. Again, Figure 28 shows that when set up in the flexural mode, the response to the even-number harmonics is poor, but there is a clear series of peaks at 1331 Hz, 3638 Hz (weak), 7092 Hz, 11682 Hz (weak), 17334 Hz, 20019 Hz, 24194 Hz (weak). These are in the ratio 1 : 2.73 : 5.33 : 8.78 : 13.02 : 15.04 : 18.18, compared with the theoretical values of 1 : 2.76 : 8.93 : 13.34 : 18.64. It is clear from this that the ratio at 15.04 (20019 Hz) is a different mode. When supported centrally to record simultaneously flexure and torsion, the same series of peaks is detected, again with the even numbered flexural peaks appearing stronger, but additionally there are peaks at 9997 Hz, 20178 Hz, and 30151 Hz which form a ratio series close to 1 : 2 : 3, identifying them as the torsional modes. In sideways flexure there are strong peaks at 3770 Hz, 10095 Hz, 19043 Hz, 30102 Hz (weak) which form the ratio 1 : 2.68 : 5051 : 7.98, close to the required flexural ratios, bearing in mind the relatively large width. In the longitudinal mode, there is a single strong peak at 27075 Hz.

Using these data gives a Young's modulus of 336 GPa, a shear modulus of 136 GPa and a Poisson's ratio of 0.243.

Using a similar approach to suspension as described for the Nimonic alloy above, a thermal cycle was performed. Figure 29 shows four flexural mode frequencies and the second torsional mode frequency as a function of temperature. It can be seen that the trend with temperature in all cases is monotonic, but above about 920 °C, the data not only become more scattered, but the fundamental flexural frequency and the second torsional frequency are no longer activated. Figure 30 illustrates the temperature dependence of Young's modulus and the damping coefficient of the fundamental flexural frequency. It is clear that at the upper end of the range of useful measurement, the damping is increasing rapidly. This is explained by softening of the secondary glassy phase in the material.

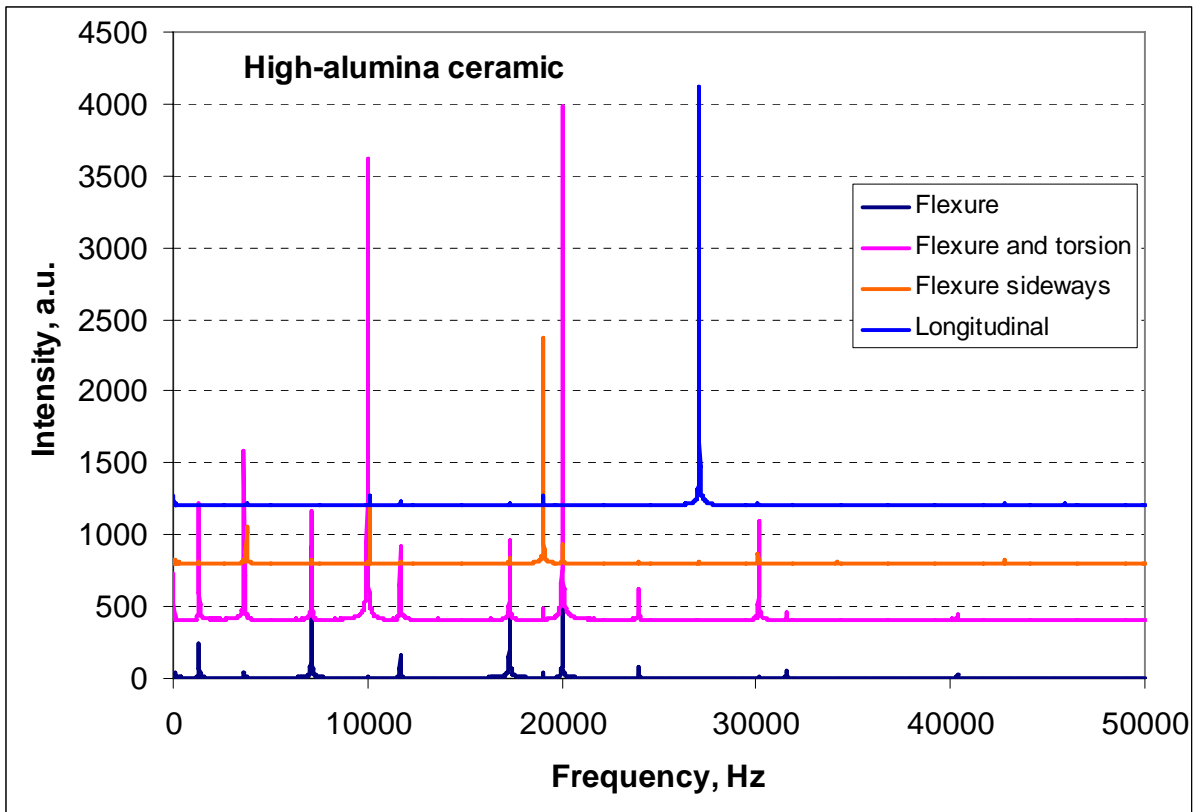


Figure 28: Room-temperature frequency spectra for flexural, flexural/torsional, sideways flexural and longitudinal modes on a high-alumina test-piece.

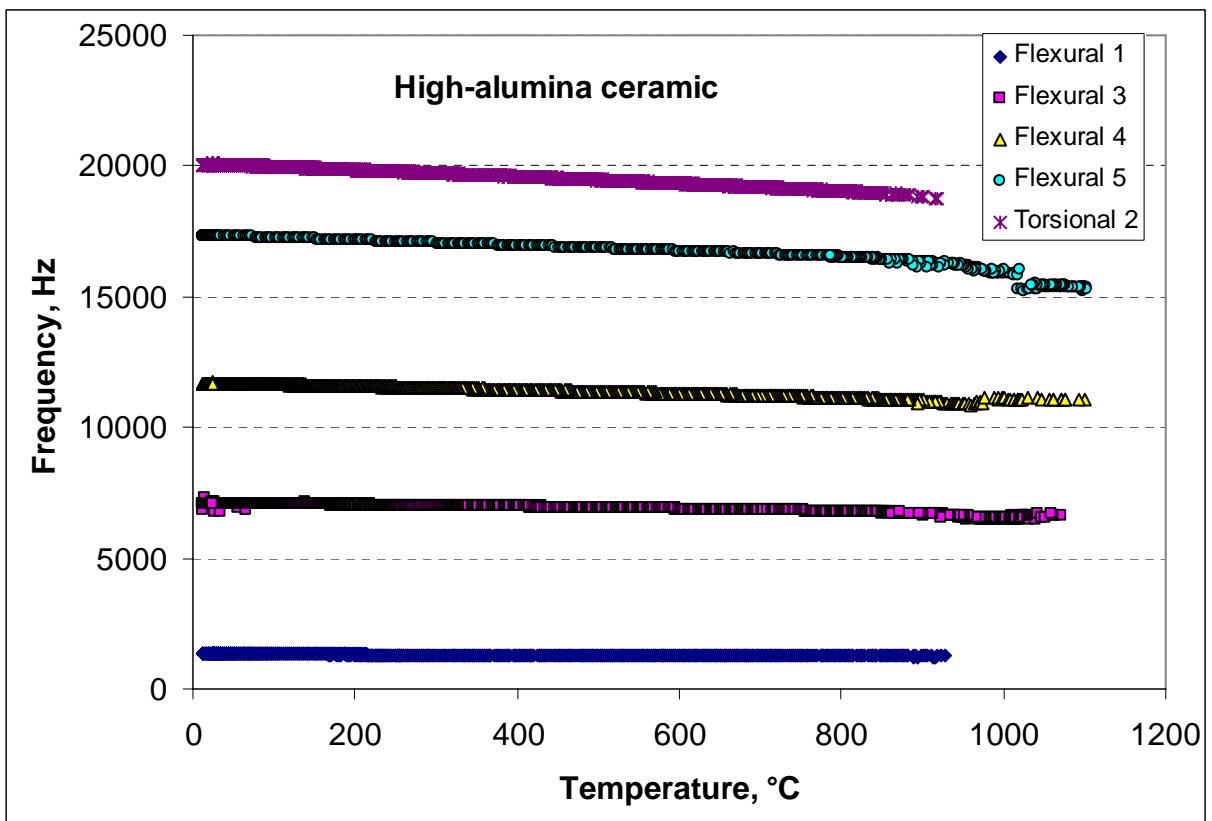


Figure 29: Flexural and second torsional frequencies as a function of temperature for high-alumina ceramic during heating and cooling.

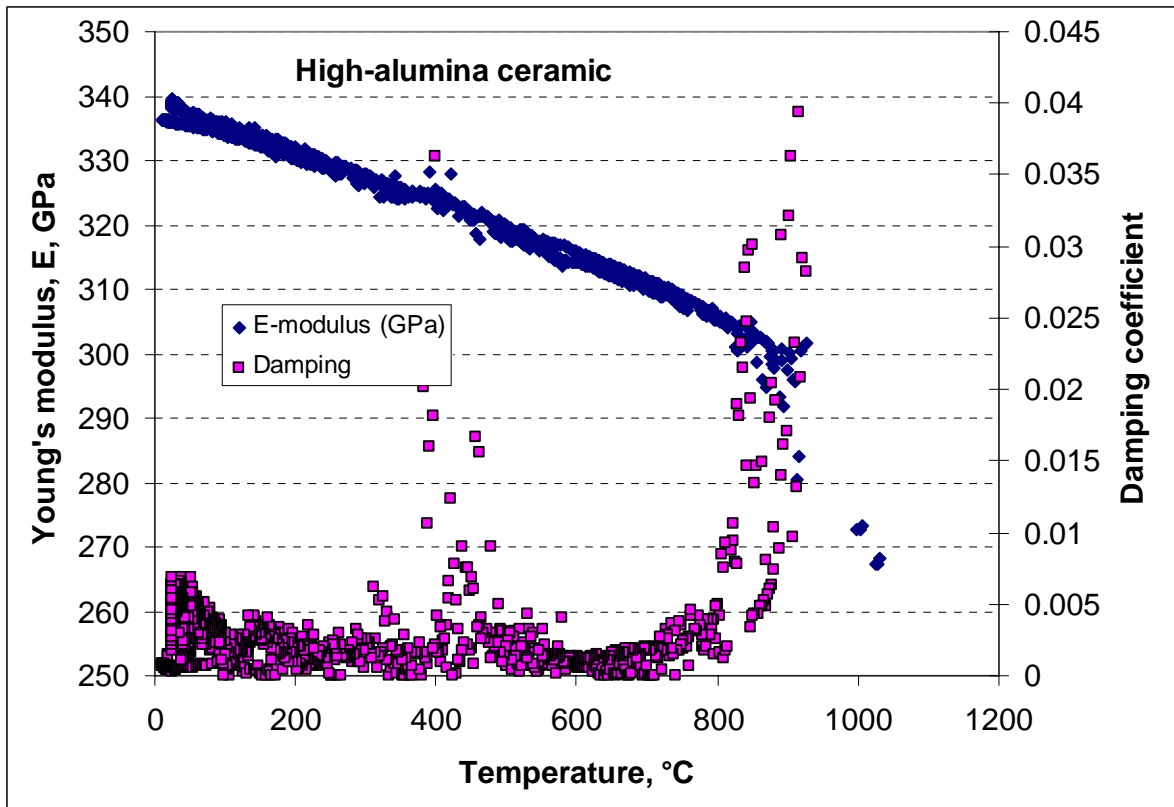


Figure 30: Young's modulus as a function of temperature calculated from the fundamental mode, compared with the damping coefficient for this frequency.

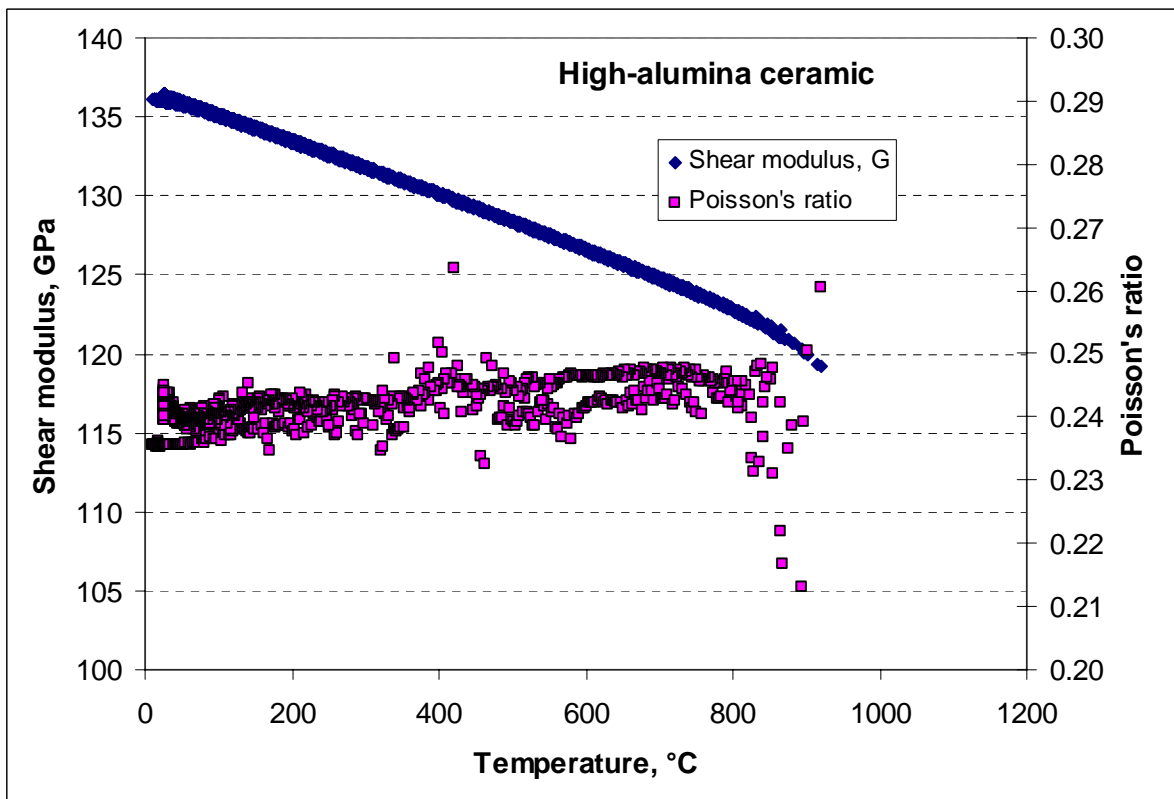


Figure 31: Shear modulus as a function of temperature calculated from the second mode torsional frequency and Poisson's ratio computed from E and G.

The shear modulus and the resulting Poisson's ratio data is shown in Figure 31. Both show monotonic behaviour to about 850 °C, above which they cannot be determined.

5.3.9 Method accuracy and uncertainty

The key elements defining the uncertainty of measurement of the resonance or the impact technique are the mass and physical size of the test-piece. Assuming that the equations relating these parameters and frequency to elastic moduli are highly accurate, a practical target of 1% overall accuracy is sensible for many applications. To achieve this level requires that each parameter is measured to rather better than this level. The typical requirements for measurement can be listed as follows:

- **Mass of test-piece:** Typically the mass can be measured to a high degree of accuracy, much better than most other parameters and is not an issue for this measurement. A suggested level of accuracy for practical applications of 0.05% is more than sufficient, *i.e.* weighing a 10 g test-piece to an accuracy of 0.005 gm.
- **Length of test-piece:** The length of the test-piece should be measured to better than 0.1%, *i.e.* on a 100 mm length, an accuracy of 0.1 mm is sufficient. Using dial-gauge or indicating callipers reading to 0.02 mm is thus more than adequate. Note that the end surfaces of the test-piece should also be flat and square to the length to better than 0.1 mm.
- **Lateral dimensions of the test-piece:** The thickness of the test-piece in the direction of flexure is the most critical measurement, since this enters into the equations raised to the third power. The width also enters to the single power. So on a rod test-piece, the diameter enters to the fourth power. In order to target an overall accuracy of 1%, the measurement of rod diameter should thus be to 0.2%, *i.e.* a 5 mm diameter rod has to be measured to an accuracy of 0.01 mm. Ideally, the rod should also be of diameter uniform to this level or better. For a rectangular section test-piece, a similar target needs to be achieved. For a test-piece of thickness 2 mm and width 10 mm, the measurement target is to better than 0.005 mm. These simple calculations show also the significance of obtaining uniform regular geometry and smooth surfaces on the test-piece. **In practical terms, therefore, it is desirable to have test-pieces not less than 2 mm thick which have been carefully ground flat and parallel faced, or not less than 4 mm diameter which have been cylindrically ground, to as high a degree of perfection as possible. It is also advisable that several measurements of diameter or of width and thickness are made along the test-piece length in order to verify the geometrical acceptability, and for average values to be computed.**
- **Density:** As an alternative to mass and dimensions, the density can be used by substitution for mass and volume in the equations. It may be possible to measure actual density by an immersion method to a higher level of accuracy than by using the mass and dimensions. The reliance on accurate cross-sectional dimensions is thus less important.
- **Frequency:** The frequency, which enters in all formulae as the second power, should ideally be measured to better than 0.1%, *i.e.* to 1 Hz in 1 kHz. Generally this is perfectly feasible with most kinds of frequency counting device. It has been found

experimentally, that devices based on quartz crystal clocks are accurate to typically an order of magnitude better than this.

Note that in the above it is assumed that each of the measuring devices is calibrated to an accuracy better than the reading requirement.

The above assessment assumes that the test-piece is a homogeneous isotropic body. This may not be the case. There are several issues:

- The material may have variations in phase content or porosity throughout its volume. In such a case, the data have to be accepted as being only representative.
- The material may have a texture, a preferred orientation of grains in certain directions or in certain areas. **It is recommended that users try and develop an understanding of the material before starting to prepare test-pieces. Ensure that the test-pieces are taken from regions and orientations of specific interest in the artefact.**
- The machined surfaces may be rough, to the extent that using a micrometer to measure the diameter or thickness will record a value based on the peaks of the roughness, which the mechanical stiffness will be based primarily on the thickness represented by the troughs of the roughness. **It is recommended that the surfaces have a minimal roughness, certainly less than the target accuracy of dimension measurement.**
- The machined surfaces may be mechanically damaged by the machining process, which may result in surface hardening or the introduction of cracks. While any residual stresses will not in principle affect the modulus measurement, the presence of damage will. It is recommended that the test-pieces are annealed before testing to heal any damage and normalise the microstructure near the surface.

The remaining issue is the accuracy of the calculation equations. The examples above show that the equations are mutually consistent to a level of probably better than 0.5%. They have been developed over many years, and evaluated using test-pieces that are relatively large and thus have minimal dimensional inaccuracies. Thus in practice, overall, the greatest uncertainty comes from the preparation and measurement of the smallest dimension of the test-piece.

To illustrate further the importance of dimensional tolerances in dynamic modulus measurement, the example below shows an uncertainty budget developed for a rectangular bar tested by impact excitation, calculated using Equation 9, and ignoring the contribution of the geometric factor, T , which can be considered negligible for a bar where $L/t > 20$, and following the same procedures as those presented in Section 4.5.

Table 9: Example uncertainty budget for the impact excitation technique

Source of uncertainty	Uncertainty	Measured Value	Uncert (%)	Prob distrib	Divisor	c_i	$U(E)$ (%)
Mass, m	± 0.001 g	2.340 g	0.043	Rect.	$\sqrt{3}$	1	0.025
Frequency, f	± 0.1 Hz	2380 Hz	0.004	Rect.	$\sqrt{3}$	2	0.004
Width, b	± 0.005 mm	6 mm	0.083	Rect.	$\sqrt{3}$	1	0.048
Thickness, t	± 0.005 mm	1.5 mm	0.333	Rect.	$\sqrt{3}$	3	0.577
Length, L	± 0.1 mm	65 mm	0.154	Rect.	$\sqrt{3}$	3	0.267
Combined Standard Uncertainty							0.64
Expanded uncertainty ($k = 2, 95\%$)							1.28

In this case the sensitivity coefficients, c_i are calculated from the partial derivatives below, and $U(\%) = \text{Uncert}(\%) * \text{divisor} * c_i$.

$$E = 0.9465(mf^2 / b)(L^3 / t^3)T$$

$$\frac{\partial E}{\partial m} = 0.9465(f^2 / b)(L^3 / t^3)T = \frac{E}{m} \quad \text{and } c_i = 1$$

$$\frac{\partial E}{\partial f} = 0.9465(2mf / b)(L^3 / t^3)T = \frac{2E}{f} \quad \text{and } c_i = 2$$

$$\frac{\partial E}{\partial b} = 0.9465(-mf^2 / b^2)(L^3 / t^3)T = -\frac{E}{b} \quad \text{and } c_i = 1$$

$$\frac{\partial E}{\partial t} = 0.9465(mf^2 / b)(-3L^3 / t^4)T = -\frac{3E}{t} \quad \text{and } c_i = 3$$

$$\frac{\partial E}{\partial L} = 0.9465(mf^2 / b)(3L^2 / t^3)T = \frac{3E}{L} \quad \text{and } c_i = 3$$

Results clearly confirm that the greatest contribution to the uncertainty is from the thickness dimension.

From the example above, the result should be reported as: $E = 167 \pm 2$ GPa, with the caveat that the reported expanded uncertainty is based on a standard uncertainty multiplied by a coverage factor, which provides a level of confidence of approximately 95%.

5.4 Differences between dynamic and static moduli

5.4.1 Theory

It is often asked whether the elastic moduli determined dynamically and quasistatically have the same values. Theoretically it can be shown that there is a small difference. The adiabatic modulus E_a is always larger than the isothermal one, E_i . This can be argued simply on the basis that when a body is suddenly stretched, it cools, a feature that derives from the first law of thermodynamics. The thermal contraction gives rise to a strain in the opposite direction to the tensile strain applied and which is governed by the specific heat c_p and the thermal expansion coefficient α . Thus the apparent adiabatic modulus E_a is greater than the isothermal one. An approximate relationship is given by [34]:

$$\frac{1}{E_i} - \frac{1}{E_a} = \frac{\alpha^2 T}{c_p \rho}$$

A typical value for the ratio of E_a/E_i is ~ 1.005 for many metals, *i.e.* a difference of 0.5%.

5.4.2 Validation

To further compare the modulus data generated from tensile and dynamic methods, an intercomparison exercise was carried out using the BCR Nimonic 75 tensile reference material (CRM661) [13]. Details of the test matrix are given in Table 10, with measurements carried out by 3 laboratories - Labs A, B and C. Initial measurements were undertaken on 20 un-machined samples cut straight from the extruded bar, approximately 14 mm diameter x 84 mm long, using the Impact Excitation Technique (IET). A further set of repeat tests was made when the specimens were returned to Lab A, prior to sending them to Lab C for measurement. Results are presented in Table 11 and plotted in Figure 32. All measurements were made at room temperature, and results between the three laboratories generally showed excellent agreement. The mean modulus values obtained for the batch were 220.4 GPa, 220.8 GPa and 220.8 GPa for measurements carried out respectively at Labs A, B and C, and the typical uncertainty for the measurements on the extruded bar was less than 1%.

Several of the test-pieces were then machined into flat rectangular bars, 82 mm long x 3 mm thick with a width of either 6 mm or 12 mm. Room temperature dynamic tests were then carried out on 10 of the machined specimens and several test-pieces were also tested in tension for direct comparison with the dynamic measurements. As advocated in Section 4, a dedicated tensile modulus test was carried out over the elastic part of the stress-strain curve, below the proportional limit. Results from the Lab C tests are included in Table 11 and plotted in Figure 33 together with a subsequent set of tensile and dynamic measurements carried out at Lab A on the same specimens. Both Labs carried out measurements according to their in-house test procedures and analysis routines. The Lab C measurements were carried out using a high precision side-to-side averaging extensometer; the Lab A tests were made using strain gauges bonded to both sides of a rectangular test-piece. Additional tests were carried out on a couple of test-pieces using a new Surface Acoustic Wave (SAW) technique.

Figures 32 and 33 are plotted on the same scale, and it is clear that the modulus results on the machined rectangular specimens are lower than those measured on the extruded bar. It is not clear why this should be the case. The dynamic measurements are generally more sensitive to variations in dimension than the tensile tests, so it might be expected that the opposite be true. The results generally show good agreement but the tensile data has greater scatter and

uncertainties than the dynamic methods, probably due to the difficulties of measuring modulus at low strain values. SAW measurements were in good agreement with the other measurements.

Table 10: Matrix of tests carried out on Nimonic 75 (CRM 661) reference material

Testpiece	Previous work - HTMTC						TENSTAND								
	Original	Lab A	Lab B	Lab A	Lab C	New Geometry	Lab C			Lab A			SAW*		
	Geometry	RT	RT	RT	HT		RT	RT Tensile	HT dynamic	RT dynamic	RT tensile	HT dynamic			
GAQ1	○	✓	✓	✓	✓	○				✓					
GAQ2	○	✓	✓	✓		□	✓		✓	✓	✓	✓			
GAQ3	○	✓	✓	✓		○					✓				
GAQ4	○	✓	✓	✓		□	✓	✓			✓	✓			
GAQ5	○	✓	✓	✓		○					✓				
GAQ6	○	✓	✓	✓		□	✓	✓			✓	✓			
GAQ7	○	✓	✓	✓	✓	○					✓				
GAQ8	○	✓	✓	✓		□	✓		✓	✓				✓	
GAQ9	○	✓	✓	✓		○					✓				
GAQ10	○	✓	✓	✓		□	✓	✓			✓	✓			
GAQ11	○	✓	✓	✓		○					✓				
GAQ12	○	✓	✓	✓		□	✓	✓			✓	✓			
GAQ13	○	✓	✓	✓		○					✓				
GAQ14	○	✓	✓	✓	✓	□	✓		✓	✓	✓	✓			
GAQ15	○	✓	✓	✓		○					✓				
GAQ16	○	✓	✓	✓		□	✓	✓			✓	✓			
GAQ17	○	✓	✓	✓		○					✓				
GAQ18	○	✓	✓	✓		□	✓	✓			✓			✓	
GAQ19	○	✓	✓	✓		○					✓				
GAQ20	○	✓	✓	✓	✓	□	✓		✓	✓	✓	✓			

○ Original geometry - 14 mm dia. X 84 mm
 □ Machined by Lab C into rectangular bars (82mm x 12mm x 3mm or 82mm x 6mm x 3mm)
 SAW* Surface Acoustic Wave technique
 HT measurements up to 750 °C in 100°C steps.

Table 11: Results from modulus intercomparison exercise on the Nimonic 75 (CRM 661) reference material

ID	EXTRUDED BAR			MACHINED SPECIMENS				
	E (GPa)	E (GPa)	E (GPa)	Lab C		Lab A		
				E (GPa)	E (GPa)	E (GPa)	E (GPa)	E (GPa)
Lab A	Lab B	Lab C	Dynamic	Tensile	Dynamic	Tensile	SAW	
GAQ1	220.5	221.9	221.1					
GAQ2	220.5	221.4	220.8	215.4		218.2	221.0	
GAQ3	219.3	222.2	220.6					
GAQ4	220.1	221.6	220.5	216.0	213.8	217.9	218.5	
GAQ5	220.0	220.2	220.8					
GAQ6	221.3	222.1	221.5	217.2	211.3	217.0	219.7	
GAQ7	221.5	222.3	221.0					
GAQ8	219.8	220.6	221.0	217.0		215.7		218.7
GAQ9	220.3	220.5	220.9					
GAQ10	219.9	221.4	220.1	217.7	215.0	218.4	220.5	
GAQ11	221.1	220.2	220.6					
GAQ12	220.3	220.9	220.5	217.2	217.1	214.7	220.5	
GAQ13	220.2	221.0	220.2					
GAQ14	220.0	219.8	220.1	216.2		216.5	219.4	
GAQ15	219.8	219.9	220.7					
GAQ16	221.5	219.8	222.1	217.0	218.7	216.7	218.9	
GAQ17	221.1	220.7	222.2					
GAQ18	219.3	220.4	220.3	217.3	216.0	216.9		216.3
GAQ19	220.7	219.8	220.4					
GAQ20	220.2	220.2	220.8	215.6		218.6	221.5	
Mean E (GPa)	220.4	220.8	220.8	216.7	215.3	217.1	220.0	
SDev (GPa)	0.7	0.8	0.6	0.8	2.6	1.3	1.0	
Uncert (%)	0.6	0.8	0.5	0.7	2.4	1.2	1.0	

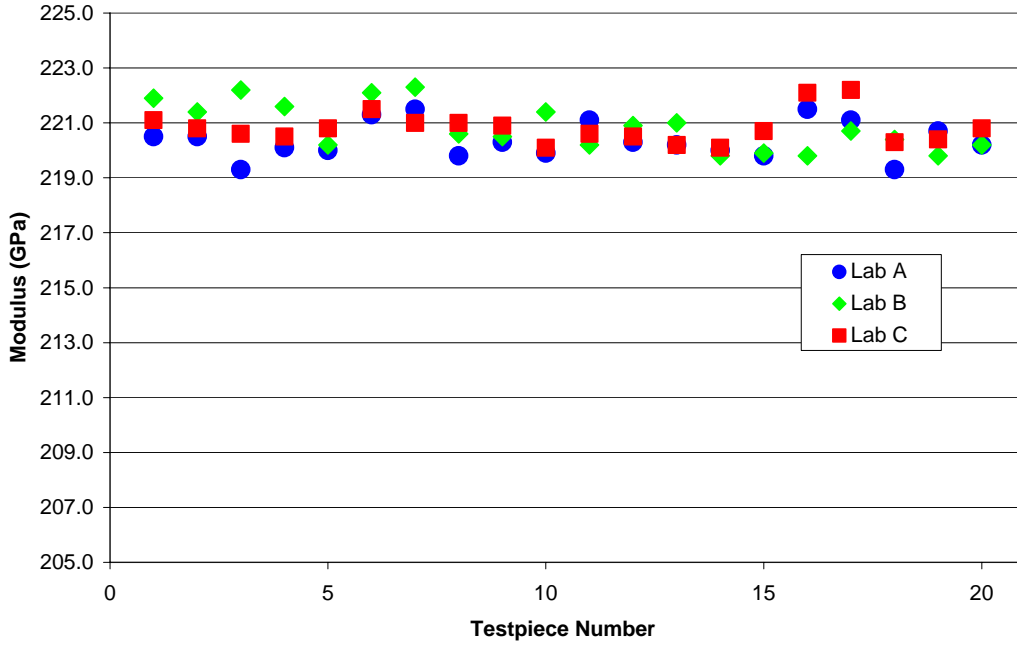


Figure 32: Comparison of dynamic modulus data from 3 laboratories on extruded bars – BCR Nimonic 75 (CRM 661) tensile reference material

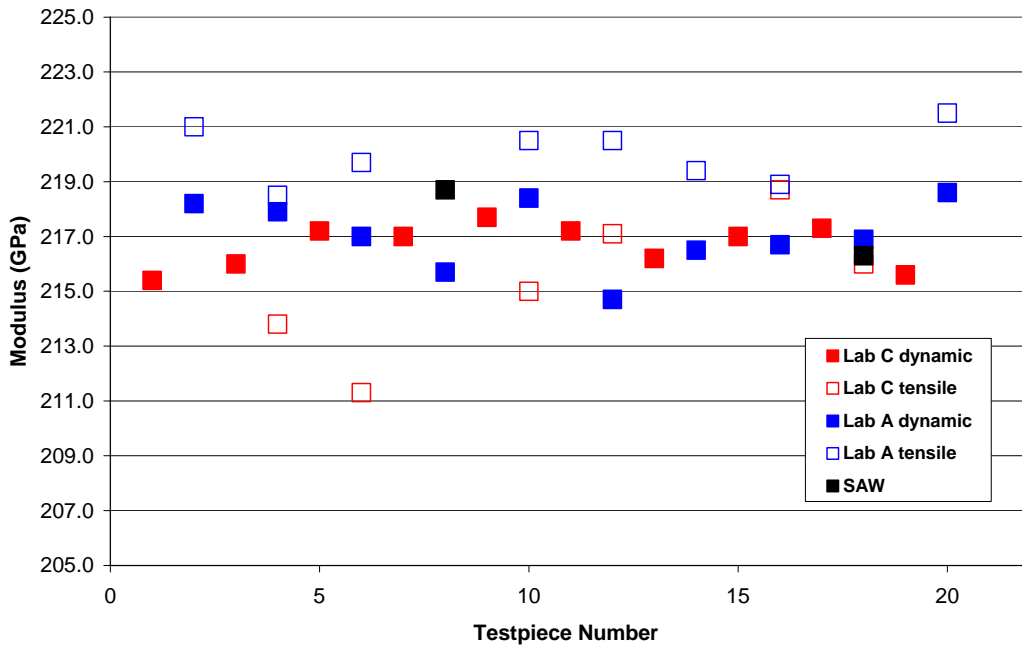


Figure 33: Comparison of the dynamic, tensile and SAW measurements on flat machined testpieces - BCR Nimonic 75 (CRM 661) tensile reference material.

5.5 Summary and recommendations on dynamic testing

Dynamic modulus methods can offer significant advantages over traditional static techniques, in particular their relative simplicity, speed and accuracy, the wide range of test-piece geometries that can be accommodated and the possibility of extending them to high temperature. However, specialist equipment is still required. It is also possible to obtain Young's modulus, shear modulus and Poisson's ratio from a single test if an appropriate test-piece geometry and set-up is used.

Generally the accuracy in modulus data from the dynamic test is of the order of 1%, but it is affected by a number of factors. To obtain high quality data there are a number of recommendations for the user to consider, including:

- Accurate control of test-piece dimensions, geometry and form. The thickness of the beam or disc, which enters into the equations as the third power, is probably the most important factor affecting the accuracy and reliability of the results.
- Machining of the faces of the test-pieces should be carried out carefully to ensure flatness and parallelism to better than 0.3%.
- Surface roughness should be as high a quality as practical as this can affect the accuracy in the measured test-piece dimensions and the subsequent calculation of modulus. A smooth, lapped surface is desirable, and a standard engineering finish should be considered as the minimum specification.
- Scaling of the test-piece dimensions is recommended to ensure that the appropriate frequencies can be obtained, and are not confused by overlapping values for different modes.
- If possible the test-piece should be examined in different modes to check and validate the selection of frequencies used for modulus calculations.
- It is recommended that the whole frequency spectra be recorded, so that the appropriate fundamental and harmonic frequencies can be used to calculate the modulus values. This is important as in some cases, and test set-ups the relevant fundamental frequencies may not be excited, or may be less obvious than higher mode responses.
- For high temperature measurements, the tracking of the frequencies at regular intervals is recommended because, as the temperature increases, the signal strength of a particular frequency may become very weak due to damping, and difficult to identify in isolation.
- For highest accuracy, the higher order geometric corrections should be applied, and at high temperature, corrections for thermal expansion of the test-piece should be made.
- The use of reference specimens, such as a stable glass, metal or ceramic or an in-house reference test-piece is recommended to check and validate the test set-up.

- Development of uncertainty budgets for the modulus measurement, which will help to identify particular areas of the test set-up that contribute most to the scatter and variability.

6 Acknowledgements

This Measurement Good Practice Guide has been produced as a part of the Metrology Tools Project on “Modulus Measurement”, which is part of the programme on Measurements for the Processability and Performance of Materials (MPP), funded by the Engineering Industries Directorate of the UK Department of Trade and Industry.

Thanks are also due to Dr Nick McCormick (NPL) who developed the NPL modulus analysis software.

7 References

- [1] EN 10002-1: *Metallic materials - tensile testing – Part 1: method of test at ambient temperature*
- [2] ASTM E8: *Standard test methods for tension testing of metallic materials.*
- [3] ASTM E111: *Standard test method for Young’s modulus, tangent modulus and chord modulus*
- [4] Lord, J.D., Loveday, M.S., Rides, M., McEnteggart, I., *Digital tensile software evaluation*, TENSTAND WP2 Report, National Physical Laboratory, July 2004.
- [5] ASTM E1876: *Standard test method for dynamic Young’s modulus, shear modulus and Poisson’s ratio by impulse excitation of vibration.*
- [6] ASTM E1875: *Standard test method for dynamic Young’s modulus, shear modulus and Poisson’s ratio by sonic resonance.*
- [7] Wolfenden, A., et al., “Dynamic Young’s modulus measurements in metallic materials: results of an interlaboratory testing program”, *Journal of Testing and Evaluation*, Jan 1989, pp2-13.
- [8] Roebben, G., Bollen, B., Brebels, A., Van Humbeeck, J., Van Biest, O., “Impulse excitation apparatus to measure resonant frequencies, elastic moduli, and internal friction at room and high temperature”, *Rev. Sci. Instrum.* 1997, **68**(12), 4511-15.
- [9] Lord, J.D.. *Review of methods and analysis software for the determination of modulus from tensile tests*, NPL Measurement Note MATC(MN)41, Dec 2002.

- [10] Unwin, W.C., *The testing of materials of construction*. Longmans, Green & Co. London, 1910, pp 237-238.
- [11] Lord, J.D., Roebuck, B., Orkney, L.P., *Validation of a draft tensile testing standard for discontinuously reinforced MMC*, VAMAS Report No.20, National Physical Laboratory, May 1995.
- [12] Ingelbrecht, C.D., Loveday, M.S., *The certification of ambient temperature tensile properties of a reference material for tensile testing according to EN 10002-1, CRM661*, EUR Report 19589 EN, 2000.
- [13] Lord, J.D., Rides, M. Loveday, M.S., *Modulus measurement methods*, TENSTAND WP3 Report, National Physical Laboratory, Jan 2005.
- [14] EN ISO 9513: 2002 *Metallic materials - calibration of extensometers used in uniaxial testing*.
- [15] Dyson, B.F., Loveday, M.S., Gee, M.G., (Eds), *Aspects of materials metrology and standards for structural performance, Chapter 8: Aspects of modulus measurements*, Elsevier Applied Science, London, 1994.
- [16] EN 10002-2 *Metallic materials - tensile testing – Part 2. Verification of the force measuring system of the tensile testing machine*.
- [17] Kandil, F.A., *Measurement of bending in uniaxial low cycle fatigue testing*, NPL Measurement Good Practice Guide No 1, March 1998.
- [18] Roebuck, B., Lord, J.D., Cooper, P.M., McCartney, L.N., “Data acquisition and analysis of tensile properties for metal matrix composites”, *ASTM Workshop on Accuracy of Load and Strain Measurements, Miami, November 18, 1992. ASTM J. Testing and Evaluation, JTEVA*, 1994, **22**(1), 63-69.
- [19] Roebuck, B., McCartney, L.N., Cooper, P.M., Bennett, E.G., Lord, J.D., Orkney, L.P., *UK interlaboratory tensile tests on Al alloy/SiC particulate metal matrix composites*, NPL Report DMM(A)77, Dec 1992.
- [20] Lord, J.D., *Intercomparison exercise to measure the elastic tensile properties of a fibre reinforced metal matrix composite*, NPL Report DMM(A)83, Dec 1993.
- [21] Sonne, H.M., Hesse, B., “Determination of Young’s modulus on steel sheet by computerised tensile test – comparison of different evaluation concepts”, *“Werkstoffprüfung 1993”*, DVM-Tagungsband.
- [22] Roebuck, B., Lord, J.D., McCartney, L.N., *Validation of a draft tensile testing standard for discontinuously reinforced MMC - VAMAS and UK MMC Forum Intercomparisons*, VAMAS Report No. 20, ISSN 1016-2186, National Physical Laboratory, May 1995.

- [23] *Guide to the expression of uncertainty in measurement*. International Organization for Standardization, Geneva. BIPM, IEC, IFCC, ISO, IUPAC, IUPAP, OIML. ISBN 92-67-10188-9, (BSI Equivalent: BSI PD 6461: 1995, Vocabulary of Metrology, Part 3. Guide to the Expression of Uncertainty in Measurement. BSI, London.)
- [24] Bell, S., *A beginner's guide to uncertainty*, NPL Measurement Good Practice Guide no. 11, August 1999.
- [25] Birch, K., *Estimating uncertainties in testing*, NPL Measurement Good Practice Guide no. 36, March 2001.
- [26] Kandil, F.A., *et al.*, (Eds), *UNCERT Manual. Manual of codes of practice for the determination of uncertainties in mechanical tests*, National Physical Laboratory, September 2000.
- [27] Timoshenko, S., Young, D.H., *Elements of strength of materials*, Van Nostrand, New Jersey, USA, fourth edition, 1962.
- [28] EN 843-2, Advanced technical ceramics - monolithic ceramics - mechanical properties at room temperature, Part 2: determination of elastic moduli.
- [29] Morrell, R., *Flexural strength testing of ceramics and hardmetals*, NPL Good Practice Guide No. 7, National Physical Laboratory, Teddington, UK, 1997.
- [30] Rammerstorfer, F.G., Hastik, F., "Der dynamische E-modul von Schleifkörpern", *Werkstatt u. Betrieb*, 1974, **107**(9), 527-33.
- [31] Prescott, J., *Applied Elasticity*, Longman, Green and Co., London, 1924, pp 307-10.
- [32] Raju, P., "Vibrations in annular plates", *J. Aeronautical Soc. India*, 1962, **14**, 37-52.
- [33] Sakata, M., Kimura, K., Mizunuma, A., "Measurement of elastic moduli from the impact sound of engineering ceramics and composites at elevated temperature", *J. Amer. Ceram. Soc.*, 1995, **78**(11), 3040-44.
- [34] Newman F.H., Searle, V.H.L., *The general properties of matter*, fifth edition, Edward Arnold (Publishers) Ltd, London, 1959, pp 152-4.
- [35] ASTM C1198-01: *Standard test method for dynamic Young's modulus, shear modulus and Poisson's ratio for advanced ceramics by sonic resonance*.

Annex 1: Equations for resonance or natural frequency methods

A1.1 Introduction

The relationships between test-piece dimensions, elastic properties and vibration modes are not simple. Equations that relate these characteristics have been developed over a century, initially as ‘thin bar’ simplified solutions to the equations of motion, and later with refinements, which account for:

- End effects
- Shear/flexure coupling
- Shape effects

Direct derivation of such relationships is complex, usually has a number of simplifying assumptions, and the outcome does not necessarily exactly match experimental results. The complexity of equations found in the current standards literature is based on fitting parametric equations to experimental results for a series of bars of a homogeneous material with different shapes and sizes (see, e.g. Spinner *et al.* [A1.1]).

Equations are now available for the following geometries:

- Rods and rectangular section bars
- Discs
- Discs with central holes (e.g. grinding wheels)
- Thin rings (e.g. piston rings)
- Thick rings
- Square plates

The equations are listed here, together with their ranges of validity. This latter aspect is important, as it affects the typical error that can arise if complex terms are omitted from calculations.

A1.2 Rectangular section bars

A1.2.1 Basic equations

ASTM standard C1259 gives the following most recent formulation for Young’s modulus E based on fundamental mode flexural and torsional frequencies for parallel faced prismatic bars of mass m , length L , width b and thickness t in the direction of flexure, of an elastically homogeneous and isotropic material. For the **flexural** mode:

$$E = 0.9465 \left(\frac{mf_f^2}{b} \right) \left(\frac{L^3}{t^3} \right) T \quad (\text{A1.1})$$

where the parameter T is given by:

$$T = 1 + 6.585(1 + 0.0752\nu + 0.8109\nu^2) \left(\frac{t}{L}\right)^2 - 0.868 \left(\frac{t}{L}\right)^4 - \left[\frac{8.340(1 + 0.2023\nu + 2.173\nu^2)(t/L)^4}{1 + 6.338(1 + 0.1408\nu + 1.536\nu^2)(t/L)^2} \right] \quad (\text{A1.1A})$$

where ν is Poisson's ratio. This standard also gives the provision that if $L/t \geq 20$, the term T can be simplified to:

$$T = 1 + 6.858(t/L)^2 \quad (\text{A1.1B})$$

which removes the need to have prior knowledge of Poisson's ratio.

If $L/t < 20$ and Poisson's ratio is not known, then it either has to be assumed, or it has to be estimated by an iterative process from Young's modulus and shear modulus determined by a torsional vibration technique (see below) until a consistent relationship between the three properties is obtained.

For shear modulus G obtained from the fundamental **torsional** frequency f_t :

$$G = \frac{4Lmf_t^2}{bt} \left[\frac{B}{1+A} \right] \quad (\text{A1.2})$$

where:

$$B = \left[\frac{b/t + t/b}{4(t/b) - 2.52(t/b)^2 + 0.21(t/b)^6} \right] \quad (\text{A1.2A})$$

is a shape dependent term, and

$$A = \left[\frac{0.5062 - 0.8776(b/t) + 0.3504(b/t)^2 - 0.0078(b/t)^3}{12.03(b/t) + 9.892(b/t)^2} \right] \quad (\text{A1.2B})$$

is an empirical correction factor. **Note that these torsion equations assume that $b \geq t$.**

The generalised case for the fundamental **longitudinal** mode is not well established other than for rods (see below) and is outside the suite of ASTM standards. However, for rectangular section specimens with t/L and b/L both $\ll 1$ and $b \sim t$ (i.e. near square specimens) the following equation can be used (Spinner and Tefft [A1.2]):

$$E = 4L\rho f_l^2 K \quad \text{where } \rho = m/Lbt \quad \text{and } 1/K \approx 1 - \frac{\pi^2\nu^2(b^2 + t^2)}{12L^2}$$

The function K is valid only for small thickness to length ratios. Other sources assume that it is the smallest dimension of the bar that is of concern, and eliminate the term b (IMCE HTVP equipment handbook citing standard NBN B15-230). This is a correction of only about 0.3% for $\nu = 0.25$ and $b/L = 0.25$, assuming $b \geq t$.

A1.2.2 Truncation of correction factors

Truncation of the correction factors can be made provided that the magnitude of the error is kept below an acceptable level, say 1%, similar to the effect of the uncertainty in measuring test-piece thickness. For example, if the function for T is evaluated (Figure A1.1), the value of $(T - 1)$ is less than 0.01 for $t/L = 0.04$, irrespective of the value of Poisson's ratio, so if the correction factor is set to unity, the error is less than 1%. For shorter, thicker test-pieces, the correction factor becomes significant and should be used.

Figure A1.1 also shows that there is no significant difference within an error level of 1% in the value of the correction factor whether the full version, T (Equation A1.1A), or partial versions, T_1 , T_2 , T_3 with progressive removal of terms from the right-hand end of the full equation, or the fully truncated version T_4 from ASTM C1259 (Equation A1.1B), if $t/L < 0.2$. The full version needs to be used for $t/L > 0.2$, which actually represents quite short stubby test-pieces. This evaluation also demonstrates that ASTM C1259 shows extreme caution in its approach.

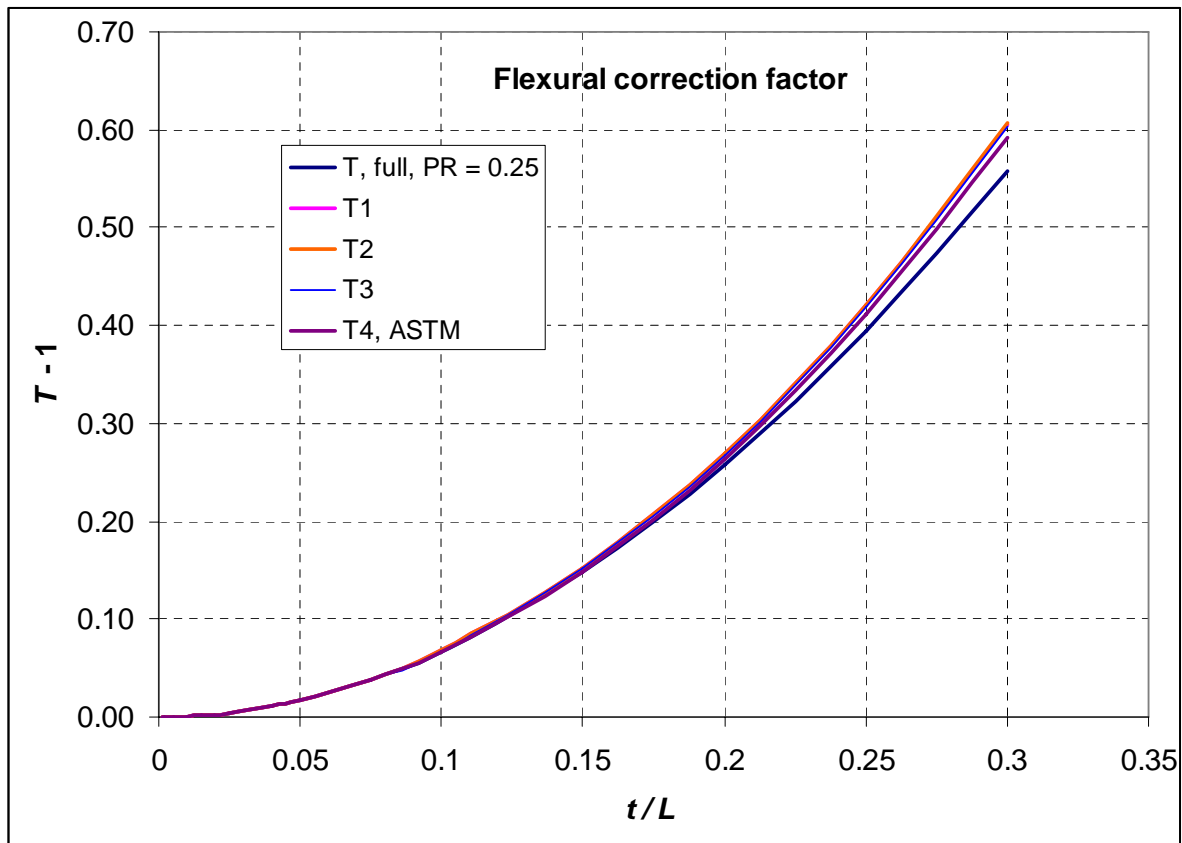


Figure A1.1: Flexural correction factor $T - 1$ as a function of thickness to length ratio.

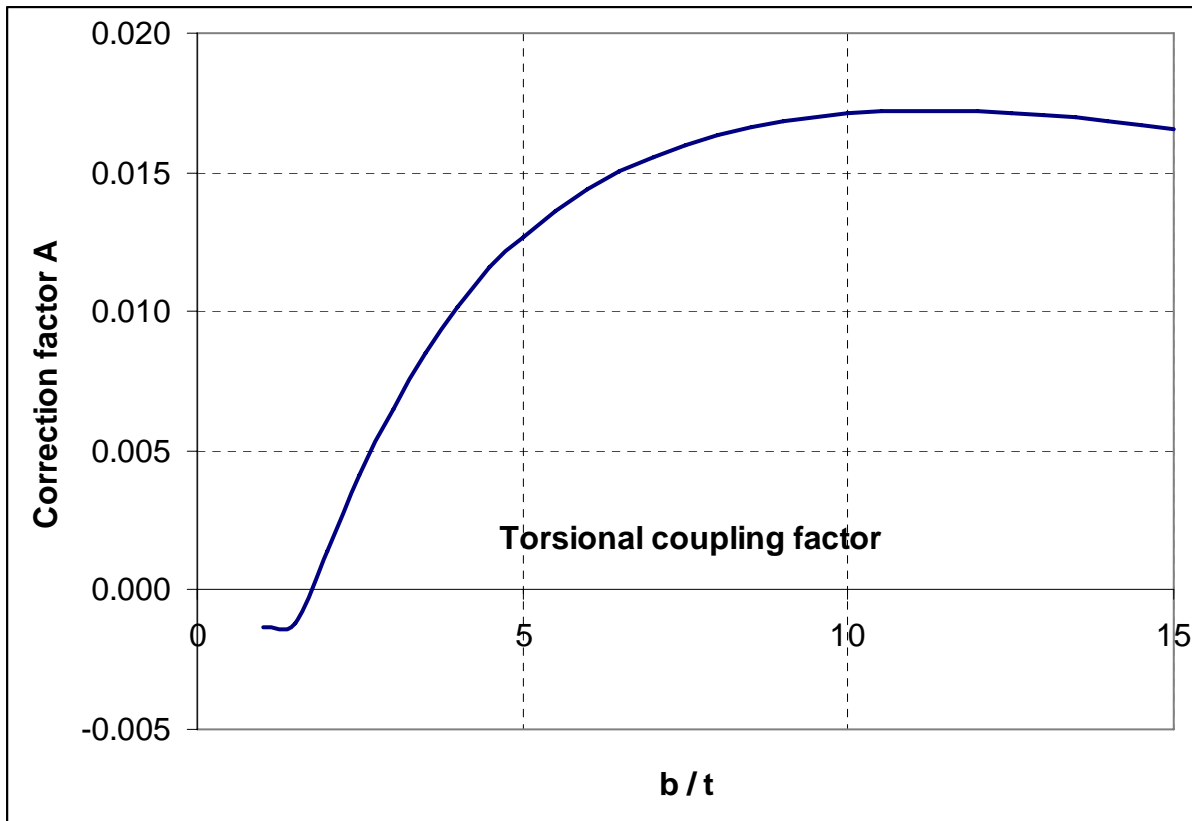


Figure A1.2: Torsion coupling correction factor evaluated from equation A1.2B.

For the torsional mode case, the calibration factor B has to be used for all geometries. The empirical correction factor A , evaluated in Figure A1.2, has a value of less than 1% for values of $b/t < 4$, and can probably be ignored in such circumstances, although this is not stated in ASTM C1259.

A1.2.3 Correction for chamfers on test-pieces

The flexural mode equations presented above are for bars with perfectly square edges. In practice, edges may be deliberately rounded or have 45° chamfers applied. An analysis for the effect of chamfers has been prepared by Quinn and Swab [A1.3]. In their analysis they correct the cross-sectional moment of inertia equation for the chamfered geometry. The cross-sectional moment of inertia of a rectangular section beam is given by:

$$I = bt^3 / 12 \tag{A1.4}$$

Substituting this into Equation A1.1 for the flexural mode modulus and then writing it using the material density:

$$E = 0.9465 \left(\frac{12mTl^3}{I} \right) f_f^2 = 0.9465 \left(\frac{12\rho btTl^4}{I} \right) f_f^2 \tag{A1.5}$$

For a test-piece with a given density, dimensions, and flexural mode frequency, but with equal chamfers on all four edges:

$$E_{cor} = E_{nom} (I_{nom} / I_{cor}) \tag{A1.6}$$

where the subscript ‘*nom*’ refers to the nominal values ignoring chamfers, and the subscript ‘*cor*’ refers to the values corrected for the chamfer. It can be shown that:

For four equal 45° chamfers of face width c :

$$I_{cor} = \frac{bt^3}{12} - \frac{c^2}{9} \left(c^2 + \frac{1}{2}(3t - 2c)^2 \right) \quad (\text{A1.7A})$$

For four equal rounded chamfers of radius r :

$$I_{cor} = \frac{b(t-2r)^3}{12} + \frac{(b-2r)r^3}{6} + \frac{r(b-2r)(t-r)^2}{2} + 4r^4 \left(\frac{\pi}{16} - \frac{4}{9\pi} \right) + \pi r^2 \left[\frac{t}{2} - r \left(1 - \frac{4}{3\pi} \right) \right]^2 \quad (\text{A1.7B})$$

This analysis assumes the density version of the equation is used, but if density has been calculated from mass and dimensions, the density also needs to be corrected, i.e.:

$$E_{cor} = E_{nom} \left(\frac{I_{nom} \rho_{cor}}{I_{cor} \rho_{nom}} \right) \quad (\text{A1.8})$$

where:

For four equal 45° chamfers of face width c :

$$\rho_{cor} = \frac{m}{L(bt - 2c^2)} = \rho_{nom} \left(1 - \frac{1}{(1 - 2c^2/bt)} \right) \quad (\text{A1.9A})$$

For four equal rounded chamfers of radius r :

$$\rho_{cor} = \frac{m}{L(bt - 2r^2(4 - \pi))} = \rho_{nom} \left(1 - \frac{1}{(1 - 2r^2(4 - \pi)/bt)} \right) \quad (\text{A1.9B})$$

The correction for moment of inertia exceeds 1% when the 45° chamfer size exceeds about 5%, or when the radius of curvature exceeds about 8%, of the thickness of a typical flexural test-piece. The correction for density based on mass and nominal dimensions is about one third of the correction for moment of inertia.

A1.3 Round section bars

The equivalent equation for fundamental **flexure** of a round bar of diameter d in flexure (ASTM C1259) is:

$$E = 1.6067 \left(\frac{L^3}{d^4} \right) m f_f^2 T' \quad (\text{A1.10})$$

where the correction factor T' is given by:

$$T' = 1 + 4.939(1 + 0.0752\nu + 2.173\nu^2) \left(\frac{d}{L} \right)^2 - 0.4883 \left(\frac{d}{L} \right)^4 - \left[\frac{4.691(1 + 0.2023\nu + 2.173\nu^2)(d/L)^4}{1 + 4.754(1 + 0.1408\nu + 1.536\nu^2)(d/L)^2} \right] \quad (\text{A1.10A})$$

Again, for long thin rods with $L/d > 20$, T' can be simplified to:

$$T' = 1 + 4.939(d/L)^2 \quad (\text{A1.10B})$$

For fundamental mode **torsional** vibration (ASTM C1259¹):

$$G = 16 \left(\frac{L}{\pi d^2 n^2} \right) m f_t^2 \quad (\text{A1.11})$$

where n is the vibration mode (= 1 for the fundamental).

Young's modulus can also be obtained from the **longitudinal** mode vibration. This is outside the scope of the suite of ASTM standards, but is given by Spinner and Tefft [A1.2] as:

$$E = 4 \left(\frac{L}{\pi n^2 r^2} \right) m f_l^2 K \quad (\text{A1.12})$$

where n is the mode ($n = 1$ for the fundamental) and, for the specific case where the wavelength λ of the vibration is large compared with the rod diameter, K is given by:

$$1/K = 1 - \frac{\pi^2 n^2 v^2 r^2}{2L^2} \approx 1 \text{ for long thin rods} \quad (\text{A1.12A})$$

i.e. when $2r/\lambda = nr/L \gg 1$. If this is not the case, then an alternative approach after Bancroft [A1.4] must be used.

A1.4 Discs

The disc method is described in ASTM C1259 Annex and CEN EN 843-2 Annex. The method relies on the identification of two separate out-of-plane fundamental vibration modes, one being a symmetrical vibration with a nodal circle of diameter about 0.7 of the disc diameter, and one being an asymmetric folding mode with two orthogonal diametral nodal lines. The former has a higher frequency than the latter. The ratio of the frequencies together with the thickness/radius ratio gives Poisson's ratio. Either of the frequencies and Poisson's ratio gives Young's modulus, Young's modulus and Poisson's ratio gives the shear modulus. The basic equation for Young's modulus developed by Glandus [A1.5] for a disc of diameter d and thickness t is:

$$E = \frac{12\pi m d^2 (1 - \nu^2) f_n^2}{K_n^2 t^3} \quad (\text{A1.13})$$

where K is a calibration factor and n is the vibration mode. ASTM C1259 gives look-up tables for obtaining first, Poisson's ratio, and then appropriate values of K for the two modes (see Annex 3).

A1.5 Discs with small central holes, e.g. grinding wheels

For out-of-plan vibration striking up the torsional mode, the relevant relationship is given by Rammerstorfer and Hastik [A1.6] as:

$$E = \frac{48\pi^2 f^2 r_0^2 \rho (1 - \nu^2)}{\lambda^4 t^2} \quad (\text{A1.14})$$

where λ is a calibration factor dependent on the inner to outer radius ratio. For values of r_i/r_o of less than 0.1, a value of $\lambda = 5.2$ is within 1% of the true value.

¹ It has been noted that in both ASTM C623 (2000) and C848 (1999), the presented equations are wrong by a factor of 2.

A1.6 Discs with large holes and thin rings tested out-of-plane

Raju [A1.7] showed that for thin rings, the term λ introduced in A1.5 was a stronger function of the radius ratio than in the region for discs with small holes. Evaluation of his data shows that a straight line fit for λ^2 is a good approximation for $r_i/r_o > 0.4$ (Figure A1.3).

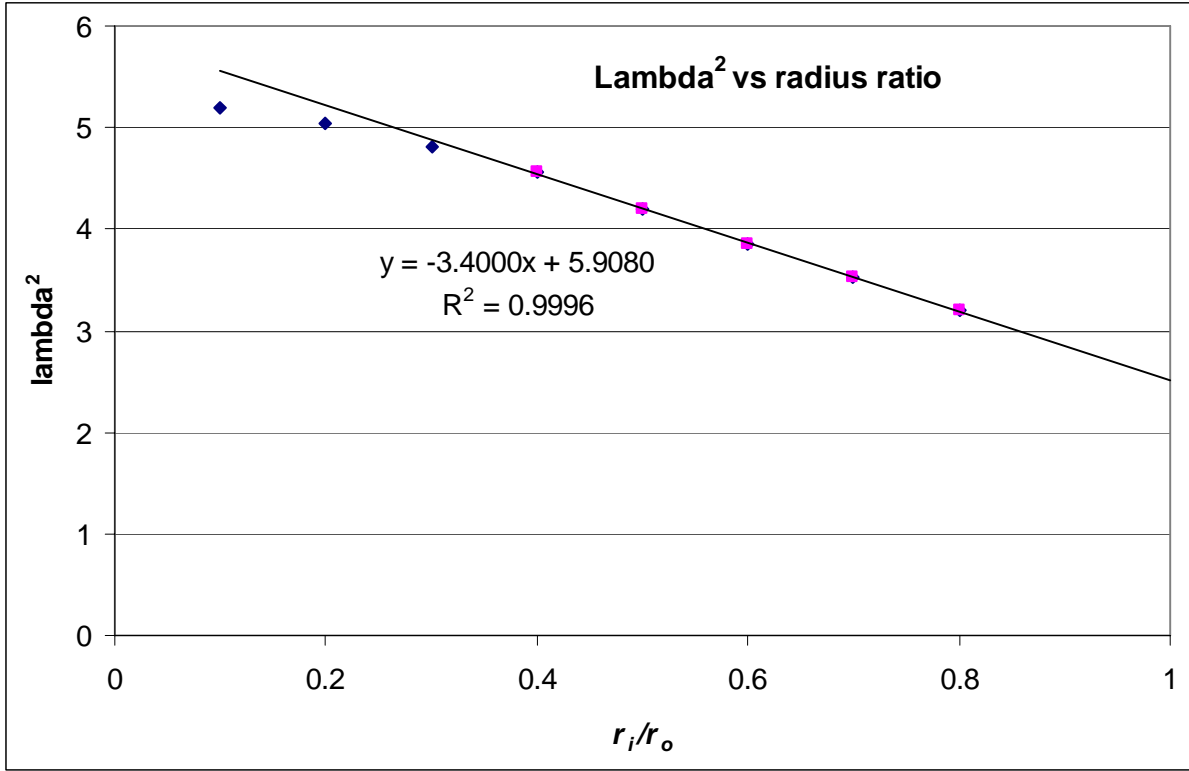


Figure A1.3: Plot of λ^2 vs. r_i/r_o with a straight-line fit to the values for $r_i/r_o > 0.4$.

A1.7 In-plane vibration of thin rings

Prescott [A1.8] showed that for a thin ring vibrating within its plane, the elastic modulus can be computed as:

$$E = \frac{\rho r^4 \cdot 4\pi^2 f_n^2 t (r_o - r_i)}{I} \cdot \frac{(n^2 + 1)}{n^2 (n^2 - 1)^2} \tag{A1.15}$$

where $n = 2, 3, 4, \text{ etc.}$, is the vibration mode, and I is the cross-sectional moment of inertia, taken as $t(r_o - r_i)^3/12$, *i.e.*, similar to the case for a bent beam. It is unclear from the original source how ‘thin’ a ring should be for this equation to be valid, but the validity is most likely to be best for the lowest vibration mode.

An evaluation was made at NPL using a 316 stainless steel ring 210 mm outside diameter, 190 mm inside diameter and 4 mm thick, and a small flexural test-bar cut from the same billet. Figure A1.4 compares the results for different in-plane modes calculated with equation A1.15 with those for flexural and longitudinal determinations using the flexural test-piece. It appears that with this ring aspect ratio, equation A1.15 gives valid results to within a consistency of 1% up to $n = 4$. For higher in-plane ring modes, the result is less accurate, an

indication that the ring is no longer ‘thin’ compared with the wavelength of the vibration. Table A1.1 shows an overall comparison of different methods applied to the ring and bar test-pieces used in this exercise, which provides evidence of the intercomparability of methods.

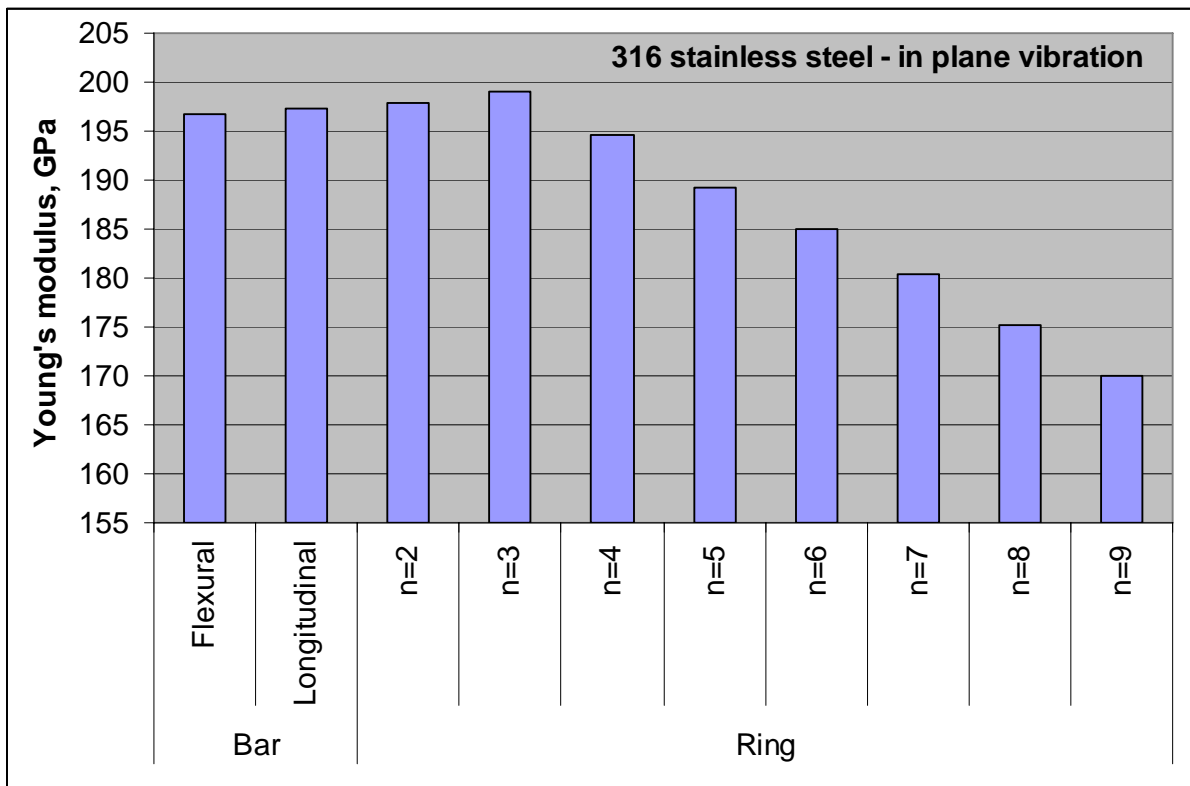


Figure A1.4: Comparison of Young’s modulus determinations using a steel bar test-piece and a range of modes of a thin ring with Prescott’s equation A1.15.

Table A1.1: Modulus measurements on 316 stainless steel bar and ring test-pieces

Bar no.	<i>E</i> , flex., GPa	<i>G</i> , torsional, GPa	Poisson’s ratio	<i>E</i> , long., GPa		
1	196.64	76.43	0.286	197.39		
2	197.04	76.51	0.288	197.37		
<i>E</i>, GPa						
Ring	Impact excitation method, in-plane	Impact excitation method out-of-plane	Ultrasonic time-of-flight, axial	Ultrasonic time-of-flight, radial	Diametral compression, 0-180° position	Diametral compression, 90-270° position
316	197.86	202.32	196.06	196.27	200.53	201.57

References:

- A1.1 Spinner, S., Reichard, T.W., Tefft, W.E., “A comparison of experimental and theoretical relations between Young’s modulus and the flexural and longitudinal resonance frequencies of uniform bars”, *J. Res. NBS*, 1960, **64A**(2) 147-55.
- A1.2 Spinner, S., Tefft, W.E., “A method for determining mechanical resonance frequencies and for calculating elastic moduli from these frequencies”, *Proc. ASTM*, 1961, **61**, 1221-38.
- A1.3 Quinn, G.D., Swab, J.J., “Elastic modulus by resonance of rectangular prisms: corrections for edge treatments”, US Army Report ARL-TN-165, July 2000.
- A1.4 Bancroft, D., “The velocity of longitudinal waves in cylindrical bars” *Phys. Rev.* 1941, **59**, 588-93.
- A1.5 Glandus, J.C., “Rupture fragile et résistance aux chocs thermiques de céramiques a usages mécaniques”, Thesis, University of Limoges, France, 1981.
- A1.6 Rammerstorfer, F.G., Hastik, F., “Der dynamische E-modul von Schleifkörpern”, *Werkstatt u. Betrieb*, 1974, **107**(9), 527-33.
- A1.7 Raju, P., “Vibrations in annular plates”, *J. Aeronautical Soc. India*, 1962, **14**, 37-52.
- A1.8 Prescott, J., *Applied Elasticity*, Longman, Green and Co., London, 1924, pp 307-10.

Annex 2: Selection of prismatic bar test-piece dimensions for resonance or impact excitation

As mentioned in the main text, if the objective of the measurement exercise is to determine both Young's and shear moduli, and hence determine Poisson's ratio, it is necessary to distinguish between flexural and torsional modes of test-piece vibration. While it is generally possible to minimise the appearance of torsional modes by minimising the chances of exciting them while driving or impacting the test-piece in flexure, it is almost impossible to avoid flexural modes while driving or impacting the test-piece in torsion. Should the unfortunate circumstances arise that the fundamental torsional mode frequency is close to or overlaps a flexural mode (typically a higher mode than the fundamental), then it becomes hard to distinguish between them, and the wrong frequency may then be selected as the torsional mode.

In order to determine the risk of overlap it is necessary to compare the frequencies for flexure and torsion. A way of doing this avoiding input of materials properties other than a Poisson's ratio figure is to compute the fundamental torsional/fundamental flexural frequency ratio (f_{t1}/f_{f1}) from the basic calculation equations, and to compare the outcome with the harmonic flexural/fundamental flexural frequency ratios (f_{fn}/f_{f1} , $n = 3, 5, 7, 9$, etc) computed from the harmonic analysis.

Using the basic calculation equations for E and G , it can be shown that:

$$\frac{f_{t1}}{f_{f1}} = \sqrt{\frac{0.1183L^2}{t^2(1+\nu)} \left[\frac{T(1+A)}{B} \right]} \quad (\text{A2.1})$$

where $T = T(\nu, t/L)$ is the correction factor appearing in the flexural mode equation, $B = B(t/b)$ is the shape parameter appearing in the torsional mode equations, and $A = A(t/b)$ is the torsional mode coupling correction. All these factors contain Poisson's ratio and geometrical ratios of thickness to length or thickness to width.

Evaluating this expression using the simplified forms:

$$T = 1 + 6.585(1 + 0.0752\nu + 0.8109\nu^2)(t/L)^2, \text{ i.e. ignoring higher terms in } t/L;$$

$$B = \left[\frac{t/b + b/t}{4(t/b) - 2.52(t/b)^2 + 0.21(t/b)^6} \right]$$

$A = 1$, i.e. assuming $b/t < 4$, such that the correction is less than 1% (see ASTM C1259);

the data in Table A.2.1 can be derived. It can be seen that the outcome is not particularly sensitive to the actual value of Poisson's ratio.

Table A2.1: Fundamental torsional to fundamental flexural frequency ratios.

Poisson's ratio	Thickness/length ratio	Fundamental torsional to flexural frequency ratio, f_t/f_f					
		$t/b = 0.1$	$t/b = 0.2$	$t/b = 0.3$	$t/b = 0.5$	$t/b = 1.0$	$t/b = 2.0$
0.2	0.001	60.500	115.201	162.662	233.132	290.326	671.655
	0.01	6.052	11.524	16.272	23.321	29.043	67.188
	0.02	3.029	5.768	8.144	11.673	14.536	33.629
	0.03	2.023	3.852	5.439	7.795	9.708	22.458
	0.05	1.220	2.324	3.281	4.703	5.856	13.548
	0.075	0.822	1.566	2.210	3.168	3.945	9.127
	0.1	0.626	1.191	1.682	2.410	3.002	6.944
	0.125	0.509	0.970	1.370	1.963	2.445	5.655
	0.15	0.434	0.825	1.166	1.670	2.080	4.813
	0.2	0.342	0.651	0.919	1.317	1.640	3.793
0.3	0.001	58.127	110.681	156.281	223.986	278.936	645.305
	0.01	5.815	11.072	15.634	22.407	27.904	64.554
	0.02	2.911	5.542	7.825	11.215	13.967	32.312
	0.03	1.944	3.701	5.226	7.490	9.328	21.580
	0.05	1.173	2.233	3.154	4.520	5.629	13.022
	0.075	0.791	1.505	2.126	3.046	3.794	8.777
	0.1	0.602	1.146	1.618	2.319	2.888	6.682
	0.125	0.491	0.934	1.319	1.890	2.354	5.446
	0.15	0.418	0.796	1.123	1.610	2.005	4.638
	0.2	0.330	0.628	0.887	1.271	1.583	3.663

Computation of the flexural harmonic ratios is more complex, and involves numerically solving the dynamic flexural mode equations. Following Huang [A2.1] and Kromp *et al.* [A2.2, A2.3], the Timoshenko equation for flexural motion of a bar with correction for shear and rotatory deformation is given by:

$$EI \frac{\partial^4 w}{\partial x^4} + \rho b t \frac{\partial^2 w}{\partial x^2} - \rho I \left(1 + \frac{E}{kG} \right) \frac{\partial^4 w}{\partial x^2 \partial t^2} + \frac{\rho^2 I}{kG} \frac{\partial^4 w}{\partial t^4} = 0 \quad \text{where } k = \frac{5 + 5\nu}{6 + 5\nu} \quad \text{A2.2}$$

The term k is a shear coupling factor to account for the fact that shear stress is not uniform. The solution to this equation is given as the series of roots b_n to the characteristic equation for free-free boundary conditions:

$$2 - 2 \cosh \alpha b_n \cos \beta b_n + \frac{\{b_n [b_n^2 r^2 (r^2 - s^2)^2 + (3r^2 - s^2)]\}}{\sqrt{1 - (b_n r s)^2}} \sinh \alpha b_n \sin \beta b_n = 0$$

with

$$r^2 = \frac{I}{b t L^2} = \frac{t^2}{12 L^2} \quad \text{for a rectangular section beam,}$$

$$s^2 = \frac{r^2 E}{kG} = r^2(2.4 + 2\nu) \text{ for an isotropic material with } E/G = 2(1 + \nu)$$

$$\text{and } \frac{\alpha}{\beta} = \frac{1}{2} \sqrt{\mp(r^2 - s^2) + \sqrt{(r^2 - s^2)^2 + 4/b_n^2}} \tag{A2.3}$$

The values of b_n are directly related to the frequencies of vibration, so the ratios of b_n/b_1 give the required frequency ratios. Equation A2.3 has to be solved numerically with appropriate input values of t/L and ν , such as an interval halving method. For demonstration purposes, a spreadsheet method has been used in which the value of b_n is iteratively adjusted to balance the equation. Table A2.2 gives numerical frequency ratio data for two values of Poisson’s ratio and a range of typical test-piece thickness to length ratios, t/L . Again, it can be noted that the outcome is not particularly sensitive to Poisson’s ratio.

Table A2.2: Calculated flexural frequency ratios

Poisson’s ratio	Thickness/length ratio	Frequency ratio, harmonic/fundamental				
		f_2/f_1	f_3/f_1	f_4/f_1	f_5/f_1	f_6/f_1
0.2	0.001	2.757	5.404	8.933	13.344	18.638
	0.005	2.757	5.404	8.933	13.344	18.638
	0.01	2.757	5.404	8.933	13.344	18.637
	0.02	2.756	5.404	8.932	13.343	18.636
	0.03	2.756	5.403	8.932	13.342	18.633
	0.05	2.756	5.402	8.929	13.336	18.622
	0.075	2.756	5.400	8.922	13.317	18.578
	0.1	2.755	5.395	8.904	13.260	18.410
	0.125	2.753	5.384	8.857	13.082	17.717
	0.15	2.750	5.362	8.742	12.506	-
	0.2	2.735	5.228	7.754	-	-
0.3	0.001	2.757	5.404	8.933	13.344	18.6379
	0.005	2.757	5.404	8.933	13.344	18.6379
	0.01	2.757	5.404	8.933	13.344	18.6379
	0.02	2.757	5.404	8.933	13.344	18.6378
	0.03	2.757	5.404	8.933	13.344	18.6376
	0.05	2.757	5.404	8.932	13.343	18.6339
	0.075	2.756	5.403	8.929	13.332	18.6011
	0.1	2.756	5.400	8.915	13.280	18.4298
	0.125	2.755	5.392	8.871	13.089	17.6216
	0.15	2.753	5.371	8.747	12.412	-
	0.2	2.739	5.224	7.589	-	-

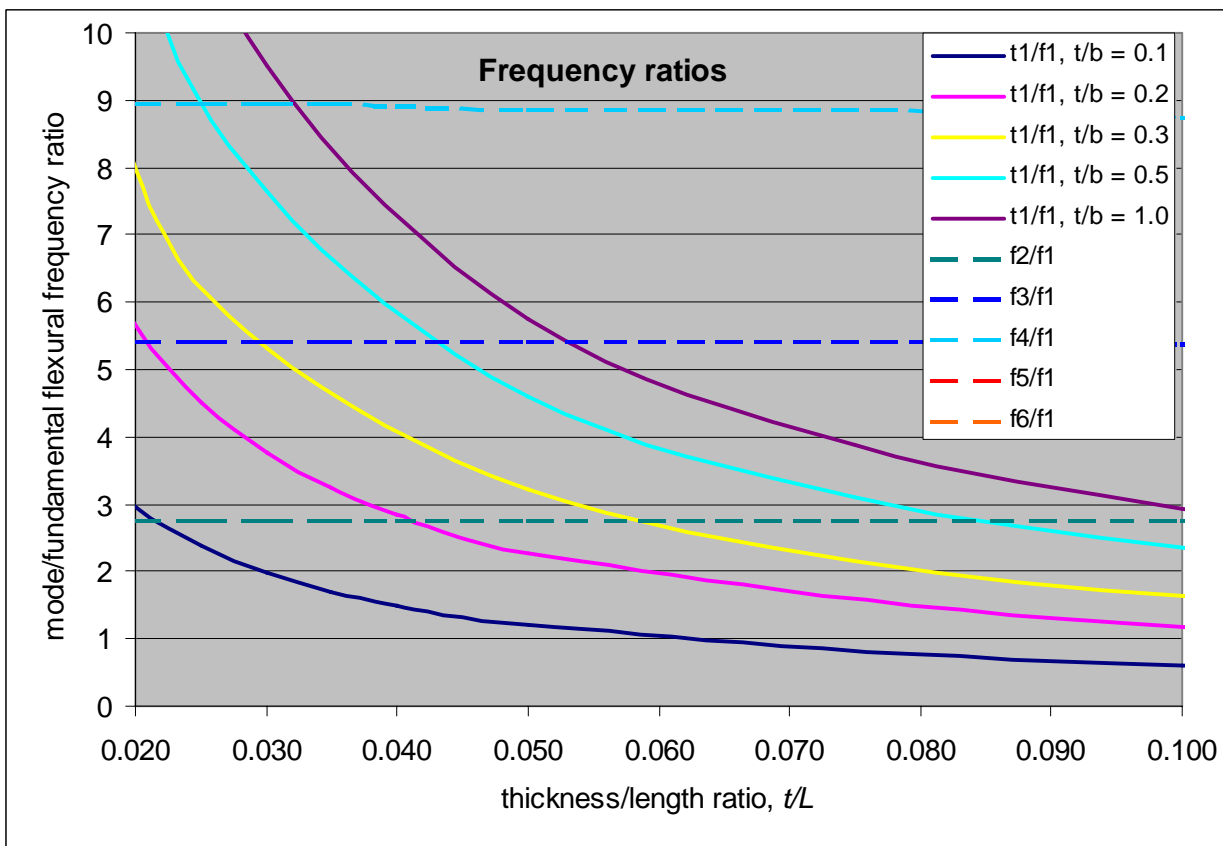
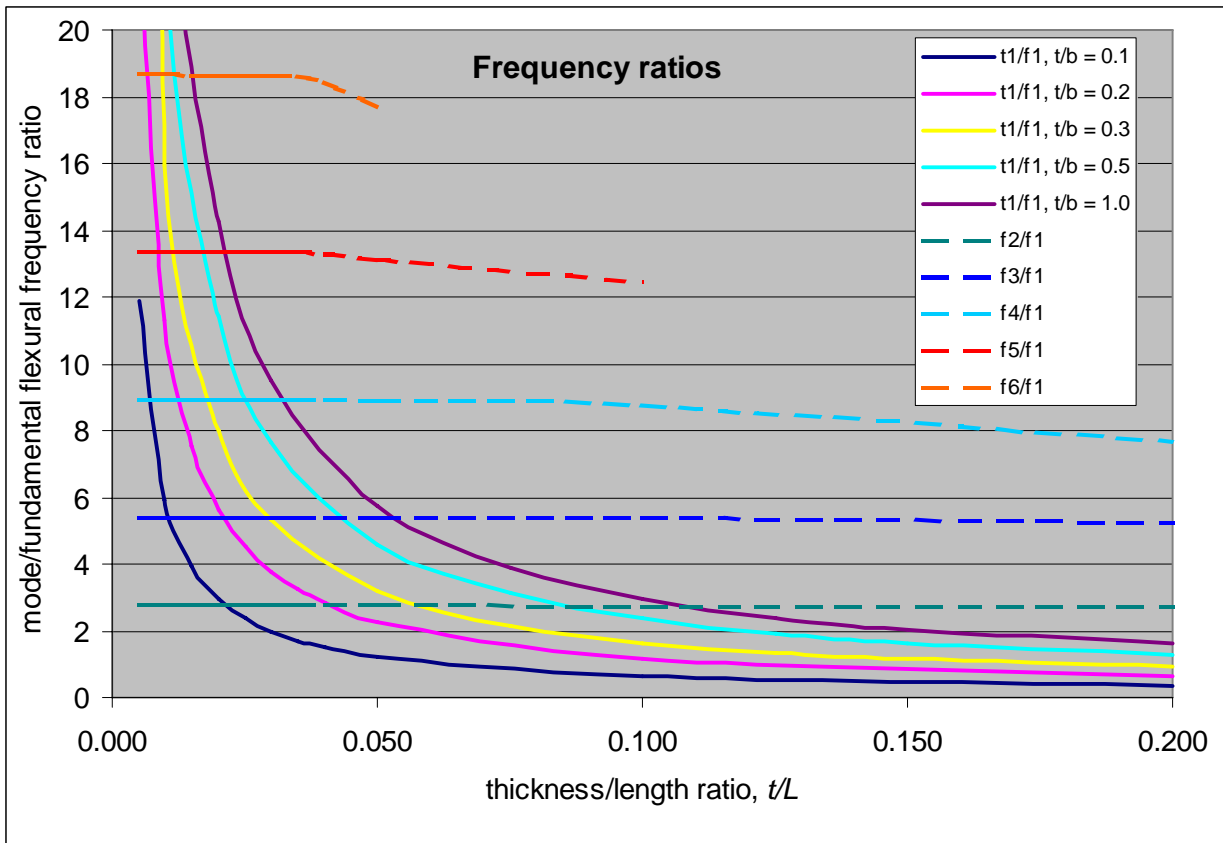


Figure A2.1: Comparison of the ratio of fundamental torsional to fundamental flexural frequency with the ratio of flexural harmonic to fundamental flexural frequency (lower figure with smaller plotted range).

For the purposes of choosing test-piece dimensions for **avoiding overlap** of the torsional mode frequency with the fundamental flexural mode, these two sets of data have been plotted in Figure A2.1. The near-horizontal set of lines represent the flexural harmonic to fundamental flexural frequency ratio as a function of test-piece thickness to length ratio. The curved lines give the ratio of the fundamental torsional to fundamental flexural frequency for a range of different thickness to width ratios. Where these two families of lines overlap, the fundamental torsional mode will be close to or overlap the flexural mode. Test-piece shapes which avoid regions of cross-over should be avoided.

It should also be noted that torsional harmonics are roughly in the ratio 1 : 2 : 3 : 4: *etc.*, so it is a relatively simple matter to estimate torsional harmonic overlap as well.

For example, some test-piece shapes which might commonly be selected, but which **should be avoided**, are as follows:

<i>t/b</i>	<i>t/L</i>
0.1	0.01, 0.02
0.2	0.02, 0.04
0.3	0.03, 0.06
0.5	0.045
1.0	0.055

It may be the case that the ringing quality of the test-piece material is sufficiently good that even quite closely spaced frequencies can be resolved, but the above dimensional ratios should generally be avoided to avoid ambiguity of selection of frequency for modulus calculation. This aspect becomes more important with high temperature measurements, where the torsional and flexural frequencies can shift differently with temperature, and peaks can merge.

References

- A2.1 Huang, T.C., “The effect of rotatory inertia and of shear deformation on the frequency and normal mode equations of uniform beams with simple end conditions”, *J. Appl. Mech.*, 1961, **28**, 579-84.
- A2.2 Lins, W., Kaindl, G., Peterlik, H., Kromp, K., “A novel resonant beam technique to determine the elastic moduli in dependence on orientation and temperature up to 2000 °C”, *Rev. Sci. Instr.* 1999, **70**(7), 3052-58.
- A2.3 Kaindl, G., Lins, W., Peterlik, H., Kromp, K., Reetz, R., Reetz, T., “The determination of the elastic moduli of anisotropic ceramics and ceramic composites at high temperatures by a novel resonant beam technique”, *Interceram*, 2000, **49**(2), 92-101.

Annex 3: Impact excitation method applied to disc test-pieces

A3.1 Principle

A disc when struck at its centre will ring with a circularly symmetrical vibration mode ('diaphragm' or second mode) with a nodal circle at approximately 0.7 of its diameter (Figure 22). When struck on the nodal circle a folding mode ('saddle' or first mode) of lower frequency will be preferentially produced. If these two frequencies are measured, their ratio, coupled with the dimensions of the disc, gives Poisson's ratio. Either of these frequencies with Poisson's ratio and the test-piece dimensions and mass gives Young's modulus. Shear modulus is computed from Young's modulus and Poisson's ratio.

A3.2 Method

The test-piece is placed either on four small equally spaced supports positioned on the nodal circle or on a small pad of cotton wool or fibre insulation. The detecting microphone is positioned above the test-piece or, alternatively a piezoelectric transducer can be positioned as appropriately to detect the respective modes. The test-piece is struck at the centre to excite and detect the second (diaphragm) mode, and on the nodal circle (between the support points if used) to excite and detect the first (saddle) mode. The two frequencies, f_2 and f_1 , respectively, are then recorded. The correct identification of the two frequencies is best achieved by estimating the relevant frequency window for the test-piece mass, dimensions and approximate elastic properties, and by using a system that displays the entire natural frequency spectrum. This will allow the correct peaks to be identified and to be measured accurately. The ratio of the two frequencies will typically lie in the range 1.4 to 1.7 for discs with thickness to radius ratios up to 0.5.

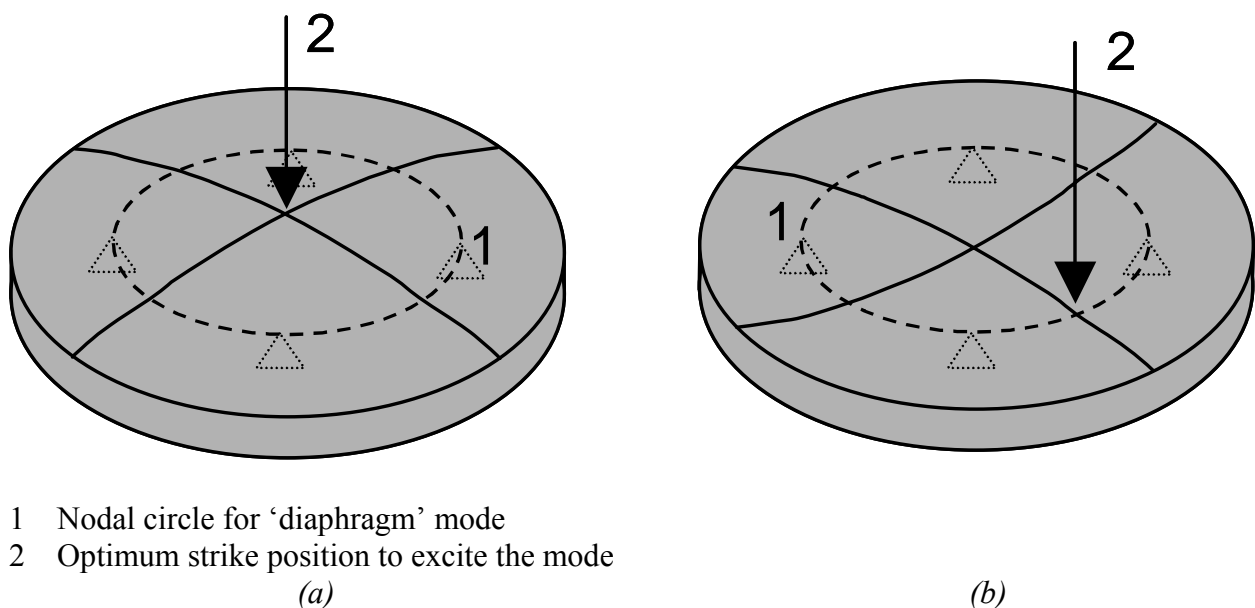


Figure A.3.1: (a) Second ('diaphragm') mode and (b) first ('saddle') mode of vibration of a disc when struck.

A3.3 Calculations

The first step is to determine Poisson's ratio from the look-up table (Table A3.1) for the relevant thickness to radius ratio, t/r , and for the relevant ratio of the first and second natural frequency modes, f_2/f_1 .

Next, determine two values of dynamic Young's modulus, E_1 , E_2 , from the following equations using the frequencies of the respective modes, together with the determined value of Poisson's ratio:

$$E_1 = 12\pi f_1^2 d^2 m (1 - \nu^2) / (K_1^2 r^3) \quad \text{A3.1}$$

$$E_2 = 12\pi f_2^2 d^2 m (1 - \nu^2) / (K_2^2 r^3) \quad \text{A3.2}$$

where:

d = disc diameter in mm

m = disc mass in g

r = disc radius in mm

f_1 = first (saddle) mode frequency in Hz

f_2 = second (diaphragm) mode frequency in Hz

K_1 = geometric factor for first vibration mode (see Table A3.2)

K_2 = geometric factor for second vibration mode (see Table A3.3)

The derivation of these equations may be found in Martincek [A3.1] and Glandus [A3.2]

Determine the average value of dynamic Young's modulus, E , from:

$$E = (E_1 + E_2) / 2 \quad \text{A3.3}$$

Compute the dynamic shear modulus, G , from:

$$G = E / (2(1 + \nu)) \quad \text{A3.4}$$

Table A3.1 — Poisson’s ratio (ν) as a function of the ratios t/r and f_2/f_1 [A3.4]

f_2/f_1	1.350	1.375	1.400	1.425	1.450	1.475	1.500	1.525	1.550	1.575	1.600
t/r											
0.00	0.015	0.043	0.070	0.094	0.118	0.141	0.163	0.184	0.205	0.226	0.247
0.05	0.018	0.044	0.070	0.094	0.118	0.141	0.164	0.185	0.206	0.226	0.247
0.10	0.020	0.045	0.070	0.094	0.118	0.141	0.164	0.185	0.206	0.227	0.247
0.15	0.023	0.049	0.075	0.100	0.124	0.148	0.171	0.192	0.212	0.233	0.254
0.20	0.025	0.053	0.080	0.105	0.130	0.154	0.178	0.198	0.218	0.239	0.260
0.25	0.033	0.060	0.088	0.114	0.139	0.162	0.186	0.206	0.227	0.247	0.268
0.30	0.040	0.068	0.096	0.122	0.148	0.171	0.193	0.214	0.235	0.255	0.275
0.35	0.051	0.078	0.105	0.130	0.155	0.179	0.203	0.224	0.245	0.264	0.284
0.40	0.062	0.088	0.113	0.138	0.162	0.187	0.212	0.234	0.255	0.274	0.292
0.45	0.070	0.096	0.123	0.148	0.173	0.197	0.221	0.242	0.263	0.281	0.300
0.50	0.078	0.105	0.132	0.158	0.183	0.206	0.229	0.250	0.270	0.289	0.307

f_2/f_1	1.625	1.650	1.675	1.700	1.725	1.750	1.775	1.800	1.825	1.850	1.875	1.900
t/r												
0.00	0.265	0.282	0.297	0.312	0.329	0.346	0.362	0.378	0.394	0.409	0.424	0.438
0.05	0.265	0.283	0.298	0.314	0.331	0.347	0.363	0.378	0.394	0.409	0.424	0.438
0.10	0.265	0.283	0.300	0.316	0.332	0.348	0.363	0.378	0.394	0.409	0.424	0.438
0.15	0.271	0.289	0.306	0.322	0.338	0.354	0.368	0.383	0.398	0.413	0.427	0.442
0.20	0.278	0.295	0.312	0.328	0.344	0.359	0.374	0.388	0.403	0.417	0.431	0.445
0.25	0.286	0.304	0.320	0.336	0.351	0.366	0.380	0.395	0.409	0.423	0.437	0.451
0.30	0.294	0.312	0.328	0.344	0.358	0.372	0.387	0.402	0.415	0.428	0.442	0.456
0.35	0.302	0.320	0.336	0.352	0.367	0.382	0.398	0.414	0.428	0.442	0.456	0.471
0.40	0.310	0.328	0.344	0.360	0.376	0.392	0.409	0.425	0.440	0.455	0.470	0.485
0.45	0.318	0.337	0.354	0.370	0.387	0.403	0.420	0.437	0.452	0.468	0.485	0.503
0.50	0.327	0.346	0.363	0.380	0.397	0.414	0.431	0.448	0.464	0.480	0.500	0.520

Table A3.2 — Geometrical constant K_1 as a function of Poisson’s ratio (ν) and the ratio t/r [A3.4]

t/r	0.00	0.05	0.10	0.15	0.20	0.25	0.30	0.35	0.40	0.45	0.50
ν											
0.00	6.170	6.144	6.090	6.012	5.914	5.800	5.674	5.540	5.399	5.255	5.110
0.05	6.076	6.026	5.968	5.899	5.816	5.717	5.603	5.473	5.331	5.178	5.019
0.10	5.962	5.905	5.847	5.782	5.705	5.613	5.504	5.377	5.234	5.079	4.915
0.15	5.830	5.776	5.720	5.657	5.581	5.490	5.382	5.256	5.115	4.962	4.800
0.20	5.681	5.639	5.587	5.524	5.446	5.351	5.240	5.114	4.975	4.826	4.673
0.25	5.517	5.491	5.445	5.380	5.297	5.197	5.083	4.957	4.822	4.681	4.537
0.30	5.340	5.331	5.290	5.223	5.135	5.030	4.913	4.787	4.656	4.523	4.390
0.35	5.192	5.156	5.120	5.052	4.961	4.853	4.734	4.610	4.483	4.358	4.234
0.40	4.973	4.964	4.931	4.865	4.775	4.668	4.551	4.429	4.306	4.186	4.070
0.45	4.781	4.756	4.723	4.661	4.576	4.476	4.365	4.249	4.131	4.013	3.899
0.50	4.540	4.525	4.490	4.436	4.365	4.280	4.182	4.075	3.960	3.841	3.720

Expansion of region shown in bold above:

t/r	0.10	0.11	0.12	0.13	0.14	0.15	0.16	0.17	0.18	0.19	0.20
ν											
0.14	5.746	5.739	5.722	5.710	5.696	5.683	5.670	5.654	5.642	5.629	5.608
0.16	5.694	5.687	5.670	5.664	5.645	5.632	5.619	5.602	5.590	5.576	5.556
0.18	5.641	5.634	5.617	5.606	5.592	5.579	5.566	5.549	5.537	5.523	5.502
0.20	5.587	5.576	5.563	5.551	5.538	5.524	5.510	5.495	5.479	5.463	5.446
0.22	5.531	5.524	5.507	5.495	5.481	5.468	5.455	5.439	5.427	5.411	5.388
0.24	5.474	5.467	5.450	5.438	5.424	5.410	5.396	5.379	5.366	5.351	5.328
0.26	5.415	5.408	5.391	5.379	4.364	5.350	5.336	5.318	5.304	5.289	5.266
0.28	5.354	5.347	5.330	5.317	5.301	5.287	5.273	5.255	5.241	5.225	5.201
0.30	5.290	5.279	5.266	5.253	5.238	5.223	5.207	5.190	5.173	5.154	5.135
0.32	5.224	5.217	5.200	5.187	5.172	5.157	5.142	5.123	5.108	5.091	5.067
0.34	5.156	5.148	5.131	5.118	5.103	5.088	5.073	5.053	5.037	5.020	4.997

A3.4 Interferences

Disc test-pieces which are not of accurate roundness or parallelism of faces may show a doubling of each of the frequencies of natural vibration. If this happens, the average frequency of the doublets should be taken and used for the computations of modulus. It is advisable to ensure that test-pieces are ground round and parallel faced to better than 0.01 mm.

Disc test-pieces which have inhomogeneous density may also show a small variability in the recorded frequency, especially when using a piezoelectric detector in contact with a specific point on the test-piece surface, depending on where the disc is struck. Similarly, test-pieces which are anisotropic in the plane of the disc, for example if taken from an extruded sheet or from a material with a hot-pressing direction lying in the plane of the disc, may show similar variability.

Table A3.3 — Geometrical constant K_2 as a function of Poisson's ratio (ν) and the ratio t/r [A3.4]

t/r	0.00	0.05	0.10	0.15	0.20	0.25	0.30	0.35	0.40	0.45	0.50
ν											
0.00	8.240	8.226	8.151	8.027	7.863	7.670	7.455	7.227	6.991	6.754	6.520
0.05	8.378	8.339	8.252	8.124	7.963	7.777	7.570	7.350	7.120	6.885	6.649
0.10	8.511	8.459	8.364	8.223	8.071	7.885	7.679	7.459	7.228	6.991	6.751
0.15	8.640	8.584	8.485	8.349	8.182	7.990	7.779	7.553	7.316	7.074	6.830
0.20	8.764	8.712	8.611	8.469	8.294	8.092	7.871	7.635	7.390	7.141	6.889
0.25	8.884	8.840	8.738	8.589	8.403	8.189	7.954	7.706	7.450	7.191	6.931
0.30	9.000	8.962	8.860	8.705	8.508	8.280	8.030	7.767	7.497	7.226	6.960
0.35	9.111	9.081	8.977	8.814	8.605	8.363	8.098	7.819	7.535	7.253	6.979
0.40	9.219	9.193	9.085	8.913	8.692	8.436	8.157	7.865	7.569	7.276	6.991
0.45	9.321	9.292	9.178	8.997	8.766	8.499	8.208	7.905	7.598	7.295	7.001
0.50	9.420	9.376	9.252	9.063	8.824	8.550	8.252	7.940	7.625	7.313	7.010

Expansion of region shown in bold above:

t/r	0.10	0.11	0.12	0.13	0.14	0.15	0.16	0.17	0.18	0.19	0.20
\square											
0.14	8.460	8.443	8.411	8.385	8.355	8.326	8.297	8.262	8.234	8.202	8.160
0.16	8.510	8.493	8.460	8.433	8.403	8.373	8.343	8.308	8.279	8.248	8.205
0.18	8.560	8.542	8.509	8.482	8.451	8.421	8.391	8.356	8.327	8.294	8.249
0.20	8.611	8.586	8.559	8.530	8.500	8.469	8.437	8.403	8.368	8.331	8.294
0.22	8.662	8.646	8.613	8.582	8.548	8.517	8.487	8.454	8.425	8.390	8.338
0.24	8.712	8.694	8.660	8.630	8.597	8.565	8.534	8.498	8.467	8.432	8.382
0.26	8.762	8.743	8.708	8.678	8.645	8.612	8.580	8.542	8.510	8.474	8.425
0.28	8.811	8.791	8.755	8.726	8.692	8.659	8.625	8.585	8.551	8.515	8.467
0.30	8.860	8.833	8.804	8.772	8.739	8.705	8.668	8.630	8.591	8.550	8.508
0.32	8.907	8.885	8.848	8.818	8.784	8.750	8.716	8.675	8.640	8.601	8.548
0.34	8.954	8.932	8.894	8.863	8.827	8.793	8.758	8.717	8.681	8.641	8.586

A3.4 Precision and bias

At present, the precision and bias of the calculation method in this Annex have limited traceability. The tabular data given in Tables A3.1 to A3.3 are based on smooth curvefitting by Glandus [A3.2] of a small number of computed data points given by Martinec [A3.1]. Most software packages incorporating this method employ the tables in look-up and interpolation mode. Very recently, multiparameter polynomial curvefits have been published for these tables [A3.5], but this work has also highlighted the influence of rounding errors in previously published work which limit the likely accuracy of some parts of the data tables and the polynomial curvefits such that the uncertainty is typically 1.5% for Poisson's ratio and 1% for Young's modulus. For most purposes this is more than adequate, since other factors such as the precision of geometry and homogeneity of structure or density will also limit the accuracy. Experimental proof of the close equivalence of data produced by the beam impact excitation and the disc excitation methods is not yet available, so the precision and bias of the

method are not fully known, but potentially the method gives results accurate to better than 1 % in modulus and 2 % in Poisson's ratio [A3.3].

A3.5 References

- A3.1 Martinec, G., "The determination of Poisson's ratio and dynamic modulus of elasticity from the frequencies of natural vibration in thick circular plates", *J. Sound Vibration*, 1965, **2**(2), 116-27.
- A3.2 Glandus, J.C., "Rupture fragile et résistance aux chocs thermiques de céramiques a usage mécaniques", Thesis, University of Limoges, France, 1981.
- A3.3 Hendrix, M., De With, G., Morrell, R., "Young's modulus of ceramic materials – an intercomparison of methods", *Brit Ceram. Proc.* 1999, **60**(2), 565-6.
- A3.4 ASTM C1259 *Standard test method for dynamic Young's modulus, shear modulus and Poisson's ratio for advanced ceramics by impulse excitation of vibration, Annex: disc test-pieces.*
- A3.5 Salem, J.A., Singh, A., "Polynomial expressions for estimating elastic constants from the resonance of circular plates", *Mater. Sci. Eng.* 2006, **A422**, 292-7.

Annex 4: Resonance and impact excitation methods applied to single crystals

A4.1. Principle of Measurement

A4.1.1 Nomenclature and equations for cubic single crystals

Crystallographically cubic single crystals have three independent crystallographic tensor stiffnesses (C_{ij}) or compliances (S_{ij}) ($i, j = 1$ to 6), specifically $(i, j) = (1, 1), (1, 2)$ and $(4, 4)$ as defined by the following stress/strain relationship [A4.1]:

$$\begin{pmatrix} \varepsilon_1 \\ \varepsilon_2 \\ \varepsilon_3 \\ \varepsilon_4 \\ \varepsilon_5 \\ \varepsilon_6 \end{pmatrix} = \begin{pmatrix} S_{11} & S_{12} & S_{12} & 0 & 0 & 0 \\ S_{12} & S_{11} & S_{12} & 0 & 0 & 0 \\ S_{12} & S_{12} & S_{11} & 0 & 0 & 0 \\ 0 & 0 & 0 & S_{44} & 0 & 0 \\ 0 & 0 & 0 & 0 & S_{44} & 0 \\ 0 & 0 & 0 & 0 & 0 & S_{44} \end{pmatrix} \begin{pmatrix} \sigma_1 \\ \sigma_2 \\ \sigma_3 \\ \sigma_4 \\ \sigma_5 \\ \sigma_6 \end{pmatrix} \quad \text{A4.1}$$

There is an equivalent relationship for stiffnesses C_{ij} , where there are simple relationships as follows:

$$C_{11} = \frac{S_{11} + S_{12}}{(S_{11} - S_{12})(S_{11} + 2S_{12})} \quad \text{A4.2}$$

$$C_{12} = \frac{-S_{12}}{(S_{11} - S_{12})(S_{11} + 2S_{12})} \quad \text{A4.2A}$$

$$C_{44} = \frac{1}{S_{44}} \quad \text{A4.2B}$$

The **effective Young's modulus E** in a given direction is a function of these elements and the angles of this direction to the principal crystallographic directions. The simplest notation is in terms of compliances and Euler angles (θ, φ) where θ is the azimuthal angle from the [001] direction and φ is the equatorial angle from the [010] direction in the (011) plane (Figure 1).²

² Gas-turbine manufacturers are particularly concerned with the crystallographic orientation of single crystals of high-temperature nickel-base superalloys used for turbine blades. In particular it is desirable from the point of view of high-temperature creep that the blade axis corresponds to near the [001] direction. Knowledge of elastic properties in all directions is required for mechanical calculations, particularly for the determination of resonances, hence the importance of being able to determine the tensor compliances or stiffnesses.

Back-reflection Laue X-ray diffraction is used to analyse the orientation of the castings, and there is a notation associated with the evaluation of angles. In the Euler angle representation, the angle θ is equivalent in X-ray stereographic representations to 'theta' (UK notation) and 'alpha' or 'primary' (US notation). The angle φ is thought to be equivalent to 'rho' (UK notation) but does not correspond with one of the four US convention angles.

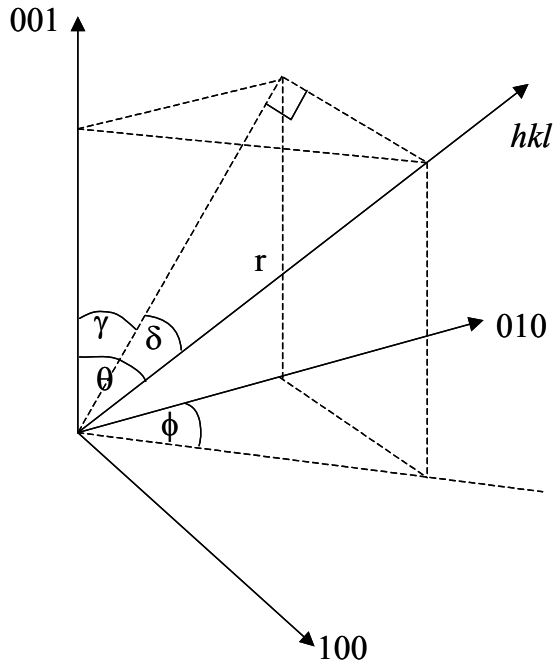


Figure A4.1: Orientation nomenclature

Following the notation of Hermann *et al.* [A.1], the apparent Young's modulus in the direction (θ, φ) is given by:

$$E(\theta, \varphi) = (S_{11} - 2SJ)^{-1} \tag{A4.3}$$

where: $S = S_{11} - S_{12} - S_{44} / 2$ A4.3A

and $J = \sin^2 \theta \cdot \cos^2 \theta + \sin^4 \theta \cdot (1 - \cos 4\varphi) / 8$ A4.3B

Thus if S_{11} , S_{12} and S_{44} are known for a given composition, $E(\theta, \varphi)$ can be calculated from equation (A.1).

The situation regarding shear modulus G is much more complex. Except in the specific circumstances of a round-section rod test-piece [A4.1], the apparent shear modulus depends on the cross-sectional geometry and its rotational orientation relative to the crystallographic axes [A.4.2]. For the case of round rods, the shape dependence disappears and a relationship of the following form can be used:

$$G_{meas}(\theta, \varphi) = ((S_{44} + 4SJ)(1 - \delta))^{-1} \tag{A4.4}$$

where δ is a coupling factor of the order 0.005. However, this may over or underestimate the true shear modulus of a non-round shape. It should also be noted that a curious and complicating consequence of directional elasticity is that applying a pure twist to an off-axis rod or bar also leads to it curving [A4.3].

A4.1.2 Angular dependency of modulus

Figure A4.2 shows the typical angular dependence of modulus for single crystal nickel alloy Rene N4 based on literature values of crystallographic compliances [A4.4]. Shear modulus is computed for the simple case of round rods. Important points to note are:

1. Young's modulus is a minimum along one of the crystallographic axes, $\theta = 0^\circ$, $\varphi=0^\circ$, *i.e.* [001] direction;
2. As θ increases at $\varphi = 0^\circ$, Young's modulus increases, nearly doubling for $\theta = 45^\circ$, $\varphi = 0^\circ$, *i.e.* [011] direction;
3. As θ increases at $\varphi = 45^\circ$, Young's modulus increases by approximately 2.5 times for $\theta = 54^\circ$, $\varphi = 45^\circ$, *i.e.* [111] direction;

It should be noted that a true Poisson's ratio only exists for contractions orthogonal to the [001] and the [111] directions. It is incorrect to employ the normal relationship for isotropic materials, *i.e.*: $\nu = (E/2G) - 1$ because unphysical results are obtained. According to [A4.1], Poisson's ratio can be specified by a single number only when the stress acts parallel to directions in the <100> or <111> families when the transverse strain is isotropic. In such cases, these are:

$$\nu = -S_{12} / S_{11} \quad \text{for strains orthogonal to } \langle 001 \rangle$$

$$\nu = \frac{-(2S_{11} + 4S_{12} - S_{44})}{(2S_{11} + 4S_{12} + 2S_{44})} \quad \text{for strains orthogonal to } \langle 111 \rangle.$$

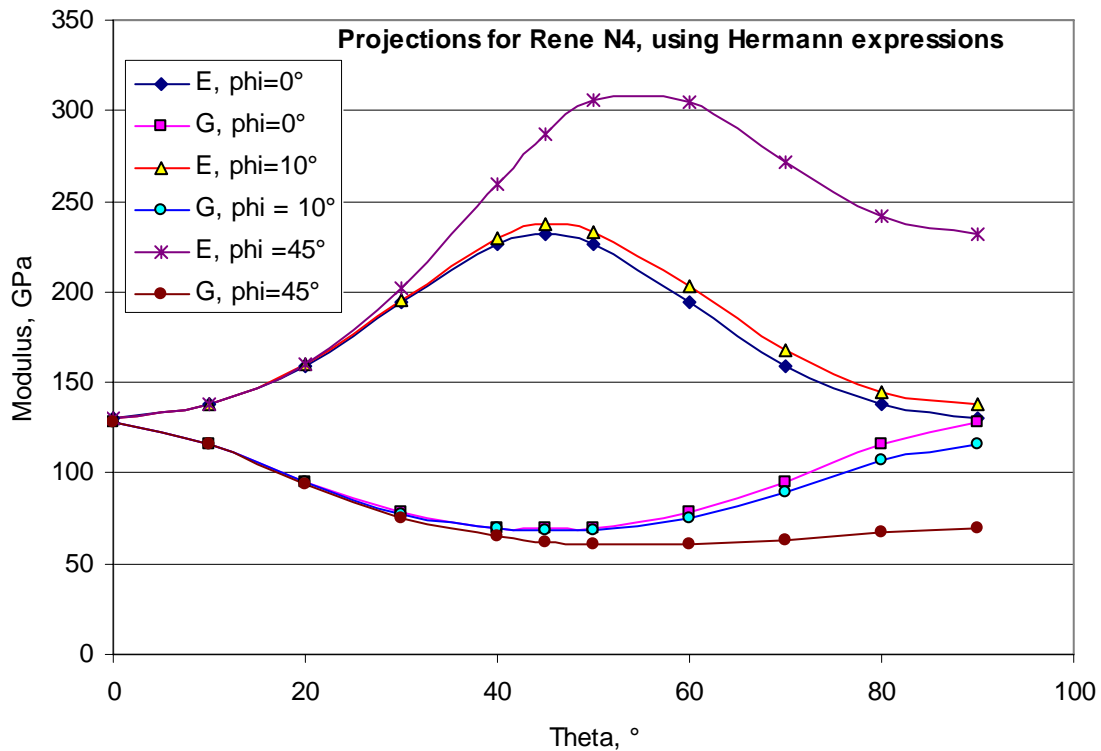


Figure A4.2: Variation in Young's modulus and shear modulus with azimuthal and equatorial angle of direction relative to the crystallographic axes for alloy RENE N4 using compliance data from reference [A4.4] and the Hermann et al. formulation [A4.2].

A.4.2 Resonance and impact excitation method applied to single crystals

Hermann *et al.* [A4.2] have used the above approach in order to evaluate single-crystal materials employing the resonance method on rod test-pieces. In this case, the resonance in flexure is straightforward, while resonance in torsion can be achieved by an appropriate suspension with the driver wire tangential to side of the rod at one end, and the sensor wire tangential to the other side at the opposite end.

The equivalent situation cannot be achieved using impact excitation because torsional vibration is difficult to initiate with a striking action. Consequently, the testing can be performed only on rectangular section bars, which introduces the problem that equation A.4 is no longer strictly valid. For this reason off-axis torsional determinations, while giving a value for the test-bar, do not easily relate to the elastic stiffness tensor.

A route around the problem has been evaluated at NPL [A4.5]. Experimentally, if the moduli of a series of test-pieces of different but known orientations are measured, the flexural and torsional modulus data can be plotted against the orientation angle function J , using equations A4.3 and A4.4 respectively, to yield values for S as the slope, and S_{11} and S_{44} as the respective intercepts at $J = 0$. In order to overcome the difficulties with the torsional data, it is advantageous where possible to select the test-bar orientations to provide:

1. An orientation as close to [001] as possible such that $J \sim 0$, and the determined value of $1/E$ is close to that of S_{11} and that of $1/G$ is close to that of S_{44} .
2. Orientations well away from [001], *e.g.* [011] and [111], such that the slope, S , of the plotted line of $1/E$ vs. $2J$ can be determined accurately, and thus an accurate value of S_{12} can be determined from equation A4.3A.

Thus, a minimum of three test-pieces is sufficient for the determination of the three tensor unknown compliances or stiffnesses.

References

- A4.1 Kelly, A., McMillan N.H., *Strong solids*, 3rd edition, Clarendon Press, Oxford, 1986.
- A4.2 Hermann, W., Sockel, H.G., Han, J., Bertram, A., "Elastic properties and determination of elastic constants of nickel-base superalloys by a free-free beam technique", in *Superalloys 1996*, ed. Kissinger R.D., Deye, D.J.; Anton, D.J., Cetel, A.D., Nathal, M.V., Pollock, T.M., Woodford, D.L., The Minerals & Metals Society, 1996, pp 229-238.
- A4.3 Lekhnitskii, S.G., *Theory of elasticity of an anisotropic body*, MIR Publishing, Moscow, 1981.
- A4.4 Dandekar, P.D., Martin, A.G., "Temperature dependence of flexural and torsional elastic constants of two nickel-based superalloys", *J. Mater. Sci.*, 1990, **25**, 3321-26.
- A4.5 Morrell, R, Ford, D.A., Harris, K., *Calculation of modulus in different for single-crystal alloys*, NPL Measurement Note DEPC (MN) 004, 2004.

